2013

A MOLECULAR MECHANISM REGULATING THE TIMING OF CORTICOGENICULATE INNERVATION

Justin Brooks
Virginia Commonwealth University

A Molecular Mechanism Regulating the Timing of Corticogeniculate Innervation

A dissertation submitted in partial fulfillment of the requirements for the degree of Doctor of Philosophy at Virginia Commonwealth University.

by

Justin McRae Brooks
Bachelor of Science
Virginia Tech, 2004

Director: Michael A. Fox, PhD
VTCRI Associate Professor
Department of Biological Sciences

Virginia Commonwealth University
Richmond, Virginia
October, 2013

Acknowledgements

I would like to thank my advisor, Dr. Michael Fox, for his mentorship and support. Through his guidance, my skills as a writer, speaker, and critical thinker have flourished, and I cannot show enough appreciation for his patience. Much gratitude goes to Dr. Linda Phillips, for taking over as my VCU advisor and always having time to meet with me on short notice. I would also like to thank the members of my PhD advisory committee: Dr. Carmen Sato-Bigbee, Dr. John Bigbee, Dr. Kurt Hauser, and Dr. William Guido. Each and every member of my advisory committee has been critical to my development with great insight and thought-provoking questions.

I would also like to extend gratitude to Dr. Jianmin Su. Dr. Su's technical expertise, work ethic, and sense of humor have kept me motivated to become a better scientist throughout the past 4 years. I would also like to thank Dr. Julie Chan and Dr. Christopher Waggener for the good times and friendship.

Much love and respect goes to my mother and father, who have supported me since day one. I would also like to thank the rest of my friends and family, especially, Catherine Smith, who has been incredibly patient and understanding.

Finally, I would like to dedicate this to the memory of Dr. Thomas Sitz, my undergraduate research advisor.

TABLE OF CONTENTS

LIST OF TABLES

There are no tables included in this document

List of Figures

Abbreviations

acan.....Aggrecan

ADAM……A Disintegrin and Metalloproteinase

ADAMTS.....A Disintegrin and Metalloproteinase with Thrombospondin Motifs

APC.... ……...Astrocyte Precursor Cell

BDNF……Brain-Derived Neurotrophic Factor

BSA.....Bovine Serum Albumin

CAM……Cell Adhesion Molecule

cDNA……..……Complementary DNA

CG...……...Corticogeniculate

chABC.....……....Chondroitinase ABC

CNTF……..CIliary Neurotrophic Factor

CNS……Central Nervous System

cRNA.....…….Complementary RNA

CS. …….....Chondroitin Sulfate

CSPG……Chondroitin Sulfate Proteoglycan

CT……..……....Corticothalamic

CTB.....……Cholera Toxin Subunit B

DAPI.....4',6-diamidino-2-phenylindole

DIG……..…….....Digoxigenin

DiI.....……1,1’-dioctadecyl-3,3,3’,3’-tetramethylindocarbo-cyanine perchlorate

DEPC.....…….Diethylpyrocarbonate

D-FISH.....……..Double Fluorescent *In Situ* Hybridization

dLGN……..Dorsal Lateral Geniculate Nucleus

dlx1.....……..Distal-Less Homeobox 1

DNA..... ……...Deoxyribonucleic Acid

E...……Embryonic Day

ECM……..Extracellular Matrix

eml..……..External Medullary Lamina

FISH…….....Fluorescent *In Situ* Hybridization

G1……..N-Terminal Globular Domain

G2.....……Globular Domain 2

G3..……..C-Terminal Globular Domain

GAG.....…….....Glycosaminoglycan

GAP-43……...Growth-Associated Protein-43

GAPDH.....…….....…Glyceraldehyde-3-Phosphate Dehydrogenase

GCL……...……....Ganglion Cell Layer

GFAP...……Glial Fibrillary Acidic Protein

GFP.....……..……Green Fluorescent Protein

Iba-1.....……Ionizing Calcium-Binding Adaptor-1

IGL..……..Intergeniculate Leaflet

IHC.....…….....Immunohistochemistry

ipRGC……Intrinsically Photosensitive Retinal Ganglion Cell

IR……Immunoreactivity

ISH.....……*In Situ* Hybridization

KS.....…….Keratan Sulfate

L1……L1 Cell Adhesion Molecule

LAR……Leukocyte Antigen-Related Protein Tyrosine Phosphatase Receptor

LGN……Lateral Geniculate Nucleus

lhx9……LIM Homeobox Protein 9

MMP……Matrix Metalloproteinase

mRNA……Messenger RNA

NCAM…… Neural Cell Adhesion Molecule

neo……Neomycin

NeuN……Neuronal Nuclei

NgR1……Nogo Receptor-1

NgR3……Nogo Receptor-3

NGS……Normal Goat Serum

Nr-CAM……Neuron-Glia Related Cell Adhesion Molecule

ODAP……Optic Disc Astrocyte Precursor Cell

OFL……Optic Fiber Layer

P……Postnatal Day

PBS……Phosphate-Buffered Saline

PCR……Polymerase Chain Reaction

PFA……Paraformaldehyde

PLL……Poly-L-Lysine

PNase……Penicillinase

POD……Horseradish Peroxidase

PTPσ……Protein Tyrosine Phosphatase Sigma

qPCR……..……..Quantitative Real Time PCR

RC.....Retinocollicular

RG.....Retinogeniculate

RGC...……..……..……..Retinal Ganglion Cell

RF……..……Retinofugal

rhADAMTS4.....……Recombinant Human ADAMTS4

RNA……Ribonucleic Acid

RTN..…….....Reticular Thalamic Nucleus

SC.....……..Superior Colliculus

SCI…….....Spinal Cord Injury

SD.....Standard Deviation

SEM…….....Standard Error of the Mean

syt1...…….....Synaptotagmin-1

TBS...…….....Tris-Buffered Saline

TIMP……...Tissue Inhibitors of Metalloproteinase

TSA...……..Tyramide Signal Amplification

UTP...…….....Uridylyltransferase

V1.....…….....Primary Visual Cortex

VGluT-1...……Vesicular Glutamate Transporter-1

VGluT-2...……Vesicular Glutamate Transporter-2

vLGN...……Ventral Lateral Geniculate Nucleus

VT.....Ventrotemporal

WT.....…….Wild Type

Abstract

A MOLECULAR MECHANISM REGULATING THE TIMING OF CORTICOGENICULATE INNERVATION

By Justin McRae Brooks, B.S.

A dissertation submitted in partial fulfillment of the requirements for the degree of Doctor of Philosophy at Virginia Commonwealth University.

Virginia Commonwealth University, 2013

Michael A. Fox, PhD
VTCRI Associate Professor
Department of Biological Sciences

Visual system development requires the formation of precise circuitry in the dorsal lateral geniculate nucleus (dLGN) of the thalamus. Although much work has examined the molecular mechanisms by which retinal axons target and form synapses in dLGN, much less is known about the mechanisms that coordinate the formation of non-retinal inputs in dLGN. These non-retinal inputs represent ~90% of the terminals that form in dLGN. Interestingly, recently reports show that the targeting and formation of retinal and non-retinal inputs are temporally orchestrated. dLGN relay neurons are first innervated by retinal axons, and it is only after retinogeniculate synapses form that axons from cortical layer VI neurons are permitted to enter and arborize in dLGN. The molecular mechanisms governing the spatiotemporal regulation of corticogeniculate

innervation are unknown. Here we screened for potential cues in the perinatal dLGN that might repel the premature invasion of corticogeniculate axons prior to the establishment of retinogeniculate circuitry. We discovered aggrecan, an inhibitory chondroitin sulfate proteoglycan (CSPG), was highly enriched in the perinatal dLGN, and aggrecan protein levels dropped dramatically at ages corresponding to the entry of corticogeniculate axons into the dLGN. *In vitro* assays demonstrated that aggrecan is sufficient to repel axons from layer VI cortical neurons, and early degradation of aggrecan, with chondroitinase ABC (chABC), promoted advanced corticogeniculate innervation *in vivo*. These results support the notion that aggrecan is necessary for preventing premature innervation of the dLGN by corticogeniculate axons. To understand the mechanisms that control aggrecan distribution, we identified a family of extracellular enzymes (the *a* *d*isintegrin *a*nd *m*etalloproteinase with *t*hromobo*s*pondin motifs [ADAMTS] family) expressed in postnatal dLGN that are known to contain aggrecan-degrading activity. Importantly, ADAMTS family members are upregulated in dLGN after retinogeniculate synapses form, and intrathalamic injection of ADAMTS4 (also known as aggrecanase-1) resulted in premature invasion of dLGN by corticogeniculate axons. Taken together these results implicate aggrecan and ADAMTSs in the spatial and temporal regulation of non-retinal inputs to the dLGN.

Chapter I

Introduction to Axon Guidance, Extracellular Matrix, and Visual System Development

A Brief History of Neuron Doctrine

The central nervous system (CNS) is composed of neurons, glial cells, and extracellular matrix molecules that perform crucial roles in the establishment of specific neural circuits. The earliest knowledge regarding CNS circuitry was developed using tissue staining techniques that were unable to fully resolve the cellular makeup of the CNS and contained many artifacts. The reticular theory which postulated that the CNS was composed of a continuous meshwork of cells and processes that were all interconnected was prevalent during the pioneering days of neuroscience. Camillo Golgi, however, revolutionized neuroscience through his invention of metallic stains, including the potassium dichromate-silver staining technique. This technique called, the "Golgi stain," was the first method capable of staining individual neurons and glial cells in their entirety, and its advent led to the morphological characterization of neurons and neuroglia as completely distinct cell types (Golgi, 1875). Despite Golgi's passionate advocacy of reticular theory, he was never able to fully describe how the nerve network was established *in vivo* because the Golgi stain was limited in that it labeled small percentages of multiple cell types in CNS, making it impossible for Golgi to fully distinguish between neuron and glial processes.

Many of Golgi's colleagues utilized his own methods to refute the reticular theory. Santiago Ramon y Cajal employed the Golgi stain on many species to create detailed drawings of the cells in CNS and the development of connectivity in spinal cord and

brain. His ability to map the fine structures of neural circuitry helped solidify neuron theory as an axiom of modern neuroscience. During this period the dendrite and axon (terms coined by Wilhelm His and Albert Von Kolliker, respectively) were categorized as distinct functional domains of the neuron. The proposition of the existence of synapses, the small contact zones between neurons that allow for unidirectional conduction (by Charles Sherrington) was another observation that shaped the central tenets of neuron theory, although their existence could not be proven until the advent of the electron microscope (Sherrington 1897; Sherrington, 1900; Palade and Palay, 1954).

Ramon y Cajal pushed the neuron theory as a basis for studying the CNS through the declaration that the CNS is composed of individual discontinous cells called neurons, which all contain a “fundamental membrane” that are extensions of the neuron (Ramon y Cajal,1909). Ramon y Cajal and his student Pio del Rio Hortega introduced gold chloride and ammoniacal silver carbonate stains which allowed for the identification of multiple types of glial cells (Ramon y Cajal, 1913; Rio-Hortega, 1919). Through the development of methods to readily distinguish differing cell types, focus could be shifted to elucidating the mechanisms that drive neuron connectivity. Neuron theory eventually became neuron doctrine and was composed of these observations: the neuron is the structural and functional unit of the CNS, neurons are composed of dendrites, soma, and axons which are fundamentally different, and conduction of nerve impulses is directional (Shepherd, 1991).

Evidence For Specific Targeting of Neuronal Connections

In 1890, Ramon y Cajal described the structure by which axons navigate in the developing nervous system called the growth cone. He also postulated that growth cones are “oriented by chemical stimulation, and move toward the secretion products from certain cells” (Cajal, 1892). Outgrowth of nerve fibers was established in tissue culture experiments using the neural crest from frog embryo (Harrison, 1907; 1910); however, there was a gap in understanding the mechanisms that drive axonal target specificity, *in vivo*. There was still much debate over whether axons initially extended throughout the CNS, and then were eliminated by competition, or if specific guidance factors drove axons to distinct targets.

Evidence for specificity in establishment of synaptic connections was discovered through JN Langley’s experiments on the preganglionic fibers of the superior cervical ganglion. Upon bisection of these fibers, Langley observed regeneration in the preganglionic axons from differing spinal cord levels to the proper postganglionic neuron. Since regenerating axons did not grow to all levels of spinal cord and then refine, this observation led him to propose a chemotactic mechanism for axon guidance (Langley, 1895).

Support for chemotactic mechanisms was exemplified in Roger Sperry’s experimentation on the frog visual system, which led to the proposal of his chemoaffinity hypothesis. Normally axons that originate from cells in dorsal retina project to ventral tectum, and axons that come from ventral retina project to dorsal tectum (Kandel et al., 2000). Other orderly projections include axons projecting from anterior retina to posterior tectum, while posterior fibers extend to anterior tectum. These orientations produce a retinal topographic (retinotopic) visual map, in which adjacent neurons in the

retina project to neighboring neurons in the brain, thus allowing the frog to see a faithful representation of the outside world (Purves et al, 2001).

To test the whether these topographic maps developed through random outgrowth of axons that are competitively eliminated based on activity or if there were specific connections from neurons in the retina to the optic tectum, Sperry detached the frog eye, inverted its positioning, and waited for the reestablishment of neuronal connections. An important feature of the amphibian nervous system is that severed retinal ganglion cell (RGC) axons regenerate and reinnervate the tectum. By rotating the retina by 180°, Sperry discovered that the frogs had inverted visual maps and that the axons in these animals projected to the proper areas of tectum despite the retinal repositioning. (Sperry, 1963). His work sparked the chemoaffinity hypothesis that growing axons are guided by gradients of molecular signals, and their positioning is directed by different concentrations of few signals. Sperry's experiments provided strong evidence to illustrate that the placement of axon processes into their respective retinotopic positions occurs through interactions of axons with molecules in the extracellular space.

Axon Guidance and Synaptic Targeting

In order for the sensory systems to distribute information to the correct relay and processing areas, axon guidance and synaptic targeting cues are necessary to set up a precise neural network. Axon guidance refers to the process by which growth cones react with their environment to select a pathway in which they travel long distances to a specific target nucleus within the nervous system (Goodman and Shatz, 1993). Axon

guidance requires ligand-receptor interactions resulting from either short range (contact-mediated) or long range secreted (diffusible) signals (Zipursky and Sanes, 2010). Contact-mediated attraction and repulsion occur at guide post cells, which contain ligands and transmembrane receptors that alter the axon's trajectory as the growth cone traverses its path and physically interacts with other cells. Secreted chemoattracant molecules can act over long distances and form gradients that direct axons, with complementary receptors, to specific brain regions, while secreted chemorepulsive signals can also act from afar but cause an axon to retract, pause, or turn depending on strength of signal [(Figure 1A) Chen and Cheng, 2009].

Molecular mechanisms that drive axon guidance can also regulate synapse formation. After an axon has selected a cellular partner, synapses between cells must communicate in order to form a functional connection (Figure 1B). The first step in synapse formation is called target recognition, in which a growing axon makes a rudimentary connection onto a postsynaptic cell or in some cases a specific region on that postsynaptic cell. Following synaptic targeting, synaptic differentiation prompts the organization of synaptic elements and establishment of reciprocal communication between the two cells, allowing each to synthesize the proper machinery for setting up a mature, fully functional synapse. Finally, mature synapses that have found suitable partners stabilize, while any improper or weak connections that have begun forming are retracted and allowed to search for a new postsynaptic partner (Fox and Umemori, 2006). Presynaptic terminals that are unable to communicate and assemble a synapse are ultimately degraded.

Extracellular Matrix Effects on Axon Pathfinding and Synaptic Development

The development of CNS circuitry requires precise spatial and temporal targeting of axons to specific partners in the distinct brain nuclei. During axon guidance and synaptic targeting, many different extracellular and molecular mechanisms drive the formation of specific connections. Axon guidance mechanisms have rigorously been studied in CNS since the proposal of the chemoaffinity hypothesis, and the advent of modern technology including genetically altered mouse models, along with high resolution imaging techniques, has advanced understanding of the biochemical mechanisms that drive axon guidance and targeting.

Many molecular axon guidance cues that have been elucidated are functional in differing areas of the CNS. Netrins are evolutionally conserved, diffusible molecules that are secreted from cells at the midline of the spinal cord, and netrins can act either as chemoattractant or chemorepulsive signals, depending on the type and density of receptors expressed on the growth cone of an approaching axon (Tessier-Lavigne and Goodman, 1996). Netrins and netrin receptors, such as DCC/Unc, contribute to the guidance of thalamocortical axons to their proper targets in cortex (Powell et al., 2008). Contact-mediated attraction and repulsion are also guided by expression of extracellular molecules, but these are inititated by complementary receptors and ligands embedded in the surfaces of cells encountered during axon outgrowth (Chen and Cheng, 2009; Kolodkin and Tessier-Lavigne, 2011). Semaphorins are a canonical repulsive guidance cue ligand which can either be diffusible or membrane-bound for contact-mediated signaling. Plexin receptors represent the major class of semaphorin receptors, and activation of these receptors can signal disassembly of growth cone cytoskeletal

molecules and initiate synaptic targeting (Zhou et al., 2008).

These guidance signals also can interact in a myriad of ways such that multiple cues can be processed in parallel, which is a mechanism by which the brain processes individual components of a single stimulus simultaneously. Signaling can work through addition or multiplication of stimuli together or through opposition of each other's effects; however, the interactions between guidance molecules often are more complex than just simple summation of positive and negative signals (Raper and Mason, 2010; Dudanova and Klein, 2013). One such example of this complexity occurs in commissural neurons, which react to both netrin and slit. Axons are guided to the midline by netrin and subsequently should be repelled by slit; however, repulsion by slit is suppressed by Robo-3/Rig-1, a Robo receptor that diminishes the effect of slit, until the midline is reached. During midline crossing, slit activation of the Robo receptor alters function of the DCC receptor, rendering the netrin signaling ineffective (Sabatier et al., 2004; Chen et al., 2008).

In addition to secreted molecules and membrane bound receptors and ligands, there are classes of extracellular matrix (ECM) molecules that have also been shown to guide axons during development and also during regeneration of injured axons in the CNS. Of particular interest are the proteoglycans, a subset of extracellular macromolecules that are expressed in CNS and provide a substrate for tethering link proteins to cells (Morawski et al., 2012). Studies involving chondroitin sulfate proteoglycans (CSPGs) during development and in the adult have revealed potent inhibitory signaling on the neuronal growth cones of many cell types. CSPGs expressed in the periphery of the retina are involved with both proper spatiotemporal

expression of RGC differentiation and directing RGC axons outward to the optic cup (Brittis et al., 1992).

CSPGs interact with many substrates in CNS including growth-promoting laminin (McKeon et al., 1995). The effect of CSPG inhibition was attenuated when laminin was coexpressed with CSPG, although the reaction for different cell types was dependent on the ratio of laminin/CSPG (Snow and Letourneau, 1992; Snow et al., 1996). These studies provided evidence that CSPGs have variable effects on diverse cell types. CSPGs also interact with cell adhesion molecules (CAMs) to regulate axon outgrowth, and evidence has shown that sensory neurons can overcome CSPG inhibition through overexpression of integrin receptors (Condic et al., 1999; Tan et al., 2011). Moreover, a recent *in vivo* study of serotonergic neurons suggests that increased expression of either β1 integrin, growth-associated protein-43 (GAP-43), or a combination of the two enables them to overcome CSPG inhibition in response to spinal cord injury (Hawthorne et al., 2011). GAP-43 has also been implicated in enhancing axon growth after injury in commissural interneurons of the cat spinal cord (Fenrich et al., 2007). Together, these studies provide support for how a complex series of interactions between cells, ECM, and growth substrates influence axon outgrowth.

Molecular factors also aid in synaptic targeting. Subcellular specificity dictates where a presynaptic axon will form a synapse on postsynaptic dendrites, soma, or axons, and this process can be mediated by extracellular guidance cues or transmembrane receptors (Sanes and Yamagata, 2009). For example, proteoglycans expressed in distinct locations aid in targeting the growth cone to motor neuron synapses, so that synaptogenesis can begin (Sanes, 2003). Neurofascin, a CAM in the

immunoglobulin superfamily, is present in a gradient in postsynaptic Purkinje cells of the cerebellum. Presynaptic axons from basket cells first innervate the soma and proximal dendrites of Purkinje cells and then work their way up the neurofascin gradient to their final subcellular locations (Ango et al., 2004). CSPGs also have been reported to play a role in mediating lamina-specific adhesion and lamina-specific axon outgrowth in the dentate gyrus of the hippocampus by entorhinal cortical afferents (Forster et al., 2001).

During early development CSPGs are derived from neurons; however, as the brain integrates circuitry from diverse sensory areas and more cells participate in the maintenance and plasticity of synaptic function, CSPGs, other ECM, and guidance factors are produced by neurons and non-neuronal "glial" cells including astroctytes, oligodendrocytes, and microglia in the brain (Domowicz et al., 1996). This level of complexity makes it difficult to ascertain the exact functions of individual cell types and ECM in the adult CNS. Astrocytes and microglia produce thrombospondins, extracellular proteases, and growth factors that potentially could alter the routing of axons (Dityatev et al., 2010; Crawford et al.,2012; Frischknecht and Gundelfinger, 2012).

Development of The Visual System from Retina to Brain

The visual system serves as an excellent model for understanding the formation of neural circuits because of its accessibility, anatomy, and role in sensory processing. The development of the visual system has been well characterized, and much of the formation of visual circuitry in the mouse occurs during the first two weeks of postnatal life. The eye is an easily accessible structure for experimental manipulations, and

RGCs provide the sole output from the retina to a plethora of retinorecipient nuclei in the brain. The retinofugal (RF) system, in particular, provides a wealth of knowledge about how RGC axons from the outer limits of the CNS can project long distances, innervate subcortical brain regions, and stop within specific, functionally distinct nuclei to begin synaptogenesis.

RGC extension is the first step in axon pathfinding. Until recently, factors responsible for initiating axon outgrowth have remained elusive due to the inability to examine growth, *in vitro* or *in vivo,* in the absence of neurotrophic factors because neurons die (Goldberg and Barres, 2000). In order to better understand whether intrinsic or extrinsic mechanisms drive axon outgrowth, a mouse model was developed that overexpressed Bcl-2 anti-apoptotic factors, and RGCs were purified and grown in the absence of glial contact (Goldberg and Barres, 2000; Goldberg et al., 2002). Under these conditions, cells were able to survive without trophic factors, but there was no axon outgrowth. Other previously published data on sensory neurons has shown similar findings (Lindsay, 1988; Lentz et al., 1999). The next step was clearly defining the extrinsic factors that could cause outgrowth. Many factors from a wide range of families, including brain-derived neurotrophic factor (BDNF), ciliary neurotrophic factor (CNTF), and oncomodulin, stimulate axon growth both *in vitro* and *in vivo* (Goldberg et al., 2002; Yin et al., 2006).

Axons, once extended from the ganglion cell layer (GCL) in the retina, grow into the optic fiber layer (OFL), and they must navigate away from the periphery towards the optic disc and out of the eye. RGC axonal extension towards the optic cup occurs from embryonic day 11 (E11) to E18 (Drager, 1985). These axons are restricted to the OFL

by a layer of neuroepithelium located just inner to the OFL. The complexities of axonal pathfinding begin at this particular step, as RGC axons that originate from different areas of the retina begin to find their way out. Axons that project ipsilateral, or to the same side of the brain as the eye, originate in the ventrotemporal (VT) crescent of retina, while fibers that project contralateral, or to the opposite side of the brain from the eye, will come from all areas of the retina. These projections do not use the same signaling mechanisms to target CNS nuclei. For example, neuroepithelial endfeet strongly express neural cell adhesion molecules (NCAMs) in rats, like L1-CAM (L1), which allows extension of some pioneer RGC fibers (Brittis and Silver, 1995; Brittis et al., 1995). Axons that follow pioneer RGCs use a different set of molecules to fasciculate and travel with the pioneer axons.

Synaptic targeting requires more than molecular cues to locate distinct cellular partners. The retina also produces spontaneous retinal waves before eye opening at postnatal day 14 (P14) that govern expression of molecular signals and alter the final pattern of innervation within thalamic targets (Chalupa, 2007; Rebsam et al., 2009). Stage 2 waves are the most relevant to the experiments included in this dissertation, and they begin around P0 in mice and last until approximately P10. Stage 2 retinal waves arrive coincident with retinotopic mapping in the CNS, and the waves allow for pruning of weak synapses and the differentiation and maturation of proper synaptic contacts. Retinal waves also help pattern eye specific segregation. These stage 2 waves are generated by starburst amacrine cells, and driven by acetylcholine release from these cells (Feller et al., 1996). They occur relatively infrequently at a rate of one every 1-2 minutes. This frequency was determined to be a driving factor for the eye

specific segregation between projections within the CNS because of the high probability that they would be sending information at alternating times, as opposed to simultaneous transmission (Butts et al. 2007).

Anterograde tracers, utilized long before transgenic mice, allowed insight to the timing of development of retinogeniculate (RG) and retincollicular (RC) projections (Godement et al., 1984). As RGCs innervate their primary targets in subcortical CNS, the complexity of visual circuit formation continues to build as relay neurons from distinct thalamic nuclei project axons to other areas of brain including some projections into primary visual cortex (V1) for higher order processing (Yamada et al.,1996; Van Hooser, 2007; Huberman and Neill, 2011). V1 spreads information to other associated areas of the cortex for further assimilation and processing of perception, as well as feedback circuits to retinorecipient thalamic nuclei.

RGCs are divided into over 20 separate classes which encode information for both image-forming and non-image-forming visual streams. ON-OFF selective RGCs react to increases (ON) or decreases (OFF) in the amount of light presented to the retina, direction selective RGCs respond to horizontal or vertical movement of an object, and other RGCs respond to and transmit information regarding colors (Chalupa and Gunhan, 2004; Demb et al., 2007; Kim et al., 2008; Quina et al., 2005; Schmidt et al., 2011; Badea et al., 2009). These particular classes constitute a subset of the image-forming stream of visual data, and they target CNS nuclei in the thalamus that are important for relaying information to areas of cortex that form perception of the visual scene. Intrinsically photosensitive RGCs (ipRGCs) that contain the photopigment melanopsin also occupy the GCL in the retina, and ipRGCs project primarily within the

non-image forming pathway of visual data to distinct nuclei in the brain that encode information regarding circadian rhythm and irradiance detection (Provencio et al., 2000; Hattar et al., 2002; Hattar et al., 2006). These cell subtypes have become important for understanding how specific guidance cues contribute to class-specific targeting, especially since the project axons to closely apposed, distinct nuclei where differential patterns of guidance cues can be identified and monitored.

Much research regarding RF circuitry in mice focuses on the lateral geniculate nucleus (LGN), which is an important subcortical relay and processing visual center located in the dorsal thalamus. In mice, the LGN contains three separate subnuclei called the dorsal LGN (dLGN), intergeniculate leaflet (IGL), and the ventral LGN (vLGN). The three LGN subnuclei have distinct functions, and they serve as a primary relay center from the retina to other subcortical areas, and, in the case of dLGN, a relay center from retina to V1. Certain image-forming RGC axons will target and primarily innervate the dLGN, while ipRGCs will advance directly to the IGL and vLGN [Figure 2. (Hattar et al., 2006; Kay et al., 2011; Fox and Guido, 2011)].

The timing of RG innervation is stereotypical with pioneer axons innervating the dLGN at E16 (Godement et al., 1984). Advances in anterograde labeling allow for examination of projections from each eye converging or diverging within retino-recipient nuclei. Intraocular injection of cholera-toxin subunit B (CTB) can be used to label retinal projections from each eye [Figure 3. (Muir-Robinson et al., 2002; Jaubert-Miazza et al., 2005)]. This allows visualization of eye specific domains in dLGN (Figure 3). During postnatal visual development, axons from the retina form many synaptic contacts onto relay neurons in dLGN. Initially, the small terminals of these weak synaptic contacts

can be labeled with vesicular glutamate transporter type-2 (VGlutT-2) antibody beginning at P3. VGluT-2 labeling of these synapses also provides insight into the timing of differentiation and maturation of RGC terminals in dLGN as the terminals increase in size until P14. These methods provide evidence that retinal terminals compete for synaptic space, mature and refine during the period of development from P4 until eye opening at P14 [Figure 3, (Guido, 2008)].

Eye-specific refinement of the retinal axons was shown in dLGN beginning around P4 when projections from each eye do not have clear borders (Guido, 2008). At P7, the axon terminals show signs of segregation, but it is not until P14, when eye opening occurs, that each eye occupies clear domain with little or no overlap between the ipsilateral and contralateral projections (Jaubert-Miazza et al., 2005). Retinal waves, a form of spontaneous retina-based activity, have been reported as major contributors to segregation of retinal axons. In addition to retinal activity, the expression profile of certain ephrins and Eph receptors have been shown to drive retinal axon refinement into eye-specific domains [Figure 3. (Pfeiffenberger et al., 2005; Rebsam et al., 2009; Sanes and Zipursky, 2010; Triplett and Feldheim, 2011)]. Recent evidence indicate that ipRGCs, which express melanopsin, the only functional opsin in the retina at birth, react to light and modulate stage 2 retinal waves and contribute to retinal refinement (Renna et al., 2011; Kirkby and Feller; 2013).

In addition to eye specific domains, retinal projections also target specific nuclei topographically, so that neurons that are adjacent in the retina project axons to neighboring neurons in retino-recipient nuclei (Luo and Flanagan, 2007). Utilizing transgenic reporter mice that label only individual classes of RGCs and mutant mice

lacking targeting molecules, multiple visual system targeting mechanisms have been well characterized; for example, gradients of ephrins and Eph receptor help arrange RGC axons in dLGN and superior colliculus (SC) (Feldheim et al., 1998; Hindges et al., 2002; Huberman et al., 2008). Retinal input instructs alignment of topographic maps from V1 and retina in the SC, such that corticocollicular mapping happens after retinocollicular mapping, and retinal input is required for precise mapping and corticocollicular fiber refinement (Triplett et al., 2009). Alignment of topographic maps is deemed necessary for proper visual perception, and this study also revealed the importance retinal activity on non-retinal (ie V1) inputs to retinorecipient thalamic nuclei. Though the thalamic nuclei were originally postulated to serve only as a relay for sensory information travelling to the cortex, recent research suggests that the thalamic nuclei serve much more dynamic roles, such as providing adjustments to retinal input from feedback provided by layer VI cortical neurons (Cudeiro and Sillito, 2006).

Retinal activity and extracellular components can drive the specificity of topographic maps and eye-specific domains within retinorecipient nuclei, but little is known about the mechanisms that affect class-specific targeting to distinct nuclei. The glycoprotein reelin has been shown to guide ipRGCs into the vLGN and IGL (Su et al., 2011). In the absence of functional reelin ipRGC axons fail to innervate the vLGN and IGL, and the ipRGC axons are misrouted to inappropriate thalamic nuclei. Mice that lack Dab1 receptor, a molecule essential for reelin function (Sheldon et al., 1997), also showed misrouting of projections, that usually terminated in vLGN and IGL, towards dLGN (Su et al., 2011). These findings suggest that ECM may play a large part in the axon guidance of both image-forming and non-image-forming pathways.

Much of what has been learned regarding class-specific targeting in visual system has focused only on circuitry between the retina and relay neurons in the thalamus. Moving forward, application of what has been learned through these studies will need to be applied to non-retinal inputs to LGN including axons from brainstem, cortex, reticular thalamic nucleus (RTN) and interneurons which provide 90% of the innervation in LGN and help process retinal signal as it proceeds to cortex.

Interconnectivity in the Thalamus

In addition to RG axons, there are numerous other cell types that innervate dLGN. In fact, RG axons form less than 10 percent of the synapses onto relay neurons, despite being the primary driver for producing synaptic responses in relay neurons (Van Horn et al., 2000). The majority of non-retinal input to dLGN are glutamatergic modulatory synapses that originate from layer VI cortical neurons in visual cortex (Erisir et al, 1997; Jones 2002). Relay neurons are also innervated by local GABAergic interneurons within the dLGN, inhibitory projection neurons from the RTN, and modulatory projections from brainstem and SC (Sherman and Guillery, 2002; Bickford et al., 2010). The development of these non-retinal inputs to the dLGN has not been well characterized because of the difficulty in labeling particular classes of neurons in confined areas of the CNS.

Recent advances in transgenic mouse reporter lines have enabled a more developed study of non-retinal inputs to the dLGN. In particular, the *golli-tau-gfp* mouse, which has layer VI cortical neurons and their projections selectively labeled with green fluorescent protein (GFP), has aided the efficient visualization of how and when

dLGN is innervated by axons from layer VI cortical neurons, also called corticogeniculate (CG) axons (Jacobs et al., 2007; Grant et al., 2012). This reporter mouse line provides an argument for class-specific targeting in cortex, as it is apparent that particular layers of cortical neurons project fibers that innervate specific locations. Layer VI axons have been shown to selectively innervate dLGN, while projections from layer V pyramidal cells also project to the LGN but terminate in vLGN/IGL areas [Figure 4. (Cosenza and Moore, 1984; Jacobs et al., 2007)].

Spatial organization of RG and non-retinal inputs onto distinct relay neurons is important in the formation of neural circuitry. Retinotopic maps begin formation in the LGN prior to afferents from the cortex, RTN, brainstem and interneurons (Bickford et al., 2010). The non-retinal synapses have been reported to provide feed-forward, feedback, and modulatory signals that alter the main stimulus coming from the retina, and they presumably must connect onto relay neurons in register with the correct retinal inputs for faithful image processing and correct behavioral outcomes (Sherman, 2012).

Subcellular specificity is also determined as the visual circuits begin to form during the first week of postnatal life. Excitatory retinal synapses form on proximal dendrites in order to drive action potentials. Inhibitory inputs from local interneurons will receive input from RGCs and form synaptic contacts in close proximity to the RGC / relay neuron interface to help tune the signal provided (Sherman and Guillery, 2002). As mentioned previously, CG synapses form more synapses onto relay neurons, but they innervate distal positions of the dendrites for the production of feedback signaling (Figure 5).

The spatial organization of retinal and non-retinal synapses may be connected with the timing of their entry into dLGN. During dLGN development, RG axons are the first projections to enter the dLGN, and they can synapse onto any area of relay neuron that is available. RG fibers form synaptic contacts onto proximal dendrites of the relay neurons, but it is unclear whether they occupy that particular area because of affinity, because they are the first projections to arrive, or because of a combination of affinity and timing (Sherman and Guillery, 2002).

The timing of CG innervation follows that of RG fibers; importantly, RG fibers begin synaptic differentiation immediately prior to the beginning of layer VI CG axon entry into dLGN (Figure 6). Though CG axons begin to invade dLGN at P4, synaptic contacts marked by vesicular glutamate transporter-1 (VGluT-1) do not begin to appear in the dLGN until P7 [Figure 6, (Seabrook et al., 2013)].

Probing the Role of Retinal Activity and Molecular Guidance on Layer VI Cortical Projections to dLGN

Recent studies using the *golli-tau-gfp* mouse have demonstrated that retinal inputs may play an instructive role in regulating the timing of CG innervation. Specifically, RG axons begin synaptic remodeling in dLGN prior to CG fiber entry, and removal of retinal input by enucleation or genetic ablation accelerates layer VI cortical innervation in dLGN (Seabrook et al., 2013). This suggests that retinal input to dLGN may be providing a stop signal that inhibits non-retinal innervation of dLGN until RG synapses have begun to function.

In light of this work, the goal of my project was to discover the molecular mechanisms that regulate the timing of CG axon innervation. As mentioned previously, there must be a balance of activity and guidance factors working to provide the perfect environment for proper synapses to form; however, little is known about molecular mechanisms that guide non-retinal inputs in the thalamus. Here I report that the inhibitory CSPG, aggrecan, is robustly expressed in the dLGN during early visual circuit formation. I sought to classify its function and regulation during this phase of development. Based on the preliminary data and the coincident delay of CG innervation of the dLGN, I hypothesized that aggrecan initially repels layer VI cortical projections from entering dLGN until proper synapses form between RGCs and relay neurons in the dLGN.

Little is known regarding mechanisms that drive how and when the CG afferents invade dLGN, but my studies support a novel role for aggrecan in the timing of layer VI CG innervation. Not only have I established a new role for aggrecan, but I also provide evidence detailing the cascade of events that mediate aggrecan distribution in postnatal dLGN. My results indicate that retinal inputs alter relay neuron expression of aggrecanases. Taken together, these experiments describe the dynamic interplay of retinal activity and molecular signaling in the establishment of layer VI innervation in dLGN.

Figure 1: Axon guidance in the CNS. (A) The blue cell projects a growth cone that responds to different extracellular cues to grow an axon to the appropriate target area. Cells secreting chemospecific attractive molecules (green) drive the initial direction of axon outgrowth. A guidepost cell, which contains inhibitory contact-mediated cues, causes the growth cone to turn, while complementary attractive and inhibitory chemospecific guidance cues push and pull the growth cone to its final target area. (B) Inhibitory cues cause the growth cone to avoid the red cell completely and search for more appropriate targets. Attractive chemospecific cues allow the growth cone to extend towards the dendrites located on the black cell, where the first steps of synaptogenesis can begin. The green cell may contain attractive elements within its dendrites, but it has not been targeted by the growth cone due to a lack of extracellular cues. Many of the same molecules that drive axon guidance over long distances can also guide the axons toward specific cells.

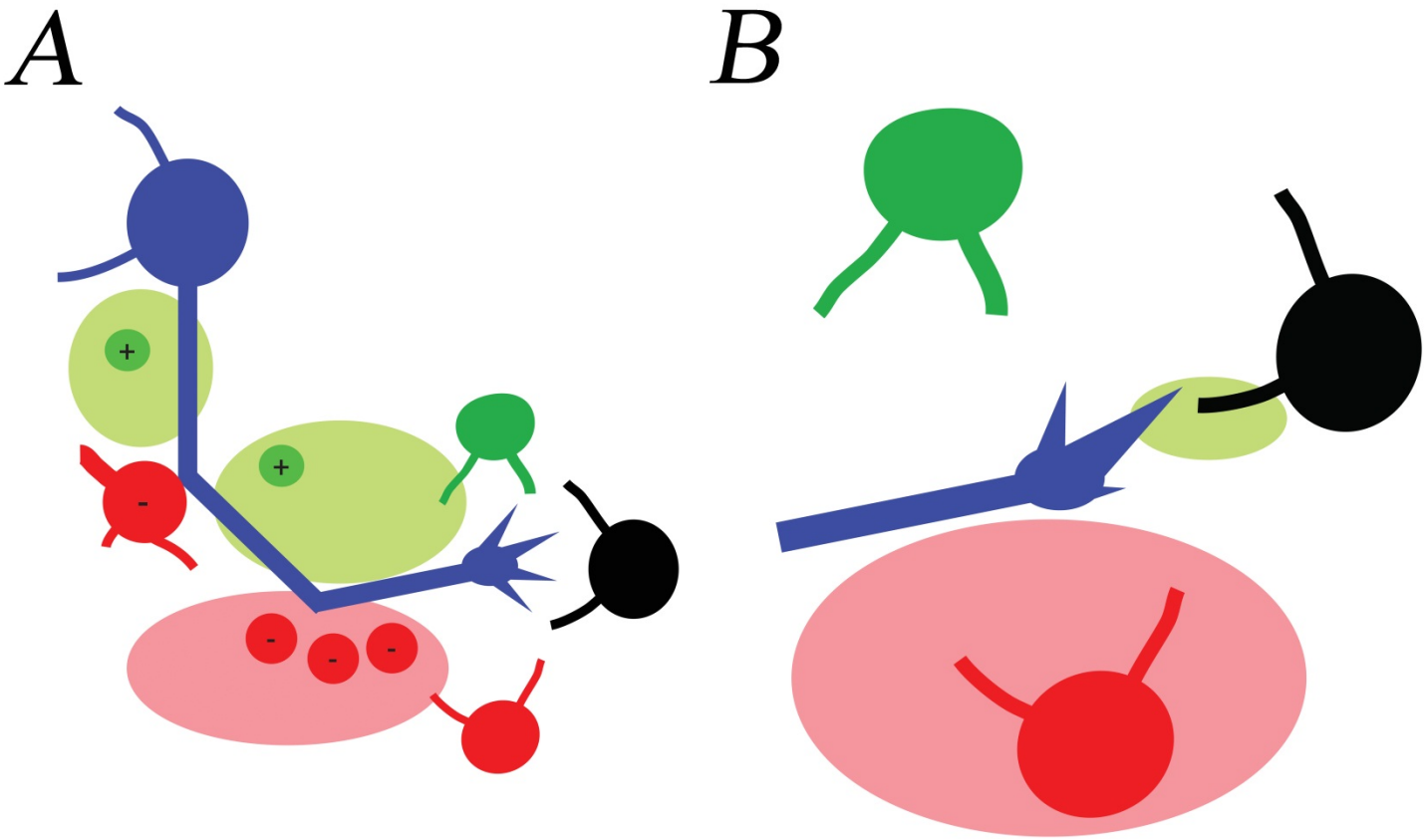
A
B
+
+
-
-
-
-

Figure 2: Class-Specific RG Targeting in LGN. RGCs project axons long distances and innervate visual nuclei in the brain. Different classes of RGCs project to distinct retino-recipient nuclei in LGN. For example, image-forming classes of RGCs (green) project to dLGN, whereas non-image forming classes of RGCs innervate vLGN and IGL.

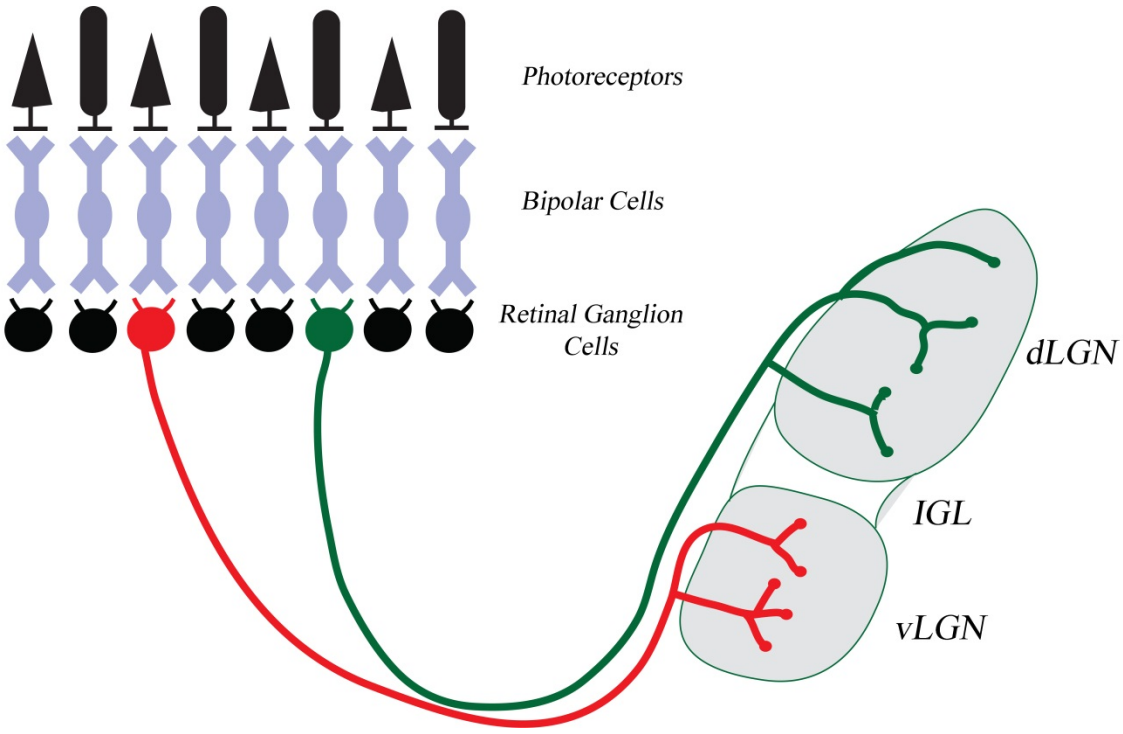
Photoreceptors
Bipolar Cells
Retinal Ganglion Cells
dLGN
IGL
vLGN

Figure 3: Eye-specific segregation and maturation of retinal terminals during the first two weeks of postnatal visual development. Top panel: CTB, conjugated to Alexa-fluor 594 (red), labels contralateral retinal axons in dLGN, and CTB, conjugated to alexa-fluor 488 (green) labels retinal axons from the ipsilateral eye. The images illustrate dLGN innervation by retinal axons from each eye at P3, P7, P10, and P14. Bottom Panel: Immunostaining with VGlutT-2 shows the maturation of retinal synapses from synaptogenesis at P3 until maturation at P14. Scale bar is 250 µm.

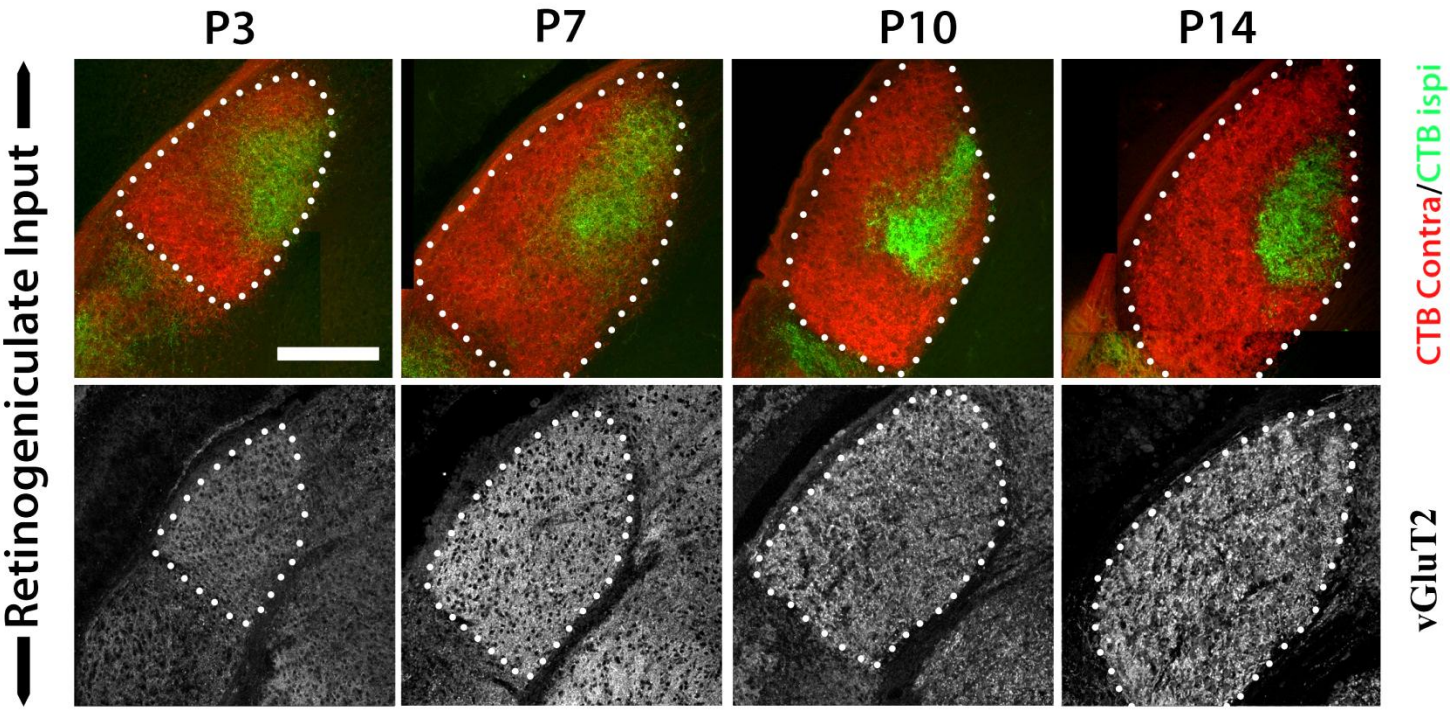
P3
P7
P10
P14
Retinogeniculate Input
CTB Contra/CTB ispi
vGluT2

Figure 4: Class-Specific CG Targeting in LGN. Cortical neurons are separated into distinct laminae, much like retinal reurons (Figure 2). Neurons in layers V and layer VI of cortex project axons to nuclei within the thalamus. In LGN, axons from layer V pyramidal cells (red) target vLGN, while axons from layer VI project to dLGN.

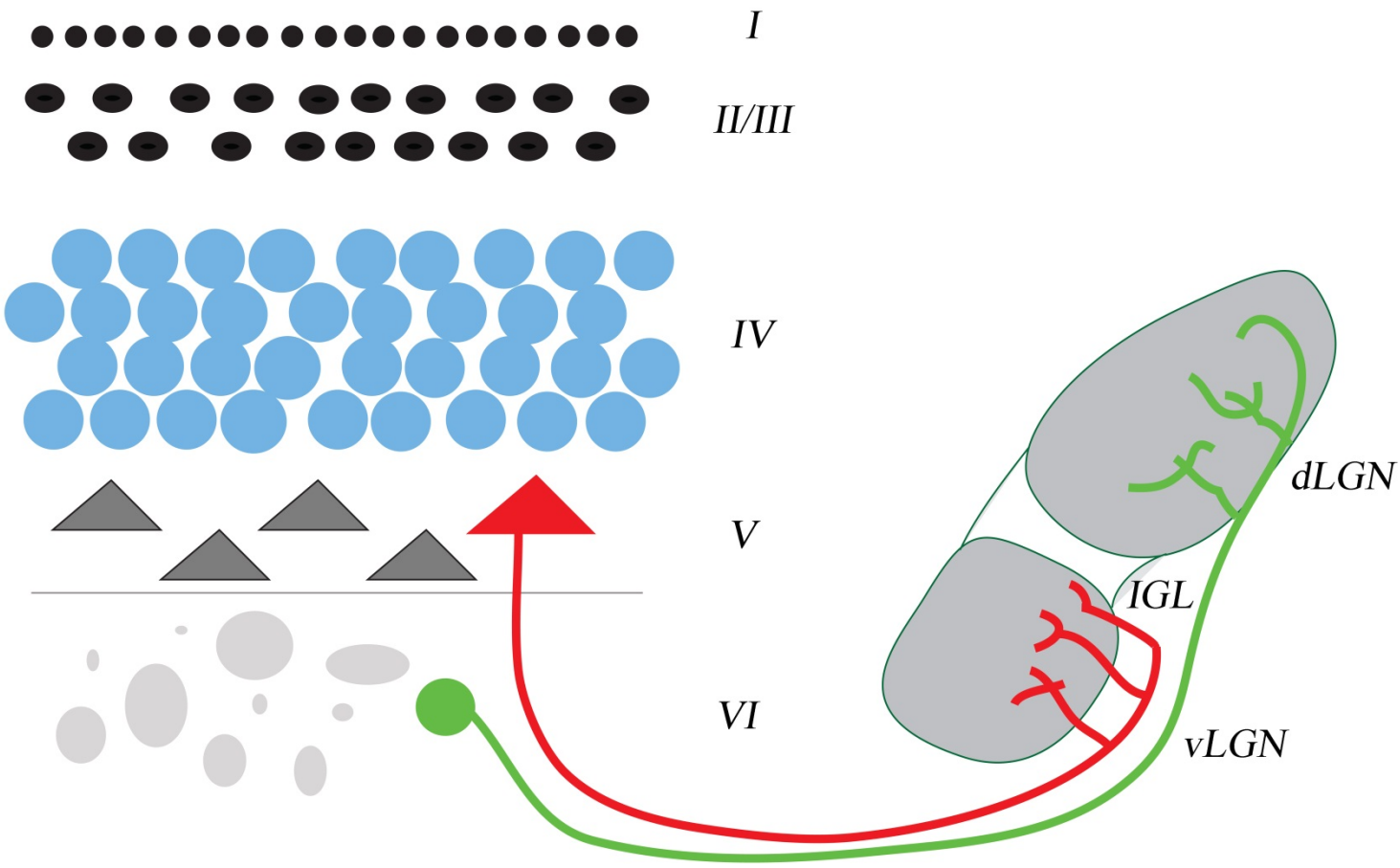
I
II/III
IV
V
VI
dLGN
IGL
vLGN

Figure 5: Schematic depicting the subcellular distribution of inputs onto relay neurons in dLGN. Retinal inputs (grey) are the primary drivers of relay neurons in dLGN and are located on proximal dendrites of relay neurons. Inhibitory and modulatory synapses from interneurons (Red) and brainstem (Blue), respectively, occupy proximal positions on dendrites and typically provide more inputs than RGCs. Inhibitory interneurons are also innervated by retinal axons to provide modulatory feed-forward inhibition of the signal. Inhibitory synapses from RTN (Purple) axons are positioned distal to RGC, interneuron, and brainstem projections. Feedback input from layer VI cortical axons are also numerous, but they generally are located on the distal dendrites of relay neurons. [(+) denotes excitatory glutamatergic inputs, (-) denotes inhibitory GABAergic inputs, and (m) denotes modulatory acetylcholinergic input].

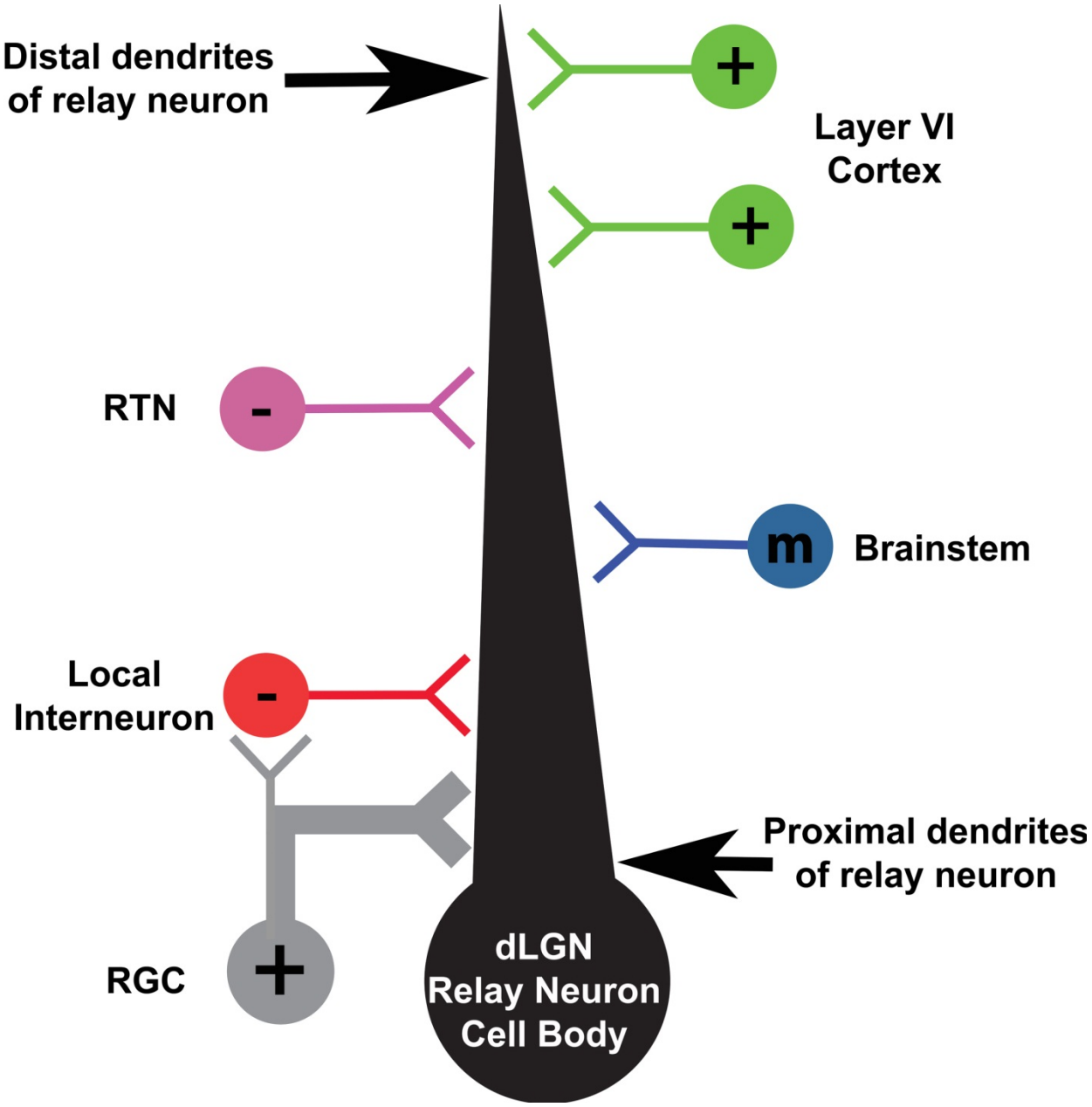
Distal dendrites
of relay neuron
+
Layer VI
Cortex
+
RTN
-
m
Brainstem
Local
Interneuron
-
Proximal dendrites
of relay neuron
RGC
+
dLGN
Relay Neuron
Cell Body

Figure 6: CG innervation and synapse labeling during the first two weeks of postnatal development. Top Panel: GFP-immunoreactivity (IR) in the *golli-tau-gfp* mouse reveals the timing of layer VI cortical fiber innervation in dLGN from P3 – P14. Bottom Panel: Immunostaining using VGlut-1 reveals the timing of synapse development between layer VI CG axons and relay cells. Scale bar is 250 µm.

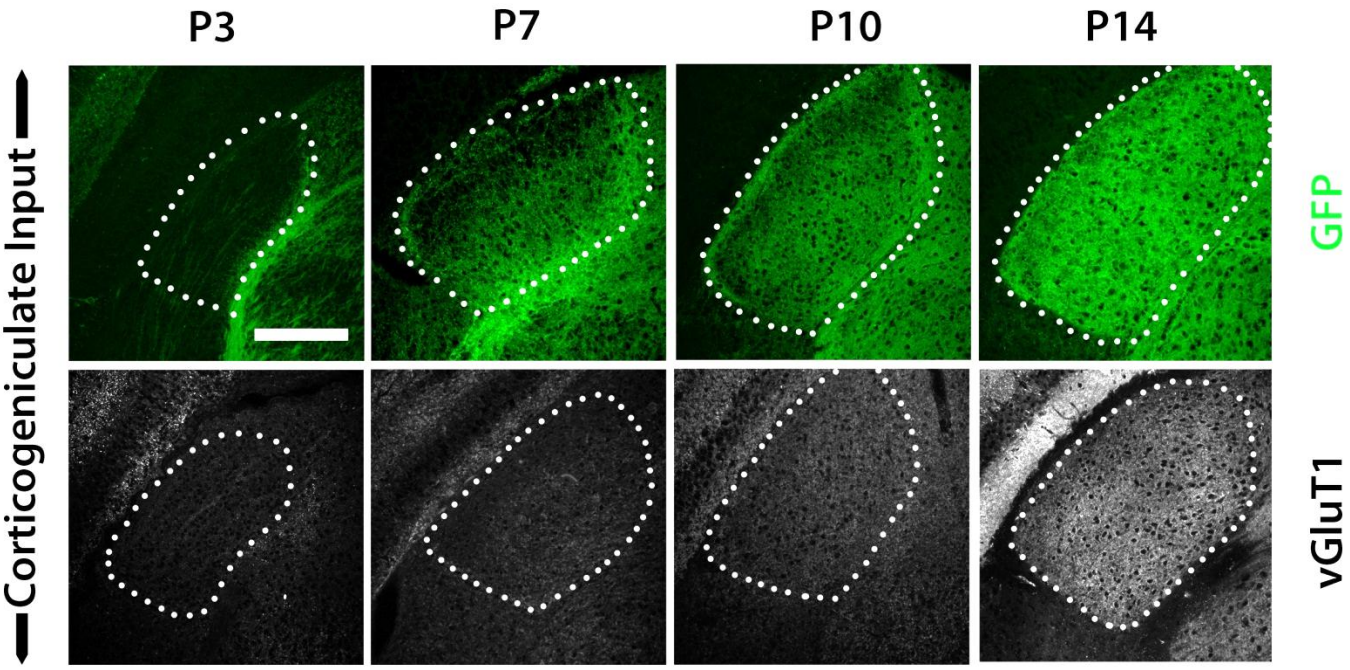
P3
P7
P10
P14
Corticogeniculate Input
GFP
vGluT1

Chapter II

Experimental Methods

Mice

CD1 and C57/BL6 wild-type mice were purchased from Charles River (Wilmington, MA) or Harlan (Indianapolis, IN). *acan*^{cmd} heterozygous mice which lack functional aggrecan, were purchased from The Jackson Laboratory (Bar Harbor, ME). The generation of *math5*$^{-/-}$ and *golli-tau-gfp* mice were described previously (Wang et al., 2001; Jacobs et al., 2007). Genomic DNA was isolated from tails using the HotSHOT method as previously described (Truett et al., 2000; Su et al. 2010) and genotyping was performed with the following primers purchased from Integrated DNA Technologies (Coralville, Iowa): *math5,* ATG GCG CTC AGC TAC ATC AT and GGG TCT ACC TGG AGC CTA GC; *neomycin (neo)*, GCC GGC CAC AGT CGA TGA ATC and CAT TGA ACA AGA TGG ATT GCA; *gfp*, AAG TTC ATC TGC ACC ACC G and TCC TTG AAG AAG ATG GTG CG; *cmd*, CCA TCT CCT CAG CGA AGC AG and CTA CAA GGA CAG TGA CTT TG. The following conditions were used for genotyping: *math5,* 35 cycles using a denaturation temperature of 94ºC for 30 seconds, annealing at 59ºC for 30 seconds, and elongation at 72ºC for 45 seconds; *neo*, 35 cycles using a denaturation temperature of 94ºC for 30 seconds, annealing at 56ºC for 30 seconds, and elongation at 72ºC for 45 seconds; *gfp,* 35 cycles using a denaturation temperature of 94ºC for 30 seconds, annealing at 55ºC for one minute, and elongation at 72ºC for one minute; *acan*^{cmd}, 32 cycles using a denaturation temperature of 94ºC for 15 seconds, annealing at 58ºC for 20 seconds, and elongation at 72ºC for one minute.

Further treatment of *acan*^{cmd} polymerase chain reaction (PCR) products using BpmI restriction endonuclease (New England Biolabs, Ipswich, MA) was performed according to previous reports (Watanabe et al, 1997). All analyses conformed to National Institutes of Health guidelines and protocols approved by the Virginia Polytechnic Institute and State University and Virginia Commonwealth University Institutional Animal Care and Use Committees.

Antibodies

The following antibodies were purchased: mouse anti-phosphacan (3F8) (Developmental Studies Hybridoma Bank, University of Iowa; 1:100 dilution); rabbit anti-GFP (Invitrogen, Grand Island, NY; 1:250 dilution), mouse anti-chondroitin sulfate proteoglycan protein core epitope (cat315) (Chemicon, Temecula, CA; 1:2000 dilution), anti-mouse/rat neurocan (R&D systems, Minneapolis, MN; 1:50 dilution), rabbit anti-mouse versican (GAG alpha domain) polyclonal antibody (Millipore, Billerica, MA; 1:500 dilution), mouse anti-brevican (BD Biosciences, San Jose, CA; 1:500 dilution), rabbit anti-VGluT-1 (Synaptic Systems, Goettingen, Germany; 1:500 dilution), rabbit anti-VGluT-2 (Synaptic Systems, 1:500 dilution), rabbit anti-glial fibrillary acidic protein (GFAP; DAKO, Carpinteria, CA; 1:2500 dilution), rabbit anti-ionizing calcium-binding adaptor 1 (Iba-1; WAKO, Richmond, VA; 1:500 dilution), monoclonal mouse anti-neuronal nuclei (NeuN; Chemicon 1:200 dilution). Fluorescently conjugated secondary antibodies were purchased from Invtirogen (1:1000 dilution).

Immunohistochemistry (IHC)

IHC was performed as previously described (Su et al. 2010, 2011). After mice were transcardially perfused with phosphate-buffered saline (PBS; pH 7.4) and 4% paraformaldehyde in PBS (PFA; pH 7.4), brains were removed and post-fixed in PFA for 12 hours at 4°C. Brains were cryopreserved in 30% sucrose solution for 24 hours, embedded in Tissue Freezing Medium (Electron Microscopy Sciences, Hatfield, PA), and cryosectioned (16–20 μm coronal sections). Sections were air-dried onto Superfrost Plus slides (Fisher Scientific, Pittsburgh, PA) before incubating in blocking buffer [2.5% bovine serum albumin (BSA), 5% Normal Goat Serum (NGS, 0.1% Triton-X in PBS for at least 30 minutes]. Primary antibodies were diluted in blocking buffer and incubated on the tissue sections for >12 hours at 4°C. After washing in PBS, fluorescently conjugated secondary antibodies diluted 1:1000 in blocking buffer were incubated on sections for 1 hour at room temperature. After thorough washing in PBS, sections were stained with 4',6-diamidino-2-phenylindole [(DAPI) 1:10,000 in water] and were mounted with Vectashield (Vector Laboratories, Burlingame, CA). For versican-IHC, tissue sections were digested with chondroitinase ABC (chABC; 0.01U/ml in blocking buffer [Sigma, St Louis, MO]) for >30 minutes at 37°C prior to incubating with blocking buffer. Images were acquired on a Zeiss AxioImager A2 fluorescent microscope, a Zeiss Examiner Z1 LSM710 confocal microscope or a Zeiss LSM 700 confocal microscope. When comparing different ages of tissues or between genotypes, images were acquired with identical parameters. A minimum of three animals (per genotype and per age) were compared in all IHC experiments. Spatial coverage of dLGN by aggrecan and GFP-labeled layer VI fibers was examined using threshold analysis as described previously (Jaubert-Miazza et al., 2005). Briefly, acquired images

were cropped after background fluorescence was subtracted and grayscale images were normalized using Adobe Photoshop. dLGN was encircled and isolated from optic tract, vLGN/IGL and medial thalamus. The image was then binarized using a threshold value of 50 in order to distinguish signal from background fluorescence. Total pixels in dLGN were calculated, as were the total number of pixels representing fluorescent signal (Jaubert-Miazza et al., 2005). Area of coverage was calculated by dividing signal area/total area of dLGN in 3-4 dLGN samples representing the middle of the dLGN. Plot profiles were obtained using imageJ software. Images were imported into imageJ software and a line scan was analyzed using the plot profile command. Data was exported into Microsoft excel where displacement distances were converted to µm. Fluorescent intensities represent averages for every three pixels (1.8 µm) for each image over the first 50 µm displacement into dLGN, and data was plotted in a line graph for images collected from n≥3 animals.

Dissociated Cortical Cultures

Cerebral cortices were dissected from E15-E18 *golli-tau-gfp* embryos and were digested in 0.25% trypsin at 37°C for 15 min. Following digestion, soybean trypsin inhibitor was used to inactivate trypsin and cortical tissue was transferred to serum-free medium (Neurobasal medium with 0.5mM L-Glutamine, 25 uM L-Glutamate, 10ug/ml Gentamicin with B27 supplement). A single cell suspension was generated by triturating tissues through a 1000ul pipette tip and $5x10^3$ cells were added to each well of a poly-L-lysine (PLL) treated 8-well lab-Tek chamber slide. In addition to being pre-treated with PLL, chamber slides were “spotted” with various extracellular substrates to assess

neurite outgrowth. Briefly, various concentrations (1 µg/ml, 5 µg/ml and 10 µg/ml) of aggrecan (Sigma), chABC or recombinant human A Disintegrin and Metalloproteinase with Thrombospondin Motifs- type-4 (rhADAMTS4, R&D Systems) were mixed with BSA conjugated to Alexa-Fluor 594 (Invitrogen) (2 µg/ml) and 2µl spots were placed onto the slide surface in separate chambers and allowed to incubate in a humidified chamber at 37 °C for two hours. The ability of chABC or rhADAMTS4 to degrade aggrecan was assessed by pre-incubating 10 µg/ml aggrecan with 50U/ml chABC in PBS or 10 µg/ml rhADAMTS4 before mixing with BSA- Alexa-Fluor 594. After plating, cortical neurons were cultured for 3 days at 37°C in 5% CO_2 before being fixed with 4% PFA (in PBS) and imaged. Layer VI neurons (and their neurites) were immunolabeled with anti-GFP antibodies and I counted the numbers of neurons whose neurites were able to grow into the "spotted" substrates. Only neurites from cell bodies that lie within 50 µm of the spot of interest were counted. A minimum of four experiments (each with at least 3 replicates) was compared in all *in vitro* experiments.

Fluorescent In Situ Hybridization (FISH)

FISH was performed on 16–20 µm cryosectioned coronal sections as described previously (Su et al. 2010, 2011). Sense and anti-sense riboprobes were generated against *syt1*, *adamts4* and *adamts15 (*Image Clone ID *syt1*: 5363062; *adamts4*: 5345809; *adamts15:* 30619053; Open Biosystems, Huntsville, AL). Riboprobes were synthesized using digoxigenin- (DIG) or fluorescein-labeled uridylyltransferase (UTP) (Roche, Mannheim, Germany) and the MAXIscript *in vitro* Transcription Kit (Ambion, Austin, TX). Riboprobes were hydrolyzed into ~0.5 kb fragments. Coronal brain

sections were prepared and hybridized as described previously (Yamagata et al. 2002; Fox and Sanes 2007). Bound riboprobes were detected by horseradish peroxidase (POD)-conjugated anti-DIG antibodies and fluorescent staining with Tyramide Signal Amplification (TSA) systems (PerkinElmer, Shelton, CT). For double FISH (D-FISH), after the first TSA reaction sections were washed in Tris-buffered saline (TBS), incubated in 0.3% H_2O_2 for 30 min, and reacted with the second POD-conjugated antibody. Images were obtained on a Zeiss AxioImager A2 fluorescent microscope or a Zeiss Examiner Z1 LSM710 confocal microscope. A minimum of three animals per genotype and age was compared in FISH experiments.

RNA isolation, Microarray, and quantitative Real-Time Polymerase Chain Reaction (qPCR)

LGN subnuclei were isolated from P3 and P8 vLGN and IGL (vLGN/IGL) or dLGN. Mice were decapitated, brains were removed and 400 µm coronal sections were cut in ice-cold diethylpyrocarbonate-treated PBS (DEPC-PBS) with a vibratome. vLGN/IGL or dLGN were micro-dissected and tissues from at least 5 littermates were pooled per sample. RNA was isolated using the BioRad Total RNA Extraction from Fibrous and Fatty Tissue kit (BioRad, Hercules, CA). For microarray analysis, RNA purity assessment, first and second strand cDNAs preparation, cRNAs generation, hybridization to Agilent Whole Genome 44k×4 mouse arrays, and data analysis with Agilent Feature extraction and GeneSpring GX v7.3.1 software packages were performed by GenUs Biosystems (Northbrook, IL). To be considered differentially expressed genes must have been 2-fold higher in the averaged sample sets (n=3,

$p<0.05$). 3 samples were analyzed per region. For qPCR, RNA was purified from pooled samples isolated from P2, P3, and P7 in both *math5*$^{-/-}$ and *golli-tau-gfp* vLGN/IGL or dLGN as described above. cDNAs were generated with Superscript II Reverse Transcriptase First Strand cDNA Synthesis kit (Invitrogen, La Jolla, CA). qPCR was performed on a Chromo 4 Four Color Real-time system (BioRad) using iQ SYBRGreen Supermix (BioRad) as described previously (Su et al. 2010) or the Step One Plus Real-Time PCR System (Applied Biosystems) was used with the GoTaq qPCR Master Mix (Promega). The following primer pairs were used: *actin,* TTC TTT GCA GCT CCT TCG TT and ATG GAG GGG AAT ACA GCC C; *acan,* CCC TCA GAG TCA CAA AGA CCA and TTC GCA GGG ATA AAG GAC TG; *adamts4*, GTC ATG GCT CCT GTC ATG G and CCG GTT TGT CTA AGA GGC AG; *adamts8*, ATC ACC GTG AGG ATG TGG TT and CAA GAG GTT TGT GTC CGA GG, *adamts9,* TGT GGT GTT GGA GTG ATG CAG AGA and TCT GGC TTC AGA TCA GTG TGG CAT; *adamts15,* ACA CTG CCA TCC TCT TCA CC and TCT TGG GGT CAC ACA TGG TA; *adamts19,* CCT CTT TCA GCA CCT GTG GA and GTG CGG GTG ACC TAT GAT G; *gapdh,* CGT CCC GTA GAC AAA ATG GT and TTG ATG GCA ACA ATC TCC AC; *lhx9*, TCT TGC AAG GGG AAT ATC CA and GTG CCA GTG CCA TTG AAG TA; *dlx1*, CTT AGC TCT GCC TGA GAG GG and ACT TGG AGC GTT TGT TCT GG. The following cycling conditions were used with 20 ng of RNA: 95°C for 15 minutes, followed by 40 cycles of amplification (94°C for 15 seconds, 60°C for 20 seconds, 72°C for 20 seconds, read plate) and a melting curve analysis on the on the Chromo 4 Four Color Real-time system. Step One Plus Real-Time PCR System used a different program: 95°C for 2 minutes, followed by 40 cycles of amplification (95°C for 3 seconds, 60°C for 30 seconds, read plate) and a

melting curve analysis. Relative quantities of RNA were determined using the ΔΔ-CT method (Livak and Schmittgen, 2001). A minimum of n=3 experiments (each in triplicate) was run for each gene, at each age examined and, to be considered differentially expressed, genes must have been 2-fold higher in the averaged sample sets (n=3, $p<0.05$). Each individual run included separate actin or Glyceraldehyde-3-Phosphate Dehydrogenase (GAPDH) control reactions.

Intrathalamic Injections and Analysis of Corticogeniculate Spatial Innervation

P0-P1 *golli-tau-gfp* mice were anesthetized by hypothermia and injected stereotactically through the skull using a glass pipette and the Picospritzer (5 msec at 8 PSI) with either 0.05 U/μl chABC (Sigma), 0.05 U/μl penicillinase [(PNase) Sigma] or 10 μg/mL rhADAMTS4 (R&D systems). Two injections, one near rostral dLGN (~3.7 mm caudal to the olfactory bulb) and one near caudal dLGN (~4.7 mm caudal to the olfactory bulb) were placed in dorsomedial thalamus ~1.0 mm from midline in order to preserve cytoarchitecture and minimize trauma to dLGN. Two days post injection, mice were euthanized, perfused, and tissue prepared for cryosections or vibratome. Spatial extent of innervation by GFP labeled fibers was calculated using the threshold analysis method described above.

Retinal Projection Labeling

Intraocular injection of CTB conjugated to Alex Fluor 488 or Alexa Fluor 594 (Invitrogen) was performed as described previously (Su et al. 2010). Briefly, mice were anesthetized by hypothermia (<P7) or by isoflurane (>P7). The sclera was pierced with

a glass pipette and excess vitreous humor was extracted. Another pipette containing CTB (0.1 – 0.2%) was reinserted into the previous hole and CTB, using Picospritzer and a prescribed volume (1-3 µl at P0-P10 and 3-5 µl for ages >P10) of solution, was injected into the eye. After 1-2 days mice were killed, and brains fixed in 4% PFA solution for 1 day, and brains were cryopreserved in 25% sucrose solution for 1 day. 16 µm coronal sections were cut using a cryostat or 40 um coronal sections were attained using a vibratome. In mice that die perinatally or for posthumous retinal projection labeling, the lens of the eye was opened and vitreous humor removed. Lipophilic DiI [1,1'-dioctadecyl-3,3,3',3'-tetramethylindocarbo-cyanine perchlorate (Sigma)] crystals were placed into the cavity in close contact with the retina. The heads were submerged in PFA and incubated at 37°C for ~6 weeks. Brains were prepared for coronal sectioning using the vibratome. Images of DiI-labeled retinal projections to the brain were taken on the same day as slides are prepared. Images were obtained on a Zeiss AxioImager A2 fluorescent microscope or a Zeiss Examiner Z1 LSM710 confocal microscope.

Chapter III

Developmental Regulation of Aggrecan

Introduction

CG fibers comprise up to 50% of the innervation to relay neurons, constituting one of the largest sources of input to the dLGN (Erisir et al, 1997; Jones, 2002). Afferents from layer VI cells in visual cortex project directly to dLGN and help shape signaling by relay neurons through tuning of receptive field properties and influencing RG signal transmission (Sherman and Guillery, 2002). The mechanisms driving layer VI cortical innervation of dLGN have been difficult to characterize due to the vast number of synapses and lack of tools that distinguish between cell types; however, the generation of the golli-*tau-gfp* transgenic reporter mouse line has improved the ability to investigate early development of CG projections. In the *golli-tau-gfp* transgenic reporter mouse, layer VI soma and processes are selectively labeled with a tau-GFP fusion protein whose expression is driven by the golli promoter of the gene encoding myelin basic protein (Landry et al., 1998; Xie et al., 2002).

Cortical projections, in these animals, traverse from the internal capsule and begin invading the thalamus by P0. While these layer VI afferents innervate dorsal thalamic nuclei immediately, the dLGN remains devoid of layer VI projections until P4 [Figure 6 (Jacobs et al., 2007; Grant et al., 2012)]. The timing of CG axon entry coincides with the remodeling of retinal axons and appears to be orchestrated by RG inputs (Seabrook et al. 2013). Due to the delay in CG innervation, I proposed a mechanism by which extracellular guidance cues prevent premature innervation of

dLGN by layer VI GFP-expressing axons, a process which appears to be regulated by retinal inputs.

Identification of aggrecan localized in dLGN during cortical axon "waiting"

To identify guidance cues localized in dLGN, I initially profiled the transcriptome of P3 and P8 dLGN, with the assumption that mRNA of repulsive cues inhibiting premature CG innervation would be down-regulated as cortical axons began to enter dLGN. No such molecules were identified (data not shown). As an alternative approach I applied a candidate screen for CSPGs in neonatal dLGN. Many members of the lectican family of CSPGs have been characterized as inhibitory to outgrowth of axons (Kwok et al. 2008; Zimmerman and Dours-Zimmerman 2008); therefore, I sought to determine the distribution of 5 prominent CNS CSPGs in LGN: brevican, neurocan, versican, phosphacan and aggrecan.

Brevican, neurocan, versican, and phosphacan protein levels were detected at low levels in LGN at P0, but each had a different expression pattern in the thalamus (Figure 7). Brevican-IR was detected in areas dorsomedial to the dLGN, while neurocan-IR was very low in dLGN. Plot profiles were obtained using line scans along the vetrolateral-dorsomedial axis of LGN to examine the intensity of IR signal in each of the three areas of LGN. Plot profiles measuring brevican and neurocan-IR in vLGN and dLGN showed little signal, indicating presence of small amounts or no protein in these areas. Versican-IR was present on the retinal axons in the optic tract and in tracts traveling through the dLGN. The line scans of versican-IR indicated considerable signal but little difference between levels in vLGN and dLGN. Phosphacan had an interesting

pattern of IR, and it appeared graded from high levels of vLGN and IGL expression to low levels in dLGN (Figure 7).

In contrast to other lecticans, aggrecan-IR was significantly elevated in the neonatal dLGN and other areas of dorsal thalamus compared to both its own levels in vLGN/IGL and the IR of the other CSPGs in the dLGN. Plot profiles illustrated the magnitude of the aggrecan signal localized in dLGN compared to the low levels in the vLGN (Figure 7).

Aggrecan is a bulky ECM proteoglycan composed of multiple functional domains. The N-terminal globular domain (G1) can associate with other proteins to form large aggregates of extracellular matrix, hence the name aggrecan. G1 is followed by an interglobular domain (IGD). The chondroitin sulfate (CS) domain located towards the C-terminal end of the aggrecan molecule was considered the signaling domain (Figure 8). The CS domain was discovered to be the repellant domain of functional aggrecan, and specific CS-glycosaminoglycan (GAG) patterns have been reported to alter neurite extension *in vitro* at levels comparable to intact aggrecan (Gilbert et al., 2005). Combined with my initial aggrecan-IR results, these reports led me to investigate the relationship between the timing of aggrecan expression in dLGN and the profile of CG innervation.

Aggrecan expression during visual development

For my hypothesis to be correct, aggrecan distribution must be reduced either through lower transcription, translation, or some other type of regulatory element as layer VI cortical fibers begin to invade dLGN after P4. I conducted experiments to

determine if *acan* mRNA transcription was diminished during the first postnatal week in the *golli-tau-gfp* mouse dLGN by generating cDNAs for qPCR analysis from dissected dLGN during development. The resulting pattern of expression from P2 to P14 was contradictory to my hypothesis, indicating a steady increase in *acan* mRNA during visual circuit formation; however, they were complementary to the general pattern of *acan* mRNA expression the CNS (Figure 9A).

mRNA expression levels are not directly correlated to translation events or protein levels, but there have been reports in the literature that, during development in rodents, the antibody I used to specifically label aggrecan, cat315, also labels certain isoforms of phosphacan (Dino et al., 2006). Thus, I was inclined to examine cat315 antibody specificity, especially after reviewing the qPCR data. First, the cat315 antibody did not label the phosphacan in the vLGN in my initial search for an inhibitory guidance cue (Figure 7). Next, I tested the validity of my previous observations by immunostaining embryonic sections of brain, using cat315, from the autosomal recessive mouse mutant that lacks functional aggrecan, called the acan^{cmd} mouse (Watanabe et al., 1994). Aggrecan-IR was abolished in the brains of these mice, and these results confirmed that IR observed in the WT (wild type) dLGN at P0 is unique to aggrecan (Figure 9B inset).

After I ensured the specificity of cat315 binding to aggrecan, I probed dLGN with cat315 later during development, when axons from the layer VI GFP-labeled cortical fibers in the *golli-tau-gfp* mouse were beginning to invade dLGN, to determine if aggrecan was still present. My results showed that aggrecan was degraded throughout

the dLGN by the time that CG projections spanned the entire dLGN and VGLuT-1 labeled cortical synapses began to appear (Figure 9B; Figure 6).

Aggrecan signal degraded prior to CG fiber entry into dLGN

Aggrecan's structure has been well established, and its functions regarding plasticity and regeneration in the CNS have been characterized, but the role of aggrecan during visual circuit formation was unknown. As I performed a daily analysis of CG innervation and aggrecan, from P0 when axons began to arrive at dLGN until P7 when axons occupy nearly 50% of dLGN, I began to uncover an important developmental role for aggrecan in the orchestration of RG and CG circuitry using the *golli-tau-gfp* mouse line. At P0 when aggrecan-IR was most intense, pioneer CG axons began to enter ventral thalamus from the internal capsule, and they started to climb the external medullary lamina (eml) toward dLGN. However, they appeared to pause and wait in eml just medial to the dLGN, and, for several days, they innervated other nuclei of dorsal thalamus but not dLGN (Figure 10).

Aggrecan-IR covered the entire extracellular area of dLGN until P1 when the IR signal appeared graded with aggrecan loss beginning at the ventromedial border of dLGN and proceeding laterally. CG axons coincidentally remained outside of dLGN during the period of time when aggrecan-IR was high, and CG fiber innervation was inversely-correlated with the area occupied by aggrecan. Furthermore, CG fibers only innervated the portions of dLGN at P4 where aggrecan-IR was nearly undetectable, which led me to hypothesize that aggrecan regulates the timing of layer VI cortical axon innervation in dLGN (Figure 10).

Potential Role for retinal input in the regulation of aggrecan

A recent report analyzed the effects of retinal input on the timing of CG innervation in dLGN, using the *math5*$^{-/-}$ mutant mouse line, which lacks 95% of RGCs (Seabrook et al., 2013). That study also included binocular enucleation as a method for destroying retinal inputs, and their observations led to the declaration that removal of retinal inputs accelerates CG innervation. In order to confirm the lack of retinal innervation in dLGN of *math5*$^{-/-}$ mutants, I used DiI, a lipophilic tracer, to label RGCs and their afferents in different aged animals. WT mice exhibited distinct labeling in the brain where retinal processes were located, but the *math5*$^{-/-}$ mutants contained no DiI labeling at any age, suggesting that retinal input to the brain was completely absent (Figure 11). By crossbreeding the *math5*$^{-/-}$ mutants to the *golli-tau-gfp* reporter mice, I was able to probe the hypothesis that aggrecan protein must be significantly reduced by the removal of retinal input to dLGN at perinatal ages in order for layer VI fibers to exhibit accelerated entry into dLGN.

I analyzed the spatiotemporal distribution of aggrecan by examining IR in the *math5*$^{-/-}$ mouse line. Although innervation by layer VI fibers had not yet begun at P0, aggrecan-IR was substantially reduced in the perinatal mouse, and aggrecan was degraded in the same manner as the *golli-tau-gfp* with signal loss at the medial border of dLGN and increased IR towards the lateral edge (Figure 12A). By P1, aggrecan-IR had been substantially reduced towards the lateral edges of dLGN; coincidentally, layer VI fibers began to enter the dLGN at this early age in the absence of retinal inputs. By P2, cat315 signal could no longer be observed throughout most of dLGN except the far

lateral edges near the optic tract, and CG fibers had begun extending across the dLGN. By P3 aggrecan-IR only covered ~5% of the dLGN and layer VI CG axons were observed to innervate significantly more area of dLGN compared with *golli-tau-gfp* mice (Figure 12 B). P1-P3 images of *math5*$^{-/-}$ mutants illustrate the principle that GFP-labeled layer VI fibers only enter the dLGN and extend to portions where aggrecan-IR is minimal (Figure 13). At ages P4 – P7, aggrecan proteoglycan expression remained nearly undetectable within dLGN, and the CG fibers continued to move laterally across the dLGN spanning 80% of dLGN by P7 (Figure 12).

We compared the spatial extent of dLGN coverage by aggrecan-IR and GFP-IR in both the *golli-tau-gfp* and the *math5*$^{-/-}$ animals. Statistical analyses of both models validated the observations that aggrecan protein levels diminished during postnatal development and CG fibers only entered the dLGN where aggrecan protein coverage was sufficiently low. P0 mice had the highest levels cat315 labeling in both *golli-tau-gfp* and *math5*$^{-/-}$mice, but the *golli-tau-gfp* mice showed more uniform high intensity signal across the entire dLGN, while *math5*$^{-/-}$ mice already had significantly diminished aggrecan levels in the ventromedial dLGN. Aggrecan-IR was apparent in only 40% of the dLGN in *math5*$^{-/-}$ mice compared to the 80% in *golli-tau-gfp* tissue (Figure 14). At P1, cat315 signal in *math5*$^{-/-}$ mice only appeared in less than 25% of dLGN and in some mice, CG axons could innervate dLGN. At P1, CG axons in *golli-tau-gfp* mice remained arrested in the eml, and aggrecan-IR covered 70% of dLGN. At P2, aggrecan in the *golli-tau-gfp* animals decreased sharply with IR presented only over 40% of dLGN; however, the *math5*$^{-/-}$ mouse line exhibited extremely low aggrecan-IR with only 5-10% coverage of dLGN. The low levels of aggrecan throughout dLGN made for a permissive

environment into which CG axons could begin innervation in all *math5*$^{-/-}$ mice. By P3, aggrecan levels had decreased dramatically and layer VI cortical fibers in the *golli-tau-gfp* mouse began to project slightly out of eml into dLGN, but the *math5*$^{-/-}$ model had a significant increase in the area of dLGN covered by layer VI fibers which correlated with the early degradation of aggrecan. P3 also represented the age at which both aggrecan and GFP-IR showed significantly different levels between *golli-tau-gfp* mice and *math5*$^{-/-}$ mice. At subsequent ages, aggrecan levels continued to recede in the *golli-tau-gfp* mice, while the CG fibers continued to innervate the dLGN until P14. From P4 to P7, the *math5*$^{-/-}$ line had a much quicker cortical fiber progression and significantly more dLGN area innervated. 80% of the dLGN was covered by GFP-containing fibers at P7 in the *math5*$^{-/-}$ animals (Figure 14). Taken together, these data suggested that high levels of aggrecan in dLGN repel layer VI CG projections into dLGN.

Conclusions

Aggrecan was present at perinatal ages in high concentrations in dLGN and likely serves as an inhibitor of layer VI GFP-expressing axons that approach the dLGN. Although transcription of aggrecan increased during postnatal development, the signal of aggrecan-IR decreased within the dLGN suggesting that it must be regulated either at a translational level or by other molecules in CNS. Aggrecan-IR was inversely correlated with the invasion of dLGN by CG fibers in both *golli-tau-gfp* and the *math5*$^{-/-}$ mouse models. These data strongly support a role for aggrecan in the inhibition of layer VI axon invasion of dLGN, and they implicate retinal input in the regulation of aggrecan.

Figure 7: Aggrecan protein is enriched in perinatal dLGN. Immunostaining in dLGN of five different CSPGs: brevican, neurocan, versican, phosphacan, and aggrecan. Plot profiles accompanying each image indicate fluorescent intensities of IR in individual pixels as measured with a line scan along the ventrolateral to dorsomedial axis of LGN (see dashed line in brevican image). Grey lines represent IR in separate animals, and the black line depicts the mean of all grey lines (n=4). Plots were divided to show fluorescent intensities as the line scan transitions from vLGN to dLGN. Scale bar is 250 µm. dLGN are encircled with white dots

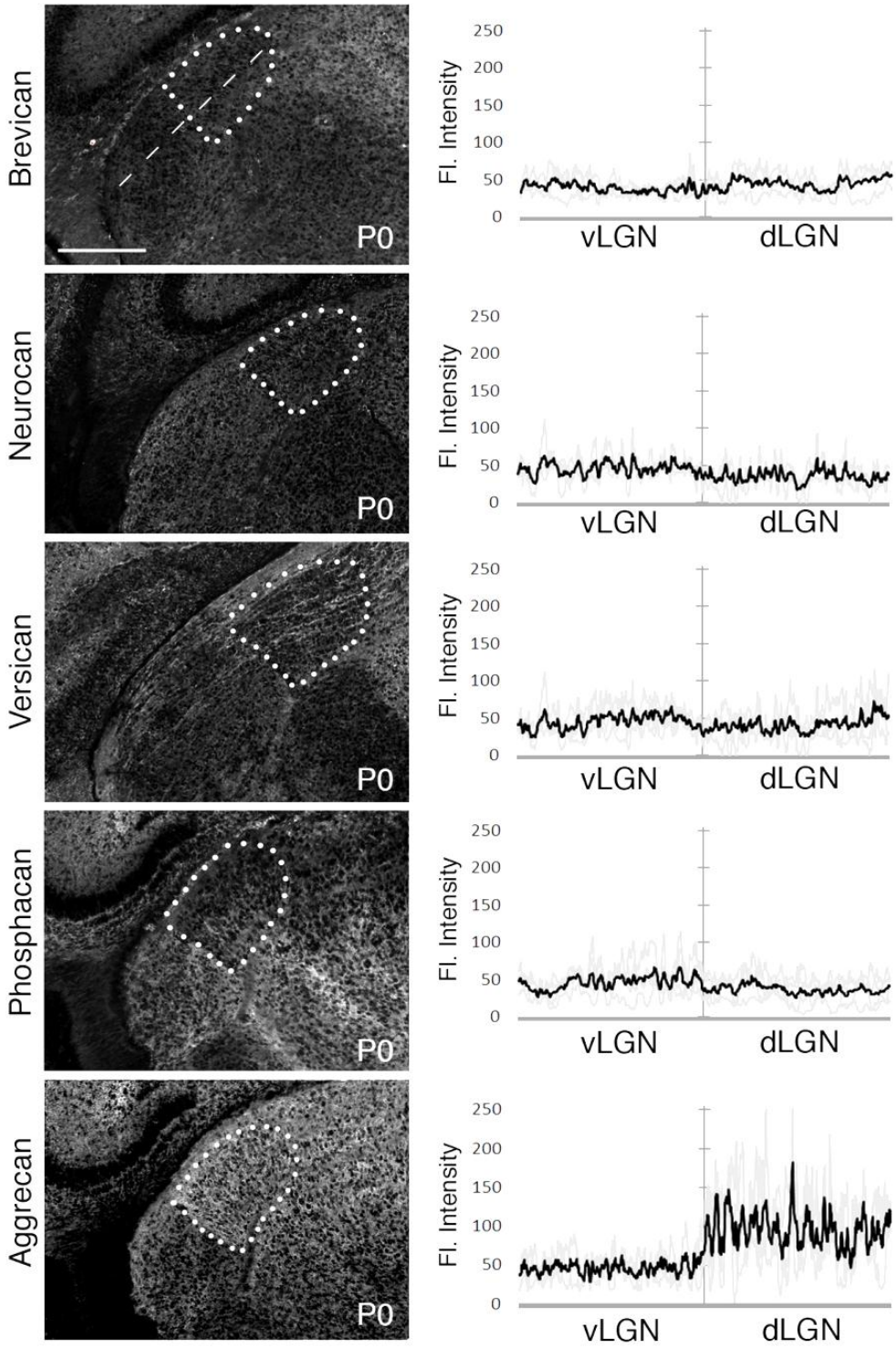
Brevican
Neurocan
Versican
Phosphacan
Aggrecan
P0
Fl. Intensity
250
200
150
100
50
0
vLGN
dLGN

Figure 8: Schematic of domains in aggrecan protein. Aggrecan is a bulky ECM protein that is composed of multiple functional domains. The N-terminal globular domain (G1) associates with hyaluronan and link proteins to form large aggregates of extracellular matrix, hence the name aggrecan. G1 is followed by the IGD, and the second globular domain (G2) has unknown function but is conserved across species for the aggrecan protein. Following G2 is a short length of protein containing keratan sulfate glycosaminoglycans chains (KS-GAGs), which precedes a long section of unfolded protein attached to CS-GAGs (Aspberg, 2013). The CS domain is reported to be the repellant domain of functional aggrecan, as specific CS-GAG patterns have been reported to alter neurite extension *in vitro* at levels comparable to intact aggrecan (Gilbert et al., 2005). Finally, the C-terminal globular domain (G3) associates with other ECM molecules to function in the organization of ECM (Aspberg, 2013).

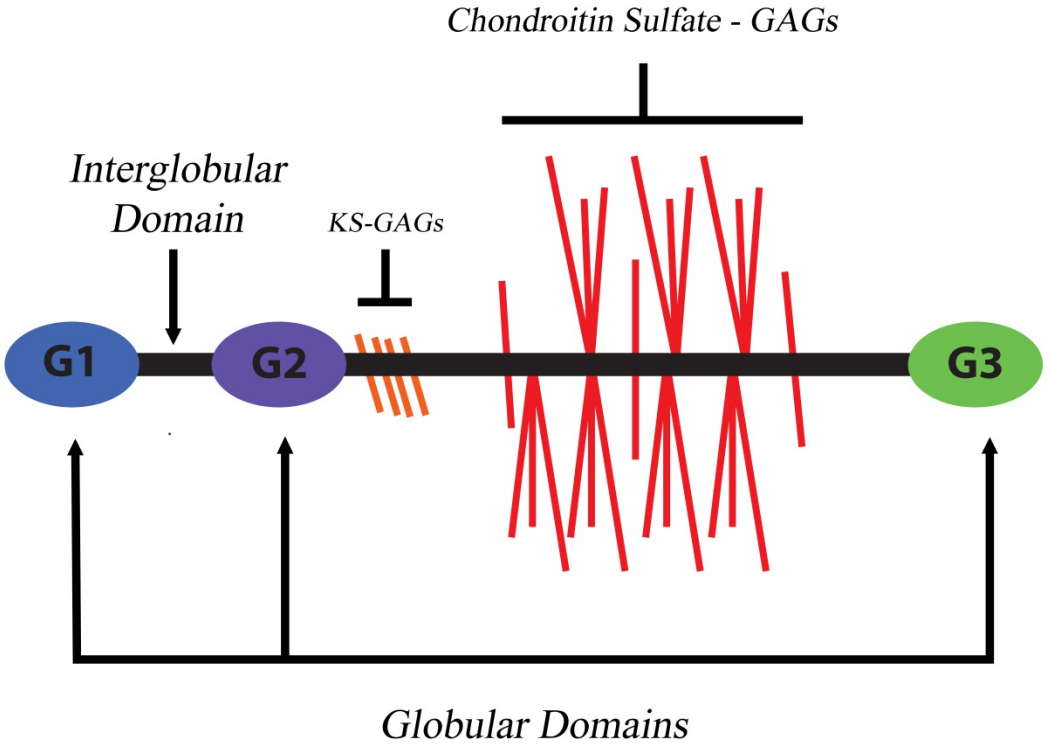
Chondroitin Sulfate - GAGs
Interglobular Domain
KS-GAGs
G1
G2
G3
Globular Domains

Figure 9: Developmental regulation of aggrecan during the first two weeks of postnatal development. (A) qPCR results illustrating increased aggrecan mRNA expression in dLGN during visual system development. Error bars in qPCR data are +/- standard deviation (SD) (B) . Immunostaining using the antibody cat315, specific for aggrecan, depicting the dramatic decline of aggrecan-IR from P0 to P10. Inset shows lack of aggrecan-IR in dLGN of *acan*^{cmd} mouse. Scale bar in B is 250 µm.

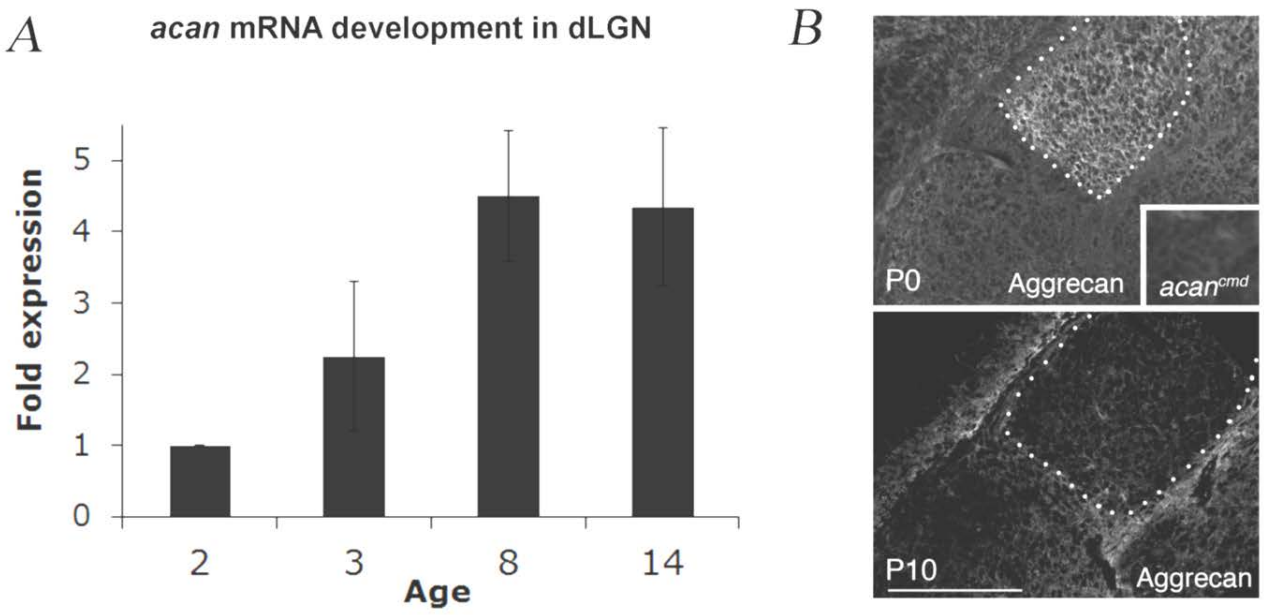
A
acan mRNA development in dLGN
Fold expression
0
1
2
3
4
5
2
3
8
14
Age
B
P0
Aggrecan
acan^cmd
P10
Aggrecan

Figure 10: Decreased aggrecan-IR coincides with layer VI CG axon innervation in *golli-tau-gfp* mice. (A) Immunostaining using antibodies to label aggrecan (top) and layer VI GFP-containing axons (middle) in *golli-tau-gfp* tissue from P0 – P7. Bottom row contains merged images of aggrecan (red) and CG fibers (green) to illustrate the lack of colocalized signal and coincident timing of layer VI dLGN innervation with aggrecan loss. dLGN are encircled by white dots. Scale bar is 200 μm. (B) The percentage of dLGN occupied by aggrecan-IR was measured in *golli-tau-gfp* transgenic mice for the first 8 days of postnatal development. The percentage of cortical innervation in these mice was also quantified. Error bars are shown +/- standard error of the mean (SEM).

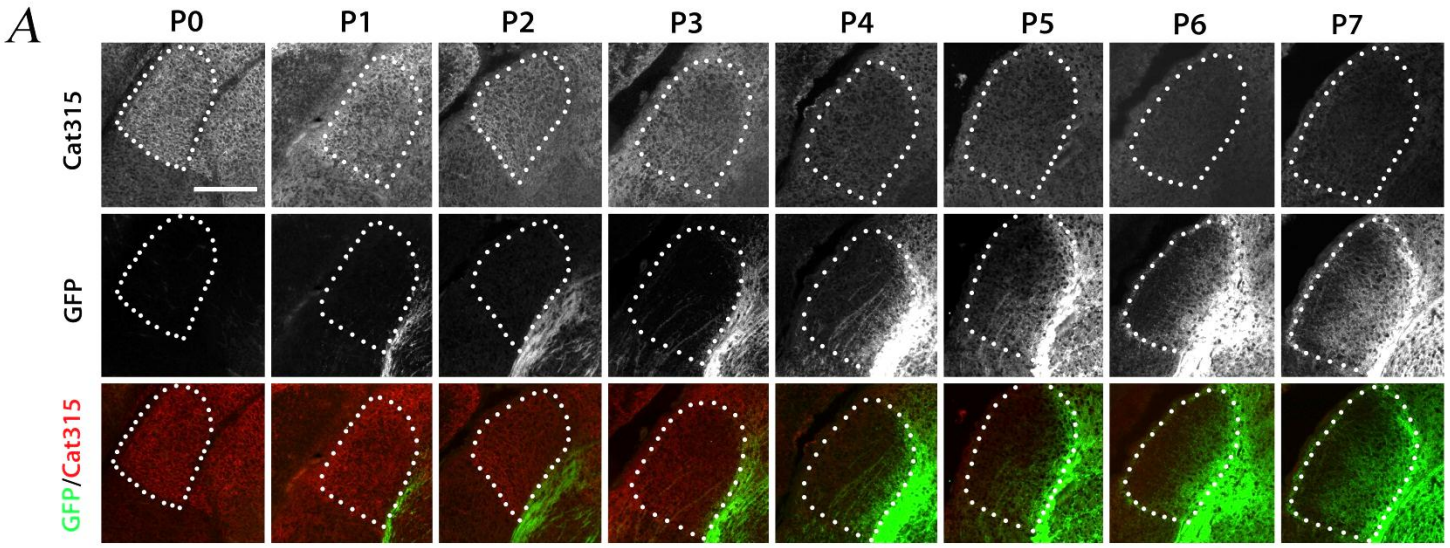
A
P0
P1
P2
P3
P4
P5
P6
P7
Cat315
GFP
GFP/Cat315

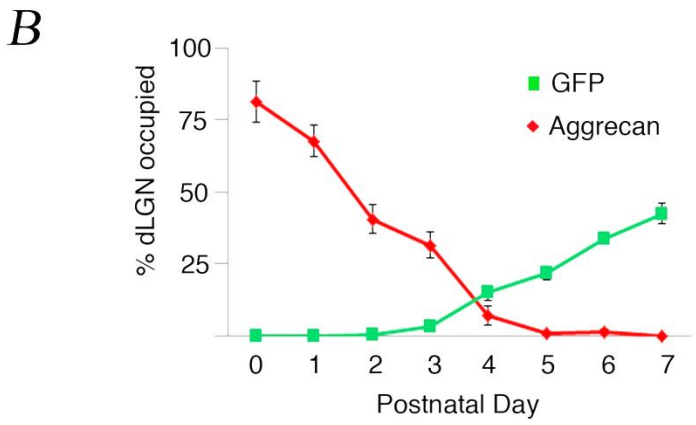
B
100
75
50
25
% dLGN occupied
GFP
Aggrecan
0
1
2
3
4
5
6
7
Postnatal Day

Figure 11: M*ath5*$^{-/-}$ mutants lack RGC innervation to LGN. Labeling of LGN in WT and *math5*$^{-/-}$ mouse lines using DiI. WT mouse (Left) labeling depicting robust fluorescent signal in the optic tract and dLGN, while the *math5*$^{-/-}$ mice (Right) lack labeling due to genetic ablation of RGCs. Scale bar is 250 µm. dLGN are encircled with white dots.

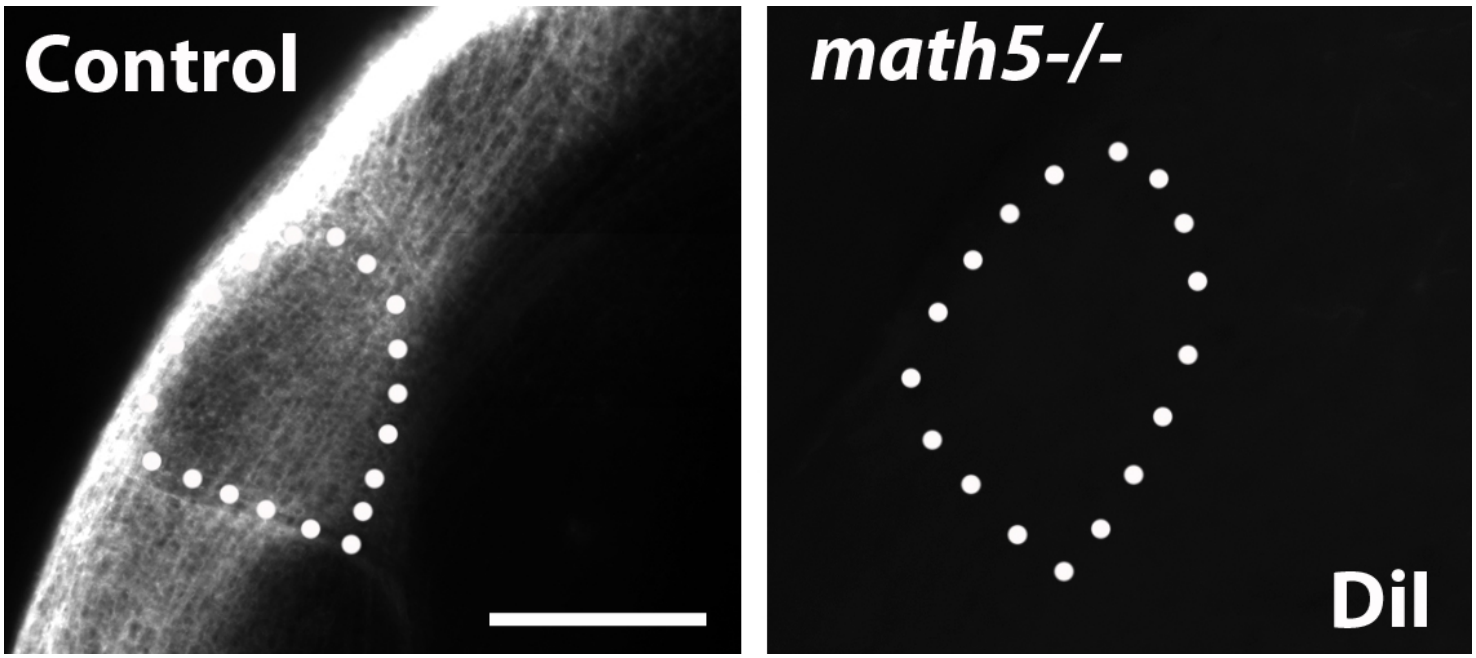
Control
math5-/-
DiI

Figure 12: Aggrecan loss in dLGN is accelerated in *math5*$^{-/-}$ mice. (A) Immunostaining using antibodies to aggrecan (top) and layer VI GFP-containing axons (middle) in *math5*$^{-/-}$tissue from P0 – P7. Bottom row contains merged pictures with aggrecan (red) and CG fibers (green) to illustrate the coincident timing of layer VI dLGN innervation with aggrecan degradation. dLGN are encircled by white dots. Scale bar is 200 µm. (B) The percentage of dLGN occupied by aggrecan-IR was measured in *math5*$^{-/-}$ transgenic mice for the first 8 days of postnatal development. The percentage of cortical innervation in these mice was also quantified. Error bars are shown +/- SEM

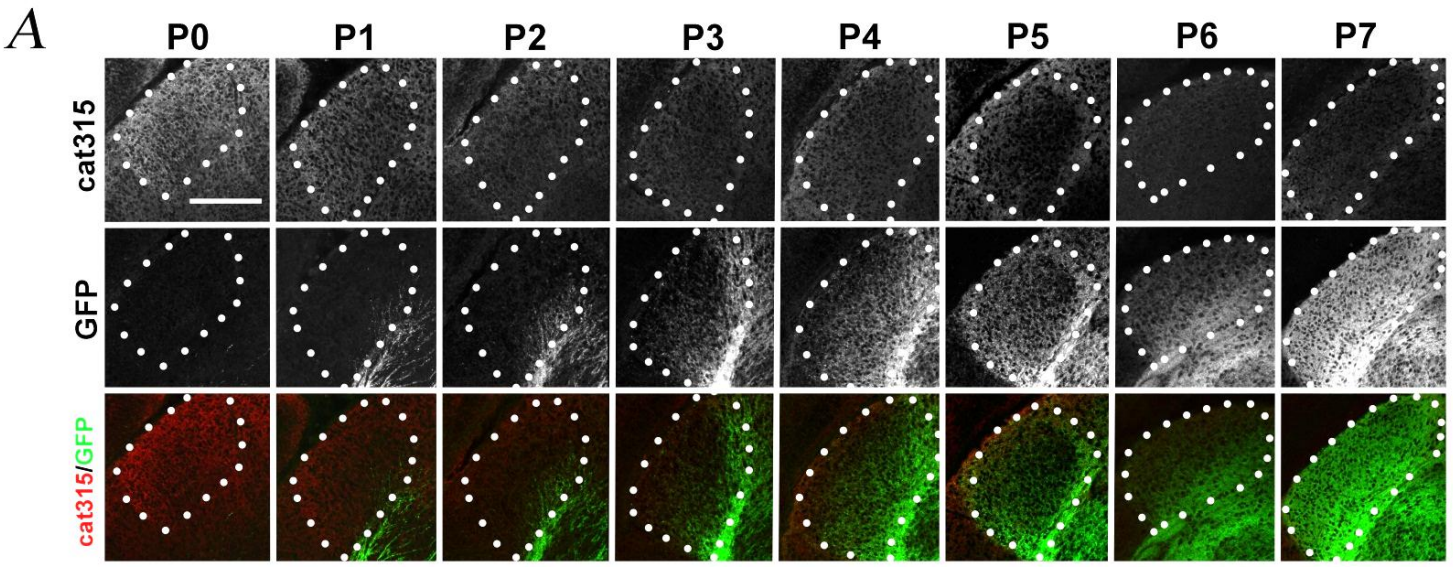
A
P0
P1
P2
P3
P4
P5
P6
P7
cat315
GFP
cat315/GFP

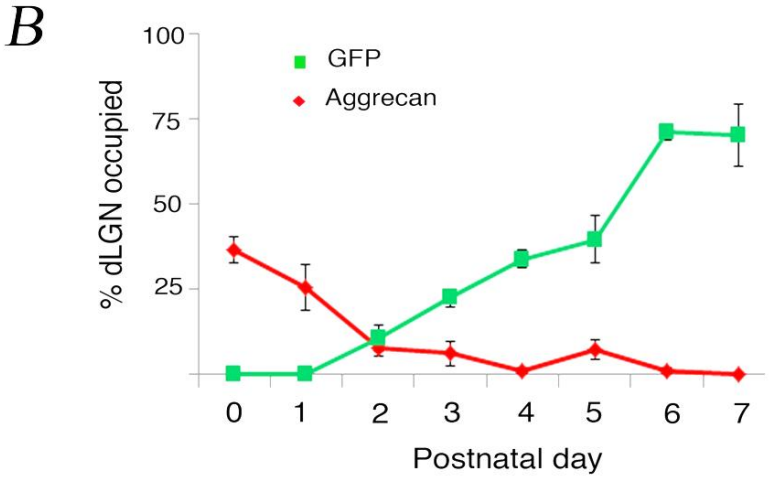
B
100
75
50
25
% dLGN occupied
GFP
Aggrecan
0
1
2
3
4
5
6
7
Postnatal day

Figure 13: Layer VI fibers enter dLGN where aggrecan-IR is lowest. P1-P3 enlarged images from the *math5*$^{-/-}$. Arrowheads depict the remaining aggrecan-IR in the lateral aspect of dLGN. Arrows highlight GFP-labeled axons prematurely invading dLGN. Note the absence of aggrecan in areas of cortical axon invasion. dLGN are encircled by white dots. Scale bar = 100 µm.

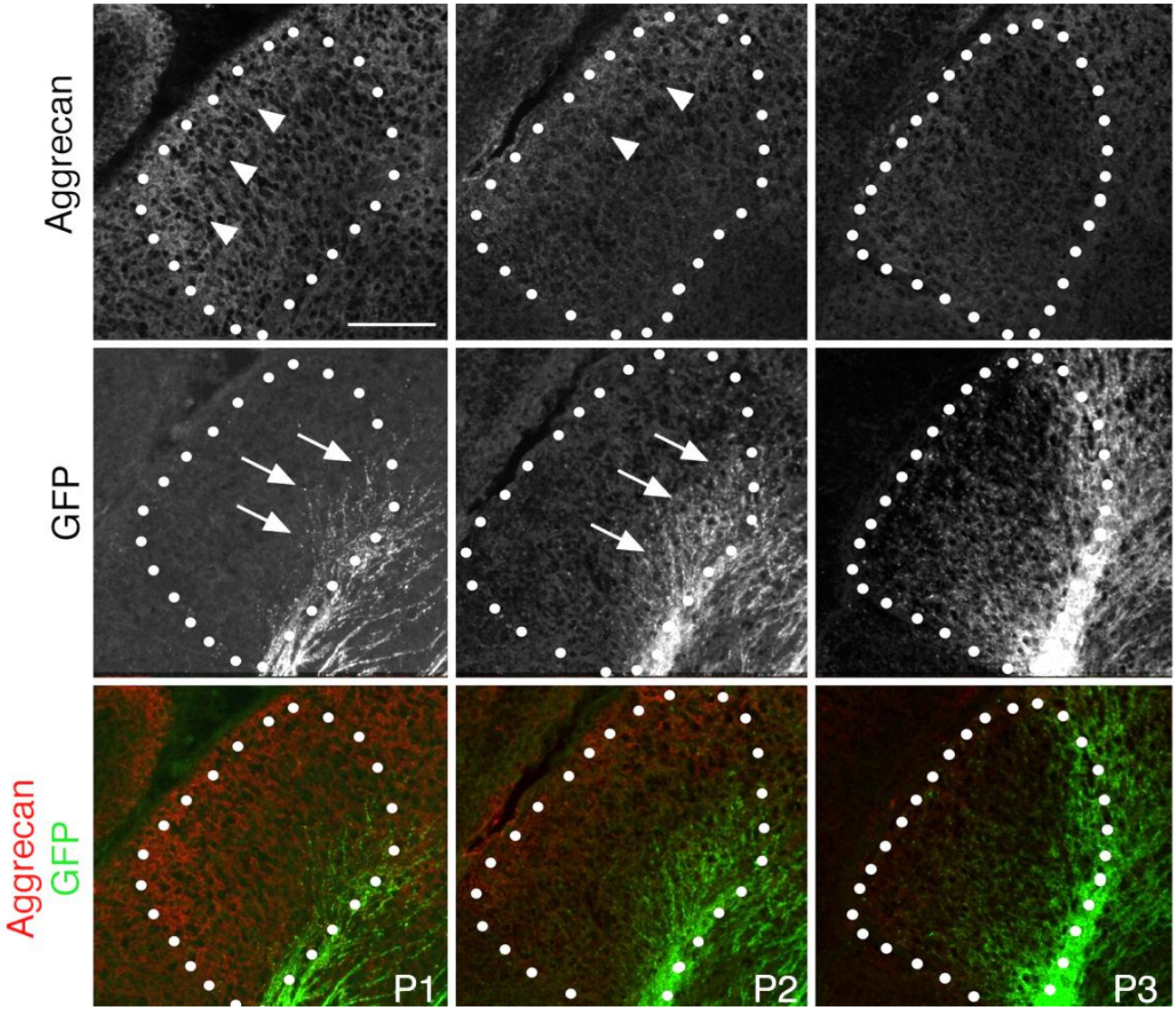
Aggrecan
GFP
Aggrecan
GFP
P1
P2
P3

Figure 14: Retinal Inputs influence the loss of aggrecan in dLGN. The % dLGN occupied by tau-GFP expressing axons (top graph) or by aggrecan-IR (bottom) was compared in *math5*$^{-/-}$ mutants and *golli-tau-gfp* controls. Error Bars are +/- SEM. * denotes a difference with statistical significance of $p<.01$ by Tukey-Kramer test.

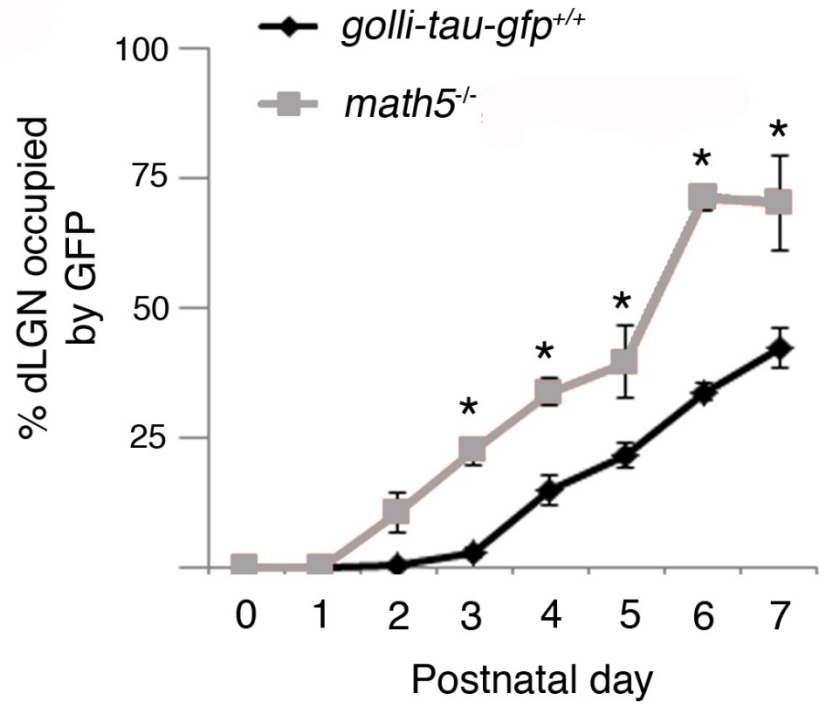
golli-tau-gfp+/+
math5-/-
% dLGN occupied by GFP
100
75
50
25
0
1
2
3
4
5
6
7
Postnatal day
*

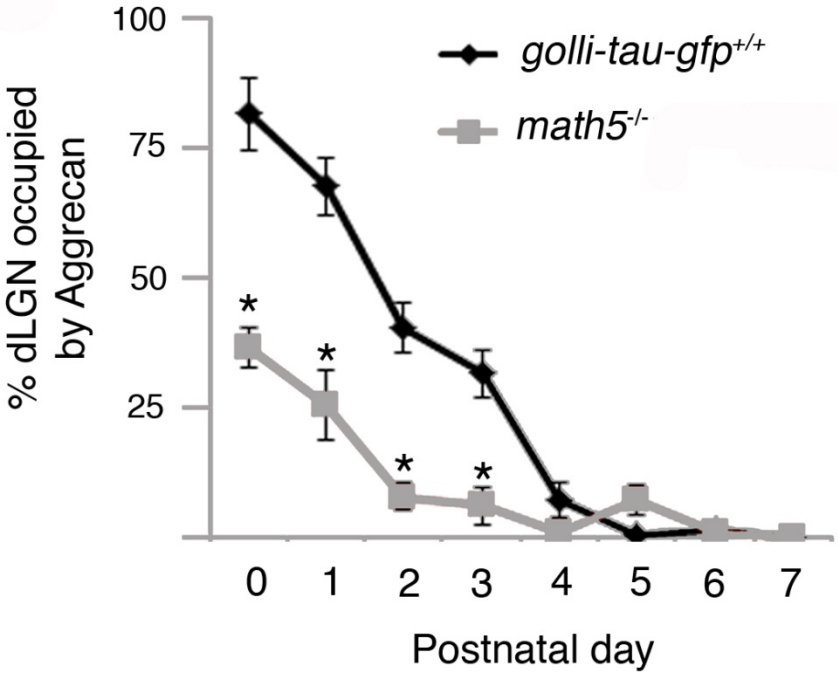
golli-tau-gfp+/+
math5-/-
% dLGN occupied by Aggrecan
100
75
50
25
0
1
2
3
4
5
6
7
Postnatal day
*

Chapter IV

Aggrecan Prevents Cortical Axon Growth into dLGN

Introduction

Although the inhibitory domain of aggrecan can repel RGC axons, regenerating fibers in spinal cord, and numerous other classes of axons, it does not repel all cell types (Snow et al., 1992; Silver et al., 2004). Serotonergic neurons in the spinal cord represent a class of cells that show enhanced outgrowth onto aggrecan rich substrate (Hawthorne et al., 2011). Having examined the expression of aggrecan and its potential role as a regulator of layer VI cortical afferents, I sought to characterize the direct effect of aggrecan protein on the growth and outgrowth of neurons located in layer VI of visual cortex. To better gauge if aggrecan was sufficient to repel CG fibers from layer VI, I used *in vitro* analysis to determine the effect of aggrecan on disassociated layer VI GFP-expressing neurons and their neurites. Once the signaling capabilities of aggrecan on layer VI axons were determined, I employed *in vivo* analyses to better understand the necessity of aggrecan in regulating the timing of CG innervation.

Aggrecan was sufficient to repel layer VI axons from dLGN

I utilized a modified stripe assay to determine whether aggrecan could repel dissociated cortical neurons. First I established that I could reproducibly grow healthy layer VI neurons in culture (data not shown). As a separate control, I spotted BSA conjugated to alexa-fluor 594, which I used to visualize the spots on the culture plates, at the same concentration that I mixed with aggrecan, to ensure that there were no

effects, either attractive or repulsive, on the growth of layer VI neurons and their processes (data not shown).

At low concentrations of aggrecan (1µg/ml), neurites from layer VI neurons could project throughout the aggrecan-containing substrates and across the borders of the aggrecan covered area (Figure 15A). At 5µg/ml and 10µg/ml, viable GFP-expressing neurons were not observed within the aggrecan containing substrates. Moreover, neurites from layer VI neurons would not extend into the aggrecan covered regions; therefore, aggrecan inhibited layer VI cortical neurite outgrowth (Figure 15 B,C). I also pretreated aggrecan with chABC, an enzyme derived from bacteria that effectively degrades the inhibitory CS-GAG side chains. Layer VI neurons could extend into regions of the chABC-treated aggrecan (Figure 15 D). The chABC treatment illustrated two important principles: First, the inhibitory domain of aggrecan was embedded in the GAG side chain domain, and it also showed that inhibition was not caused by a physical boundary due to a protein barrier. Quantification of the neurites' ability to cross into the aggrecan substrate revealed that high concentrations of aggrecan repel significantly more neurites than low concentrations of aggrecan and aggrecan that had been degraded by chABC (Figure 15 E).

Degradation of the CS domain of aggrecan alters CG innervation profile

After I established that aggrecan was sufficient to inhibit layer VI cortical neurite outgrowth *in vitro,* I was interested in testing whether premature digestion of the CS-GAGs attached to aggrecan would result in accelerated layer VI CG axon entry *in vivo*. I performed bilateral intrathalamic injections of chABC in *golli-tau-gfp* mice to determine

the necessity of aggrecan in CG timing and compared these data to age matched uninjected littermates. As an additional control to account for the CNS injury received during injection, I also injected littermates with PNase, an enzyme of comparable size and bacterial origin with no known effects within CNS tissue. I then analyzed CG innervation in each of the treatment conditions.

My experimental dosing regimen was based on previous chABC treatments used in spinal cord injury (SCI) therapies that were known to allow regenerating axons to overcome CSPG inhibition (Steinmetz et al, 2005; Massey et al., 2006; Alilain et al., 2011). These studies reported that chABC must be injected within 1mm of the area of interest in order for distribution to a specific site. After making a tiny incision in the scalp to locate coordinates on the brain to place my injection, I placed the micropipette through the cortex in the medial thalamus approximately 0.5mm from the dLGN to preserve cytoarchitecture and prevent gliosis within dLGN which might affect my results (Figure 16 A). Using a picospritzer, I delivered controlled volumes of drug into the CNS of P0-P1 *golli-tau-gfp* mice.

Upon examination of CG innervation, two days following drug delivery, I observed a significant increase in the area of dLGN covered by axons in the chABC-injected animals compared to uninjected age matched control littermates (Figure 16B, C). PNase injected *golli-tau-gfp* mice exhibited a CG innervation phenotype that was insignificantly different from uninjected age matched littermates but showed significantly lower area of coverage when compared to the chABC injections (Figure 16B,C).

Aggrecan prevents layer VI axons from entering the dLGN

ChABC non-specifically destroys the CS-GAG side chains of all CSPGs. Although I established that aggrecan was the most abundant lectican CSPG localized in dLGN during perinatal development, IHC results revealed that other CSPGs were also present in dLGN. In order to interpret the necessity of aggrecan and exclude interactions from CS-GAG chains on other CSPGs, I needed to specifically target aggrecan and ensure that CS-GAGs from other proteoglycans were not directly affected by chABC enzymatic digestion. For this I used a mouse model with a spontaneous mutation in the *acan* gene (*acan*^{cmd}). This mutation results in the translation of a non-funtional aggrecan molecule that lacks the CS domain. Due to the lack of functional aggrecan protein globally, these homozygous mutant mice exhibit many severe phenotypes including perinatal death due to an inability to breathe.

By cross-breeding the *acan*^{cmd} mouse line to the *golli-tau-gfp* mouse line, I was able to observe the effect of ridding the CNS of aggrecan, exclusively, on the timing of CG projections without destroying the cytoarchitecture or introducing pharmacological side-effects such as degradation of CS-GAGs on other proteoglycan molecules.

Aggrecan was expressed throughout the thalamus during embryonic development of mice, and aggrecan was degraded in a pattern from ventral to dorsal thalamus during prenatal and perinatal development (Data not shown). Given these observations, I believed that CG innervation would be accelerated in the *acan*^{cmd} mouse because of a lack of inhibitory cues to stop the growth cones of invading axons. My results confirmed the necessity of aggrecan in regulation of the timing of layer VI cortical projections in dLGN. In the *acan*^{cmd} mice that were homozygous for WT aggrecan and *acan*^{cmd} mutants, I compared the progression of layer VI fibers into thalamus at P0. In

WT sections of rostral LGN, GFP expressing axons began to approach the dLGN, but there were very few projections labeled. Since the LGN is a long structure, I also analyzed sections located in both the middle of the LGN and caudal LGN to see if layer VI axons were more abundant within a particular section, or if the GFP-expressing projections had progressed further into dorsal thalamus or along the eml. In the areas of middle LGN, axons were located near the most ventral areas of the vLGN of WT mice, nowhere near dLGN at this point (Figure 17 A). Finally near the caudal end of LGN, where vLGN was very large, I observed that layer VI afferents were absent from areas adjacent to the vLGN. These results starkly contrasted my findings in the *acan*^{cmd} mouse, where layer VI fibers were not only quite abundant near rostral, middle, and caudal dLGN, but I could also see that the axons had progressed much further along the eml. In all three sections, axons were present travelling as far as the IGL, with many projections lining up in eml along medial dLGN in more rostral sections. Upon closer inspection, pioneer axons (denoted by arrows) could be seen in the tract adjacent to and even coursing through parts of dLGN in rostral, middle and caudal sections (Figure 17B).

The outgrowth profile of layer VI axons into thalamus demonstrated a vast difference between animals that had normal aggrecan profile and those that could not produce functional aggrecan. In several cases, I observed multiple fine CG fibers coursing into dLGN (Figure 18).

Conclusions

In vitro experiments illustrated that aggrecan was repulsive to layer VI neurites in high concentrations, and the functional domain for inhibiting neurite outgrowth resided within the CS-GAG domain of aggrecan. An interesting observation from the *in vitro* analyses was a potential concentration dependent effect of aggrecan inhibition on layer VI neurites, suggesting a differential effect on axons within the population of layer VI cells. The destruction of aggrecan at perinatal ages with chABC *in vivo* led to accelerated CG innervation, complementing previous data from the *math5*$^{-/-}$ time series experiments that suggested early loss of aggrecan allowed accelerated CG entry into dLGN. Finally the *acan*^{cmd} mutant mouse line provided evidence that layer VI GFP-expressing fibers could innervate the dLGN as early as P0 in the absence of aggrecan. Taken together these data showed that aggrecan was sufficient to repel layer VI axons from the dLGN, and aggrecan was necessary in the proper spatiotemporal development of CG axons in thalamus.

Figure 15: Layer VI neurite outgrowth is inhibited by high levels of aggrecan *in vitro*. (A-D) Aggrecan covered substrate containing low concentration (1µg/ml), high concentrations (5 µg/ml and 10 µg/ml), and an enzymatically deactivated (10 µg/ml + chABC) concentration of aggrecan are labeled in red. Tau-GFP expressing cortical neurons labeled with GFP antibody in green. Scale bar is 50µm. (E) Quantification of the percentage of neurites capable of crossing into aggrecan containing substratum in conditions shown in A-D. Error bars are +/- SEM. ** marks a difference with statistical significance $p<.01$ by ANOVA with Tukey-Kramer post-hoc test.

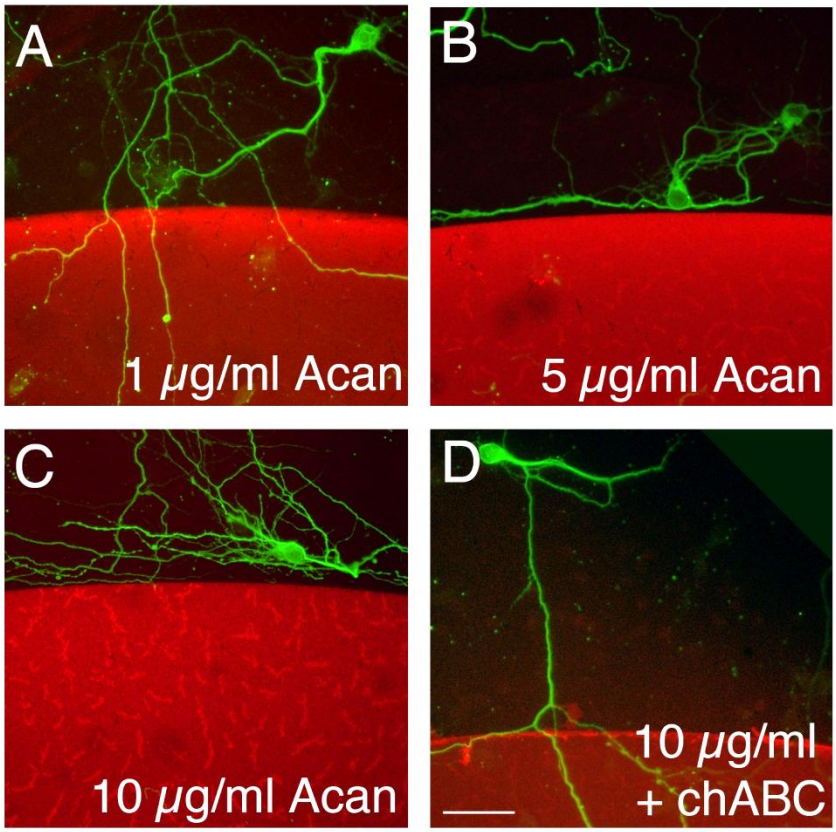
A
1 μg/ml Acan
B
5 μg/ml Acan
C
10 μg/ml Acan
D
10 μg/ml
+ chABC

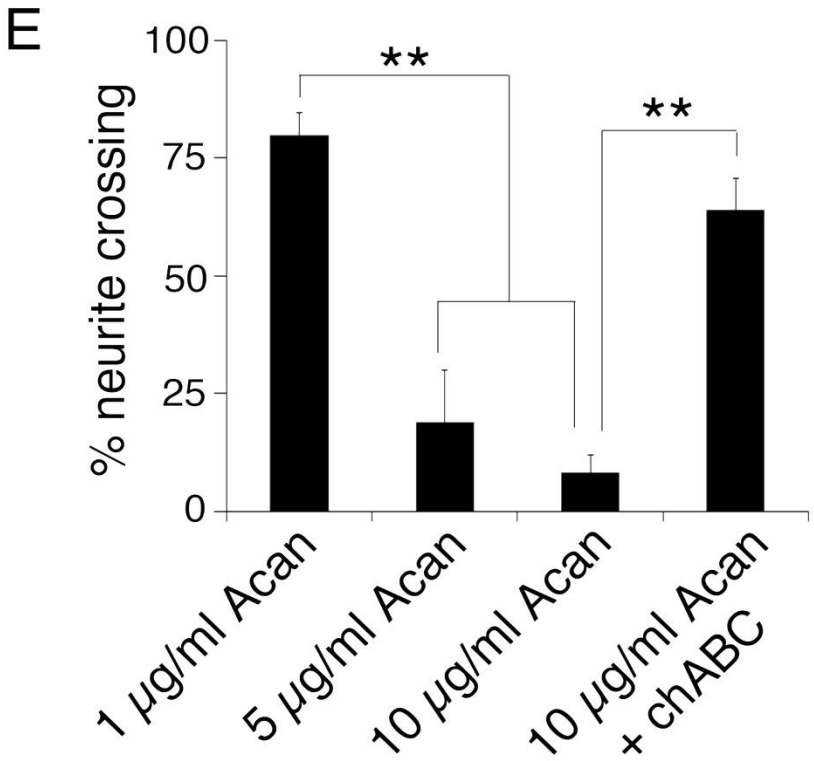
E
% neurite crossing
100
75
50
25
0
**
**
1 μg/ml Acan
5 μg/ml Acan
10 μg/ml Acan
10 μg/ml Acan
+ chABC

Figure 16: Premature digestion of aggrecan accelerates CG innervation *in vivo*. (A) Schematic depiction of the site of bilateral intrathalamic injections. (Image of cresyl violet stained coronal section of brain modified from Allen Institute for Brain Science). (B) Top row shows GFP-labeled axon invasion at P3 following injection of PNase at low (left) magnification and area highlighted by arrows at high (right) magnification. Bottom row depicts GFP labeled axon invasion at P3 following injection of chABC at low (left) magnification and area highlighted by arrows at high (right) magnification. dLGN are encircled with white dots. Scale bar for low magnification images is 150 µm. Scale bar for high magnification images is 20µm. (C) Quantification of the percent dLGN innervated by GFP-containing cortical axons at P3 following neonatal injection of PNase or chABC. Data are normalized to data obtained from uninjected *golli-tau-gfp* littermates and error bars are +/- SEM: n>7. * chABC treatment is statistically different from PNase treatment by p<.02. **chABC treatment is statistically different from uninjected controls by p<.0005.

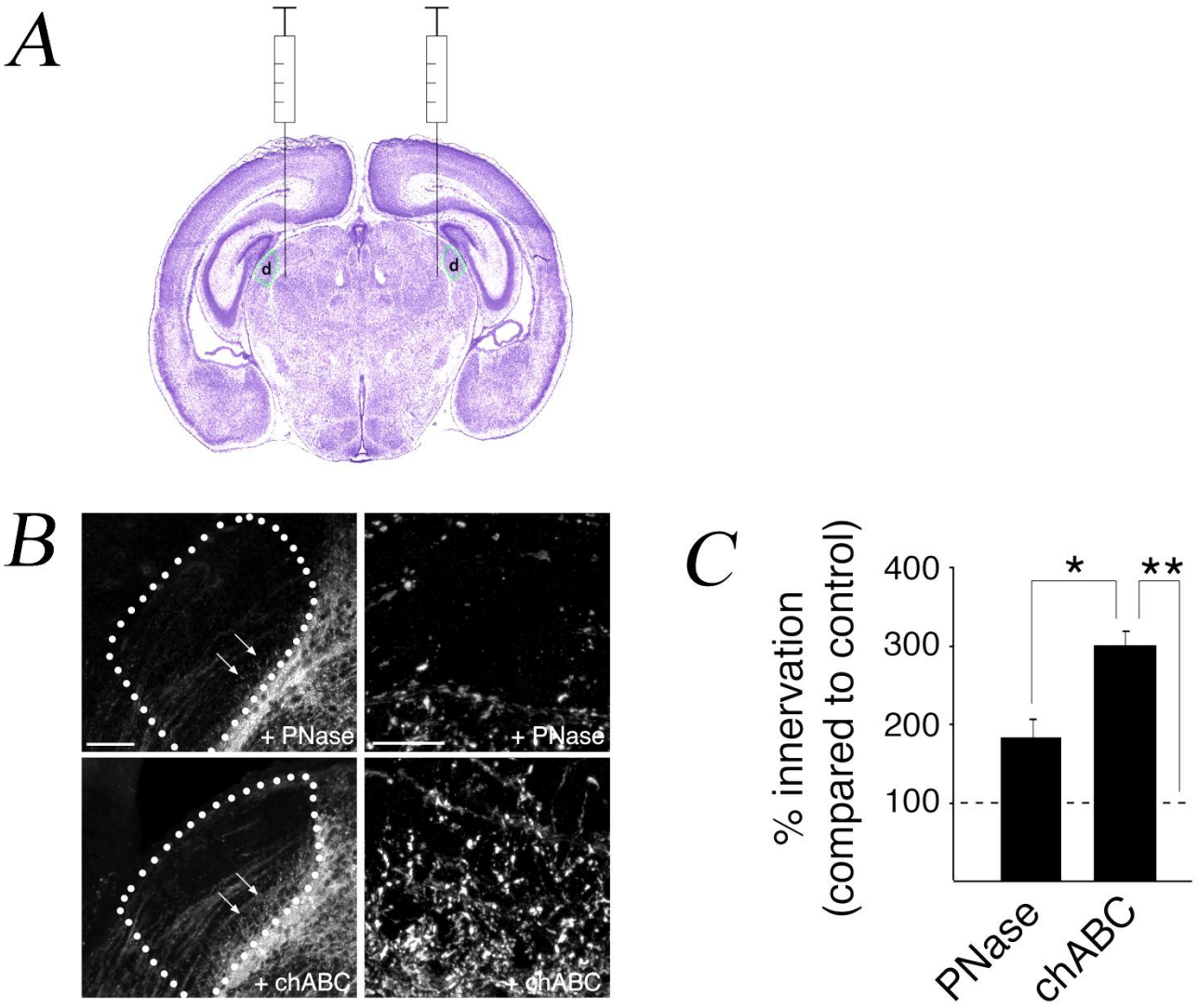
A
d
d
B
+ PNase
+ PNase
+ chABC
+ chABC
C
% innervation
(compared to control)
400
300
200
100
*
**
PNase
chABC

Figure 17: Pioneer axons from layer VI cortical neurons advance further into thalamus in the absence of functional aggrecan. Left panel shows regular (left) and inverse (right) images layer VI axon progression in sections of rostral, middle, and caudal LGN in WT *golli-tau-gfp* mouse. Arrows show how far pioneer axons have reached in each section by P0. Right panel depicts similar sections in age matched *acan*^{cmd} mutants which lack aggrecan protein. Arrows show that pioneer layer VI fibers advanced much further, and they are located within dLGN in some cases. Scale bar is 250 µm.

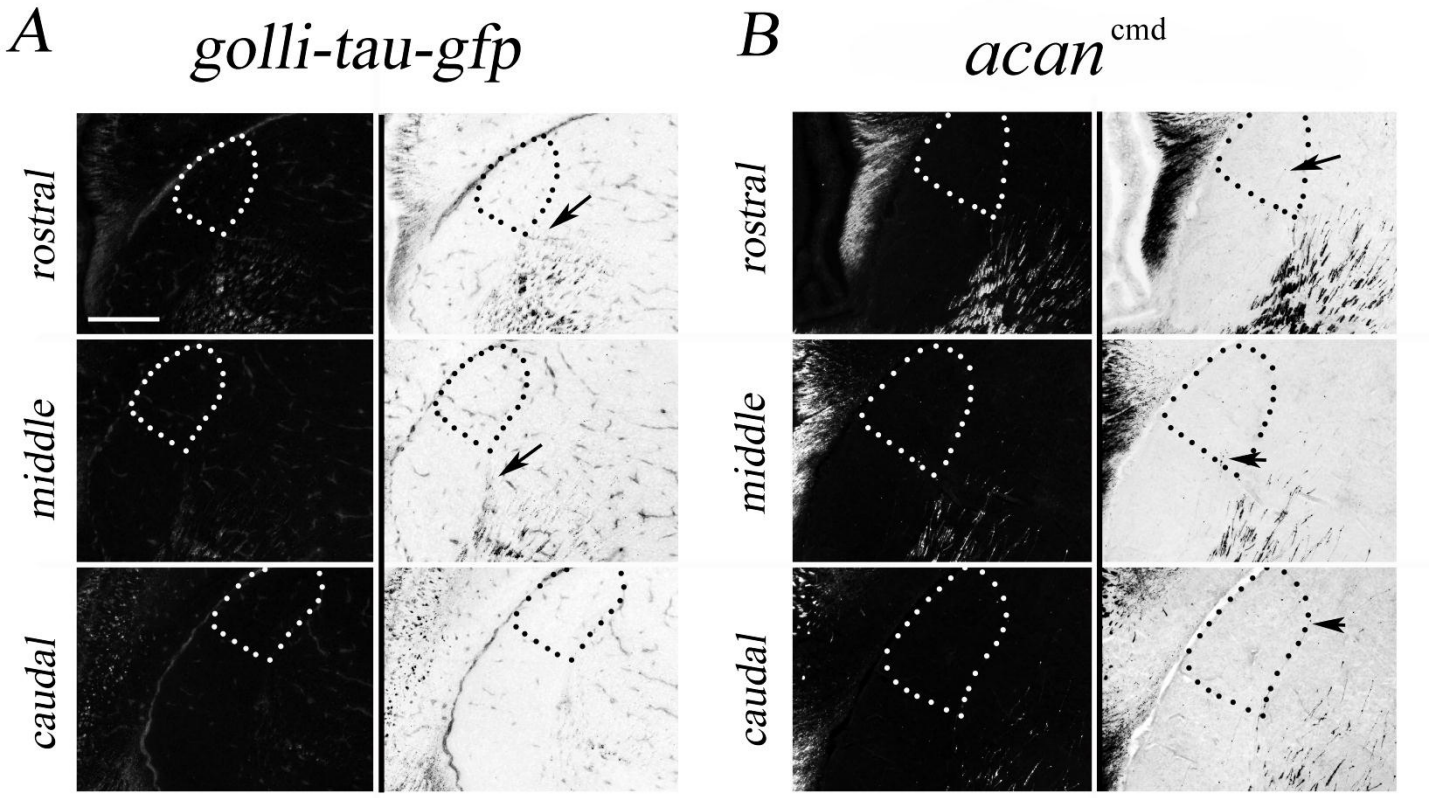
A
golli-tau-gfp
B
acan cmd
rostral
middle
caudal
rostral
middle
caudal

Figure 18: Multiple layer VI CG axons can be found in dLGN of *acan*^{cmd} mutants at P0. Low (left) magnification image shows at least two axons (highlighted by arrows) within dLGN in *acan*^{cmd} mutants. High-magnification inverse image (right) highlights the fine processes of multiple fibers (arrows) and large bulbous growth cones. Low magnification scale bar is 100µm. Scale bar in high-magnification image is 50µm.

acan^{cmd}

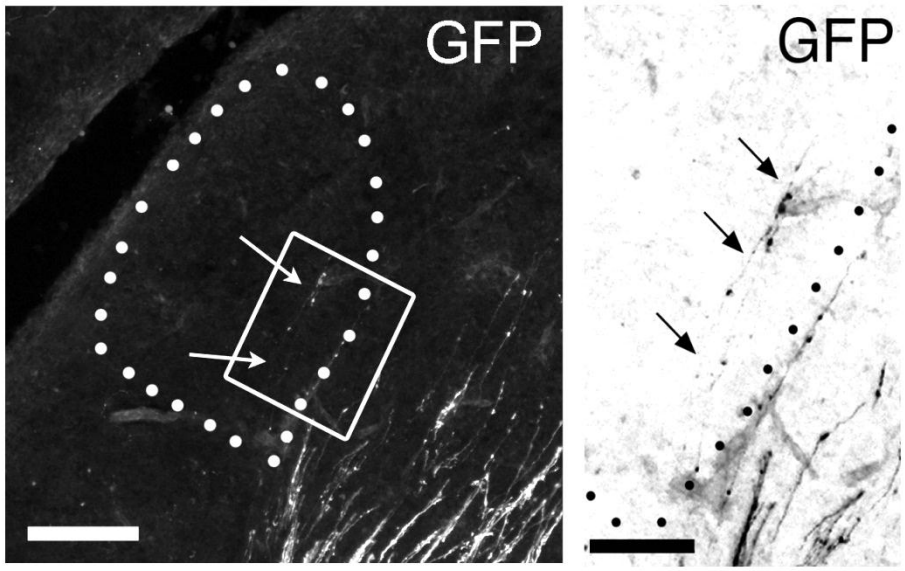

Chapter V

Retinal Inputs Regulate Aggrecanases

Introduction

Earlier in this manuscript, I introduced the phenomenon that genetic removal of retinal inputs to dLGN caused aggrecan levels to decrease and accelerated the timing of CG innervation (Figure 12). Due to the reduction of aggrecan in the *math5*$^{-/-}$ animals, I hypothesized that retinal input to dLGN relay neurons influences the distribution of aggrecan. Since I previously reported that aggrecan mRNA levels consistently increase from birth until eye opening and do not correlate with aggrecan protein levels by IR, I attempted to uncover the regulatory elements involved in aggrecan degradation.

Further exploration of literature revealed the ADAMTS family of extracellular proteases that possess aggrecanase activity. Prompted by this new information, I sought to examine the expression profiles of ADAMTS members in both *golli-tau-gfp* and *math5*$^{-/-}$ mice. Once I determined the presence of *adamts* gene transcripts *in vivo,* I was interested in exploring the mechanism by which *adamts* mRNA is regulated. I employed FISH using *adamts* probes and transcriptional profiles, comparing mRNA expression in *golli-tau-gfp* and *math5*$^{-/-}$ mice, to characterize the role of retinal input on the regulation of *adamts* family members. Furthermore, I performed plot profile comparisons of the fluorescent intensity and displacement of the layer VI afferents projecting into dLGN in *golli-tau-gfp, math5*$^{-/-}$, PNase-, chABC-, and ADAMTS4-injected mice to illustrate how premature aggrecan degradation led to advanced CG innervation.

Finally, I designed a model describing the mechanisms elucidated in this dissertation that regulate the timing of CG innervation.

Role of ADAMTS in timing of CG innervation

Despite the dramatic changes in aggrecan protein levels during postnatal dLGN development, preliminary qPCR analyses detected increases in mRNA transcript expression of the gene *acan*, which encodes aggrecan. Although there is not a 1:1 ratio that determines every transcribed gene product must be translated into protein, I was surprised by this data and suspected that there must be an extracellular enzyme responsible for the decline of aggrecan-IR signal in dLGN.

Although my initial transcriptional profiling experiments did not identify aggrecan or other potential regulators of CG timing, they demonstrated an enrichment of extracellular protease mRNAs in postnatal dLGN. Specifically, I observed an increase in several members of the *adamts* gene family in a microarray comparing expression of P3 dLGN and vLGN. At this age, when layer VI axons were just beginning to enter dLGN in the *golli-tau-gfp* mouse, I found that *adamts*4, *adamts*8, *adamts*15, and *adamts*19 were all significantly enriched in dLGN (Figure 20 A).

ADAMTS proteins are a class of extracellular enzymes that function in cleavage and degradation of a plethora of extracellular molecules. Many studies have focused on characterizing the enzymatic cleavage activities of the ADAMTS proteases, specifically on aggrecan, to determine which family members constitute the most effective “aggrecanase” (Totorella and Malfait, 2008; Stanton et al., 2011). The results of those studies concluded that nearly half of the known ADAMTS family members have an

affinity for at least one domain located on aggrecan protein including ADAMTS-1,4,5,8,9,12,15,16,18, and 19 (Figure 19).

This experiment provided evidence for a potential mechanism for aggrecan degradation at the early ages, but I also needed to ensure that *adamts* family members continued high levels of expression in order to maintain low aggrecan levels. Thus, I employed a longitudinal microarray comparing levels of mRNA expression in dLGN of P3 and P8 animals, and I observed that even more "aggrecanases" were upregulated including *adamts*1, *adamts*8, *adamts*9, *adamts*10, *adamts12, adamts*15, *adamts*19 (Figure 20 B). I confirmed significant developmental increases in mRNA expression for *adamts*4, *adamts*8, *adamts*9, *adamts*15, and *adamts*19 through qPCR comparisons in dLGN at P2 and P14 (Figure 22 B).

ADAMTS family members produced by relay neurons

The transcriptonal profiles provided me with an excellent starting point for selecting candidate molecules. Due to the unavailability of specific antibodies to label ADAMTS members, I synthesized riboprobes specific to *adamts* family members for *in situ* hybridization of developmental tissue. FISH enabled a better understanding of what cells are making the enzymes and any distinct patterns of generation or localization within the dLGN. I was successful in generating probes for both *adamts*4 and *adamts*15. D-FISH colocalization experiments, using the *adamts* probes and a probe for gene product of *syt*1 (synaptotagmin 1,) to label excitatory neurons in dLGN, allowed me to identify that both *adamts*4 and *adamts*15 were produced by relay neurons in the dLGN (Figure 21).

Although I could not be sure if one or all of the ADAMTS enzymes mediated aggrecan degradation in dLGN, my results implicated *adamts4* and *adamts15* as viable candidates. I observed that the expression of *adamts*15 in P3 WT mice occurred in a ventromedial to dorsolateral gradient in dLGN which closely resembled the pattern of early aggrecan degradation (Figure 22). By P14 *adamts*15 expression localized in the dLGN was expressed robustly in relay neurons throughout the dLGN (Figure 22).

Aggrecanases regulated by retinal input

Based upon the upregulation of aggrecanase mRNAs coincident with aggrecan degradation in *golli-tau-gfp* dLGN, I suspected that the expression or activity of these metalloproteinases may be regulated by retinal input. ISH probes for *adamts4* and *adamts15* were applied to *math5*$^{-/-}$ tissue to determine if any differences existed, pertaining to expression early in development, when aggrecan levels were already diminished in these mutants. I identified high levels of expression of *adamts4* in these mutants at P3 and P6, and I also observed *adamts15* expression in dLGN at P0, as well as, P3 and P6 (Figure 23 A).

I also performed a microarray comparing P3 dLGN mRNA expression in *golli-tau-gfp* and *math5*$^{-/-}$ mutants to determine if other guidance molecules were altered in the absence of retinal input. Although I did not find the expression of inhibitory guidance molecules, including *acan* expression, to be altered significantly in the *math5*$^{-/-}$ mutants, I discovered a modest increase in many of the adamts family members that contain aggrecanase activity, including *adamts*4*, adamts*8*, adamts*9, *adamts*15*,* and *adamts*16 (Figure 23 B). *Adamts12* mRNA levels were significantly upregulated, and there was

also a significant 27% increase amongst the entire family of *adamts* aggrecanases. Since the ADAMTS enzymes have redundant functions, I believe that these increases provide ample explanation for early aggrecan degradation in the *math5*$^{-/-}$ mice.

ADAMTS4 degradation of aggrecan allowed accelerated CG invasion of dLGN

Next I tested whether aggrecanases contributed to the timing of CG innervation by injecting constitutively active, rhADAMTS4 into the thalamus of neonatal *golli-tau-gfp* pups. ADAMTS4, dubbed aggrecanase-1, was chosen over the other ADAMTS enzymes for multiple reasons. In contrast to most other ADAMTS enzymes, active ADAMTS4 was commercially available. Second, ADAMTS4 was capable of cleaving the aggrecan molecule at multiple sites within the IGD and CS domains of aggrecan, whereas, many of the other metalloproteinases were only capable of cleaving at one particular site on the aggrecan molecule(Tortorella and Malfait, 2008). Finally, in addition to cleaving the same sites as other ADAMTS enzymes, ADAMTS4 had an affinity for aggrecan that was several orders of magnitude higher than most others (Tortorella and Malfait, 2008). This combination provided confidence that exogenous delivery ADAMTS4 was the most suitable ADAMTS family member to specifically target and degrade aggrecan *in vivo*.

I utilized the same intrathalamic injection paradigm for ADAMTS4 that I used in the chABC experiments. When I assessed the amount of CG innervation at P3, I observed that layer VI fibers in the PNase injected animals resembled the phenotype in uninjected animals, but layer VI axons in the ADAMTS treated cohort traveled further into dLGN (Figure 24A). Not only did GFP labeled fibers extend further into dLGN, but

also the amount of area occupied by CG projections as detected by threshold analysis was significantly higher for the ADAMTS4-injected animals compared to both uninjected littermates and PNase-injected animals (Figure 24B). Although both chABC and ADAMTS4 injections significantly altered CG innervation compared to controls, they did not show statistical differences between each other.

Pharmacological models of aggrecan degradation showed similar CG innervation profile to math5$^{-/-}$ *mutant mouse model*

Another compelling piece of evidence for retinal regulation of aggrecanase enzymes came from performing plot profiles using line scans to quantify axon progression from the medial to lateral boundaries of dLGN in *golli-tau-gfp, math5*$^{-/-}$, ADAMTS4-treated, chABC-treated and PNase-treated brain sections stained with GFP at P3. The plot profiles recorded both fluorescence intensity, which related to the number of axons present in any pixel, and distance traveled from eml into the dLGN providing a detailed account of the innervation profile. I performed plot profiles and averaged the data for n=8 for the *math5*$^{-/-}$ and *golli-tau-gfp* brains, and n=3 for each of the treated brains.

The *math5*$^{-/-}$ animals showed the greatest lateral extent of CG axon entry into dLGN, and they maintained the highest fluorescent intensity over the first 50µm into dLGN. Axons from both the ADAMTS4 and chABC-treated animals began entering the dLGN with intensities comparable to the *math5*$^{-/-}$ model; however, the plot profile for chABC began to diverge from the other two scans just 5.4 µm into dLGN. The

ADAMTS4 plot profile mimics the profile of *math5*$^{-/-}$ mice until nearly 15µm inside dLGN (Figure 25).

GFP-expressing axons in both the *golli-tau-gfp* and PNase-treated animals began entering the dLGN with fluorescent intensities that were ~2/3 of the signal observed in axons from *math5*$^{-/-}$ animals. This data suggested that fewer axons were entering dLGN from eml in *golli-tau-gfp* and PNase-treated mice. The plot profiles for *golli-tau-gfp* and PNase treated mice were similar and appeared "distinct" from the data obtained from either ADAMTS4-injected animals or *math5*$^{-/-}$ mutants (Figure 25). This descriptive analysis combined with the statistically significant increase in dLGN coverage by layer VI axons in ADAMTS4-injected animals suggested that ADAMTS4 could potentially be the *adamts* family member that is directly regulated by retinal input *in vivo*.

Conclusions

Microarray analyses provided evidence for upregulation of ADAMTS family members in dLGN, which was concomitant with the decreased signal in the aggrecan IHC experiments. These data confirmed a potential molecular mechanism for the regulation of aggrecan during the development of the visual system. The D-FISH results suggested that relay neurons, not interneurons or glial cells, were the primary synthetic site of *adamts* mRNA transcripts. Along with the IR labeling and transcriptome profiling in the *math5*$^{-/-}$ mouse model, the data implicate retinal inputs as serving an instructional role on aggrecanase expression. Finally, I determined that ADAMTS4 was sufficient to degrade aggrecan *in vivo* and accelerate the timing of CG innervation. Comparisons of

CG innervation, at P3 in my experimental models, illustrated that early aggrecan degradation allows for more axons to project further into dLGN. These results supported my hypothesis concerning an endogenous regulatory mechanism for CG timing in CNS; specifically, relay neuron derived ADAMTS contributed to the developmental degradation of aggrecan.

Summary

To summarize, I created a simplified model to illustrate the mechanisms that regulate the timing of CG innervation during visual system development in the mouse dLGN. At perinatal ages, immature retinal axons had already begun to innervate the dLGN and had formed many weak synapses onto relay neurons throughout the dLGN. During that period of time, aggrecan was present in the ECM across the entire dLGN. Retinal signaling of the relay neurons produced a response that inhibited expression of *adamts* family members. At around P4, retinal synapses began differentiation, where strong synaptic partners were retained, and weak synapses, or improperly formed synapses, were retracted in order to form other contacts. At that time, the inhibition of ADAMTS expression was released and aggrecan degradation had begun, allowing CG fibers entry into dLGN. As development progressed, RG synapses began to mature, ADAMTS expression was greatly increased, and aggrecan continued to be destroyed. This process allowed for CG projections to extend across much of dLGN and form weak synapses onto relay neurons. Around the time of eye opening (P14), CG fibers finally began exhibiting mature synaptic contacts as RG synapses took on their adult profile,

presumably to allow CG feedback afferents to form specific connections onto the proper relay neuron (Figure 26).

Figure 19: ADAMTS4 is capable of cleaving aggrecan at multiple sites. Matrix metalloproteinases (MMPs) cleave aggrecan at one site within the IGD. At least 5 sites have been identified as targets for ADAMTS4 cleavage on the aggrecan molecule, one site within the IGD and 4 others within the CS domain which create different size cleavage fragments (Porter et al., 2005). ADAMTS4 recognizes the IGD cleavage domain with at least 100X greater efficiency than most other ADAMTS enzymes and can overcome aggrecan inhibition more effectively than MMPs (Cua et al., 2013). The major cause of aggrecan depletion is due to cleavage at the IGD site, however, the ADAMTS4 CS-domain cleavage has been hypothesized to result in bioactive fragments that could be conducive to neurite outgrowth, based on previous reports of bioactive molecules resulting from partially digested ADAMTS fragments from other CSPGs including versican and brevican (Cua et al., 2013; Sandy et al., 1991; McCulloch et al., 2009; Viapiano et al., 2008)

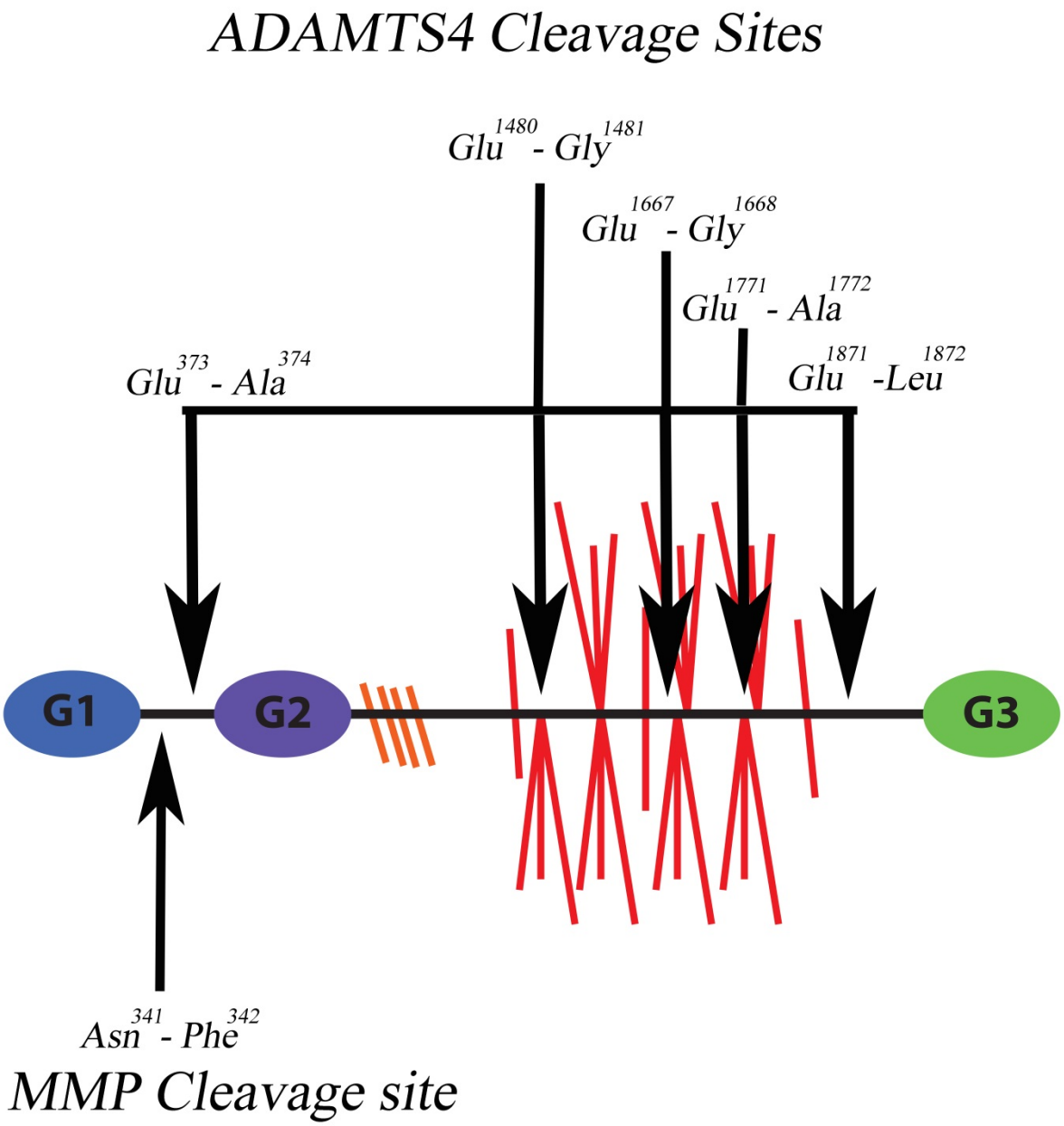
ADAMTS4 Cleavage Sites
Glu 1480 - Gly 1481
Glu 1667 - Gly 1668
Glu 1771 - Ala 1772
Glu 373 - Ala 374
Glu 1871 -Leu 1872
G1
G2
G3
Asn 341 - Phe 342
MMP Cleavage site

Figure 20: Aggrecanases are upregulated in postnatal dLGN. (A) Microarray comparison of gene expression in P3 dLGN compared to vLGN revealed that several members of the *adamts* family of proteases were upregulated in dLGN. Blue bars indicate *adamts* known to possess aggrecanse activity. Error bars are +/- SEM: n=3. * means difference is significant by p<.05 by T-Test, ** means difference is significant by p<.01. (B) Microarray comparison of gene expression in P3 dLGN compared to P8 dLGN revealed that several members of the *adamts* family of proteases increase over time during visual development. Blue bars indicate *adamts* known to possess aggrecanse activity. Error bars are +/- SEM: n=3. * means difference is significant by p<.05 by T-Test, ** means difference is significant by p<.01.

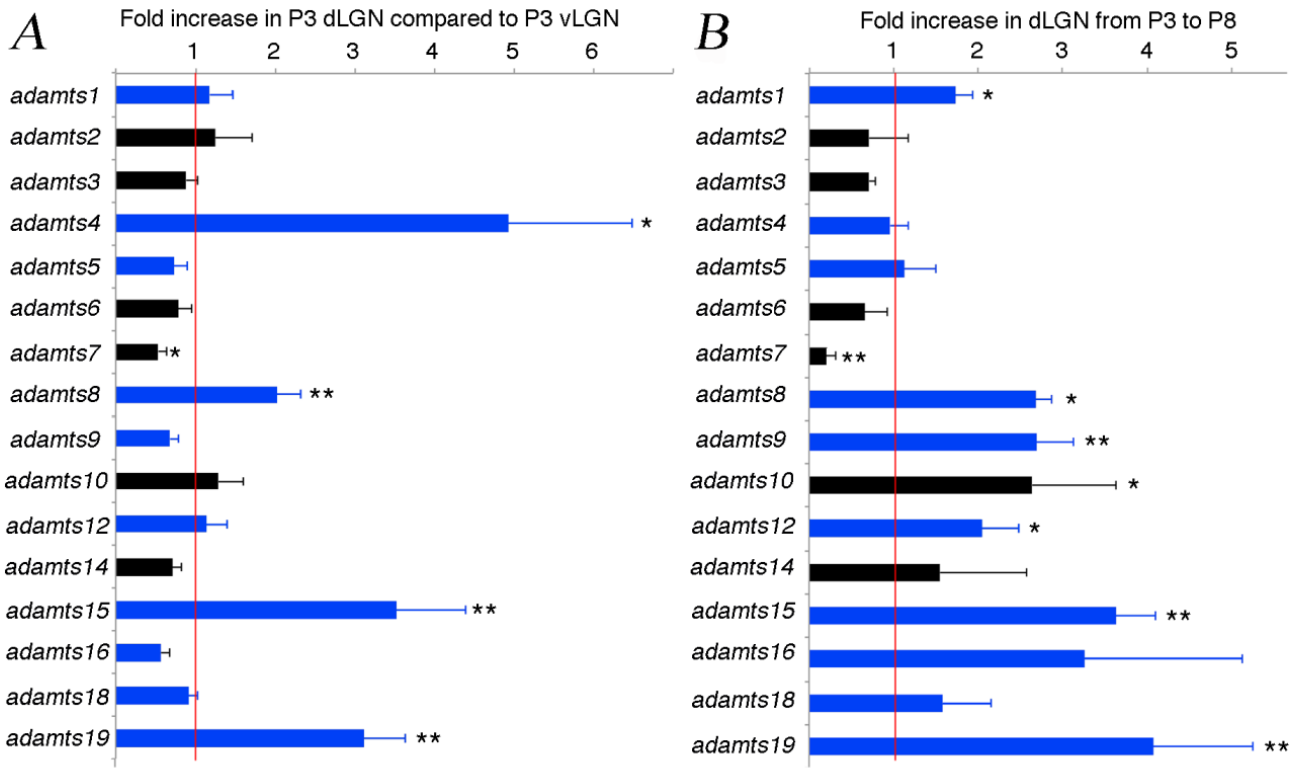
A
Fold increase in P3 dLGN compared to P3 vLGN
1
2
3
4
5
6
adamts1
adamts2
adamts3
adamts4
adamts5
adamts6
adamts7
adamts8
adamts9
adamts10
adamts12
adamts14
adamts15
adamts16
adamts18
adamts19
*
*
**
**
B
Fold increase in dLGN from P3 to P8
1
2
3
4
5
adamts1
adamts2
adamts3
adamts4
adamts5
adamts6
adamts7
adamts8
adamts9
adamts10
adamts12
adamts14
adamts15
adamts16
adamts18
adamts19
*
**
*
*
*
**
**

Figure 21: Relay neurons produce *adamts* mRNA transcripts. (Top panel) *In situ* hybridization in P14 coronal sections of dLGN revealing the presence of *adamts*15 (left) and *syt1* (middle left) illustrating colocalization (middle right). (Bottom panel) *In situ* hybridization in P14 coronal sections of dLGN showing *adamts*4 (left) and *syt1* (middle left) and colocalization (middle right). High-magnification images of each overlay (Far Right) clearly show colocalization of both *adamts15* and *adamts4* in relay neurons. Scale bar for low-magnification images is 200 µm. Scale bar for close up overlay images is 75µm.

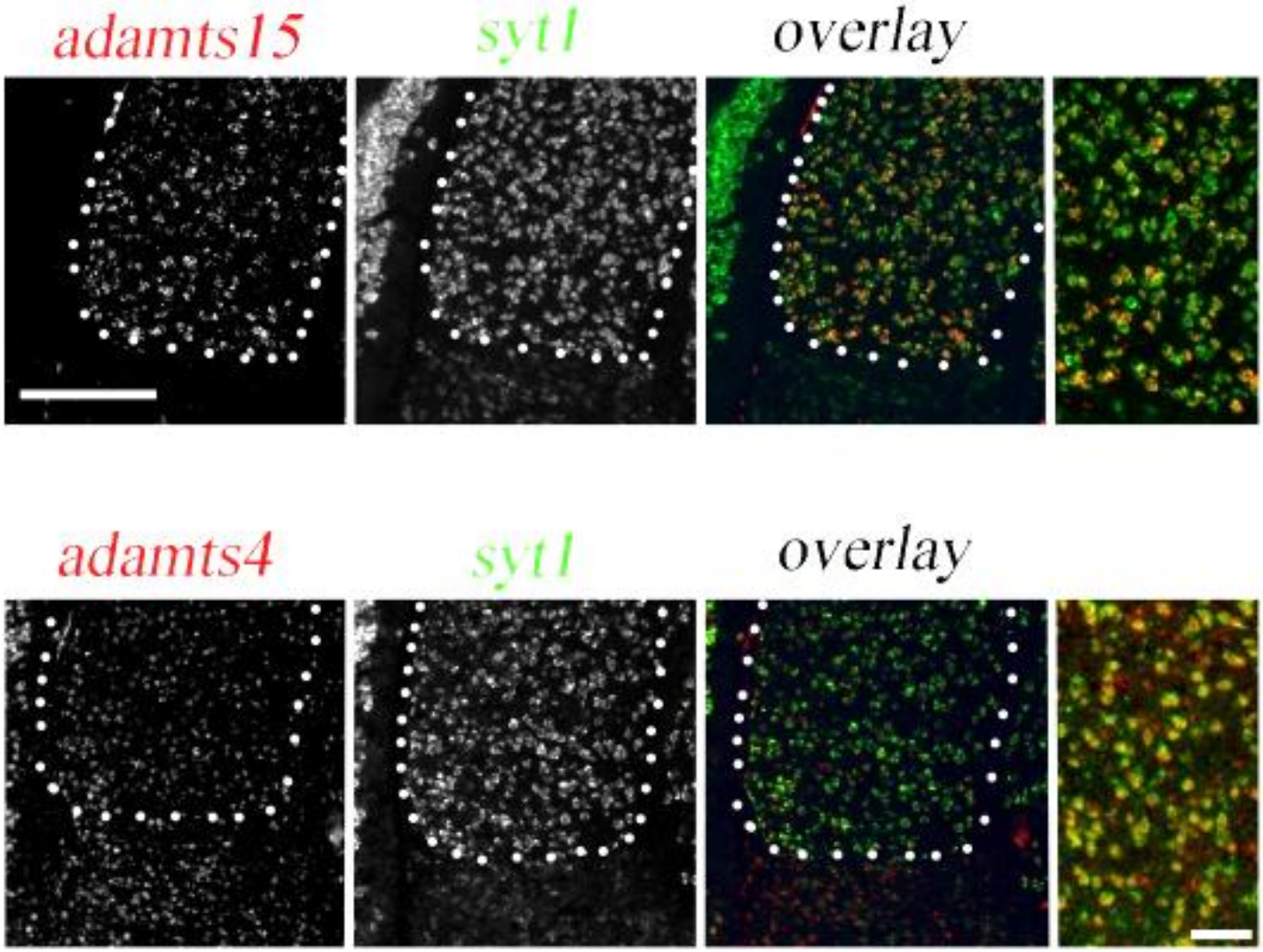
adamts15
syt1
overlay
adamts4
syt1
overlay

Figure 22: Increased longitudinal gene expression of *adamts* family members confirmed in *golli-tau-gfp* mouse. (A) ISH for *adamts*15 showing localization in dLGN at P3 and P14. Scale bar is 200µm. (B) qPCR of relative expression from P2 to P14 shows that multiple aggrecanse genes are upregulated over time in dLGN.

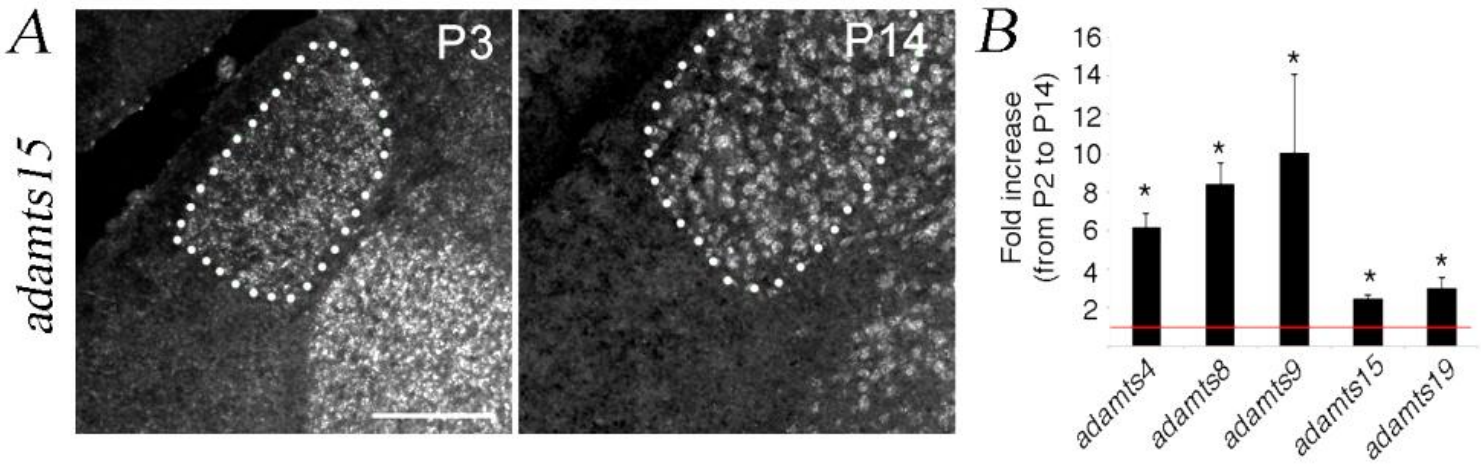
A
adamts15
P3
P14
B
Fold increase
(from P2 to P14)
16
14
12
10
8
6
4
2
*
*
*
*
*
adamts4
adamts8
adamts9
adamts15
adamts19

Figure 23: Removal of retinal inputs increases *adamts* expression in postnatal dLGN. (A) ISH for *adamts4* (top panel) showing robust expression in dLGN at P3 and P6. *Adamts*15 (bottom panel) was also detected in perinatal dLGN. Scale bar is 200µm. (B) Microarray comparison of P3 *golli-tau-gfp* and *math5*$^{-/-}$ dLGN unveiled modest changes in multiple *adamts* family members that possess aggrecanase activity (blue bars).

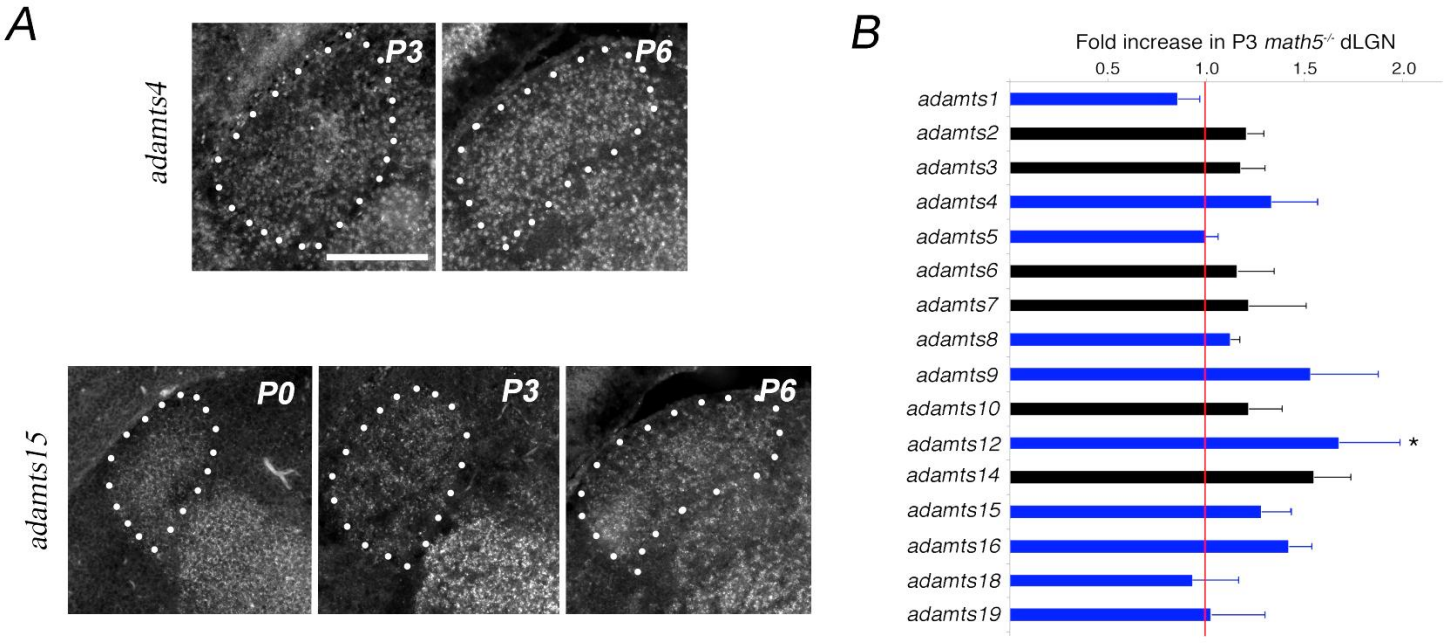
A
adamts4
P3
P6
adamts15
P0
P3
P6
B
Fold increase in P3 math5-/- dLGN
0.5
1.0
1.5
2.0
adamts1
adamts2
adamts3
adamts4
adamts5
adamts6
adamts7
adamts8
adamts9
adamts10
adamts12
*
adamts14
adamts15
adamts16
adamts18
adamts19

Figure 24: ADAMTS4 digestion of aggrecan accelerates CG innervation. (A) PNase (Top panels) injected tissue immunostained with GFP showing little CG axon entry into dLGN. Left Panel represents low-magnification image, and right panel is high-magnification image focused on boxed area. ADAMTS4 injected tissue (Bottom panels) showing layer VI fiber extending farther into dLGN. Left Panel represents low-magnification image, and right panel is high-magnification image focused on boxed area. Scale bar for low-magnification images is 150μm. Scale bar for high-magnification images is 20μm. (B) Quantification of the percent of dLGN innervated by layer VI GFP-expressing cortical axons in PNase and ADAMTS4 treated tissues. *ADAMTS treatment is statistically significantly different from PNase injections by $p<.0001$ by ANOVA with Tukey-Kramer post-hoc test.

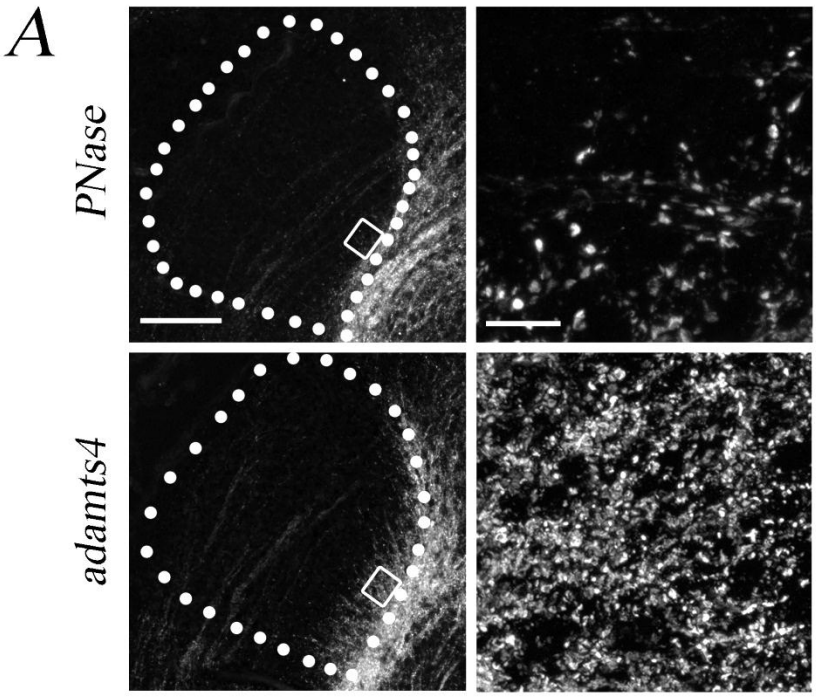
A
PNase
adamts4

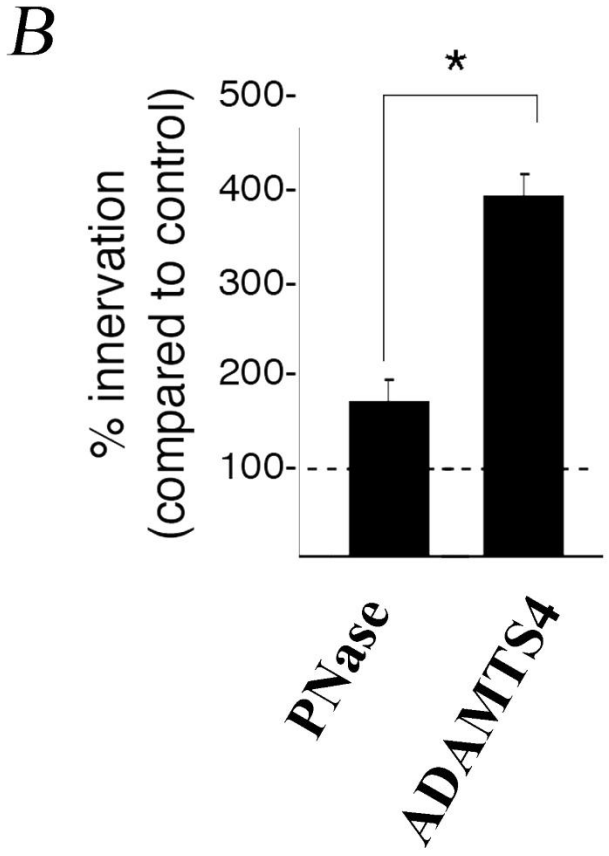
B
*
% innervation
(compared to control)
500-
400-
300-
200-
100-
PNase
ADAMTS4

Figure 25: Neonatal injection of ADAMTS4 produces CG innervation profile similar to *math5*$^{-/-}$ mice at P3. Averaged plot profiles from medial dLGN to lateral dLGN in P3 *math5*$^{-/-}$ (red), *golli-tau-gfp* (green), PNase-injected (yellow), chABC-injected (blue), and ADAMTS4-injected (black) mice depicting fluorescent intensity of invading GFP fibers, as well as, displacement from eml into dLGN. Note the clustering of *math5*$^{-/-}$, chABC-injected and ADAMTS4-injected fluorescence intensities at the medial border and displacement into dLGN.

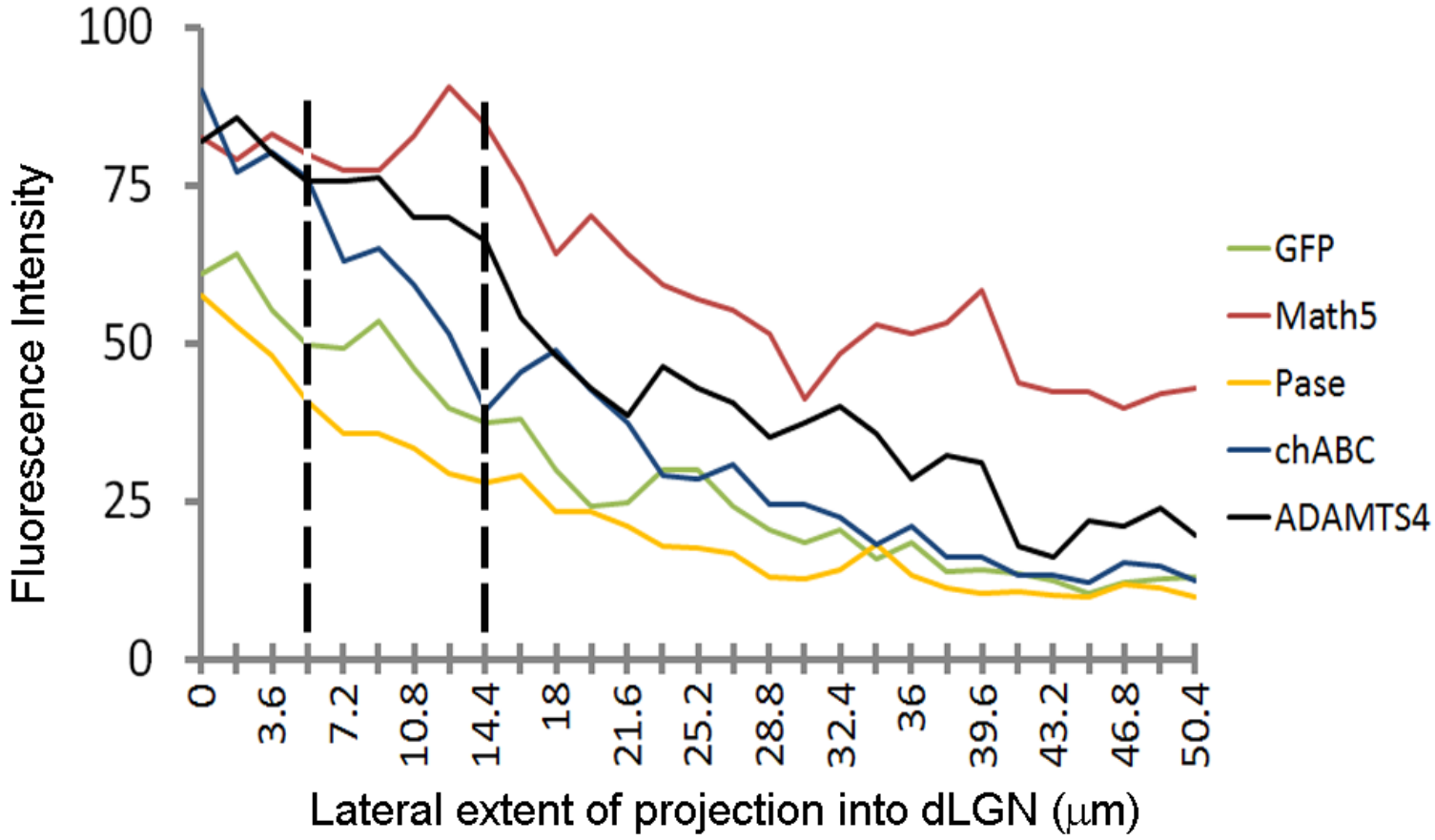
100
75
50
25
0
Fluorescence Intensity
0
3.6
7.2
10.8
14.4
18
21.6
25.2
28.8
32.4
36
39.6
43.2
46.8
50.4
Lateral extent of projection into dLGN (μm)
GFP
Math5
Pase
chABC
ADAMTS4

Figure 26: Retinal inputs instruct the timing of CG innervation through the modulation of aggrecan. Left: As immature retinal inputs (red lines) form weak connections with relay neurons (large purple circle) at neonatal ages, aggrecanases (yellow) are inhibited from being expressed and aggrecan (blue bars) is present throughout dLGN. CG axons (green lines) remain outside of dLGN. Middle: Around age P4, retinal inputs to the mouse dLGN begin differentiation to form mature synaptic contacts, the signal for inhibition of ADAMTS is released and aggrecan can be degraded. Coincidentally, CG inputs begin entering dLGN in areas where aggrecan has been degraded. Right: Retinal synapses continue to mature and become larger at P7, aggrecanase production is greatly increased leading to rapid aggrecan turnover, and CG axons begin to extend much further into dLGN and form synaptic contacts.

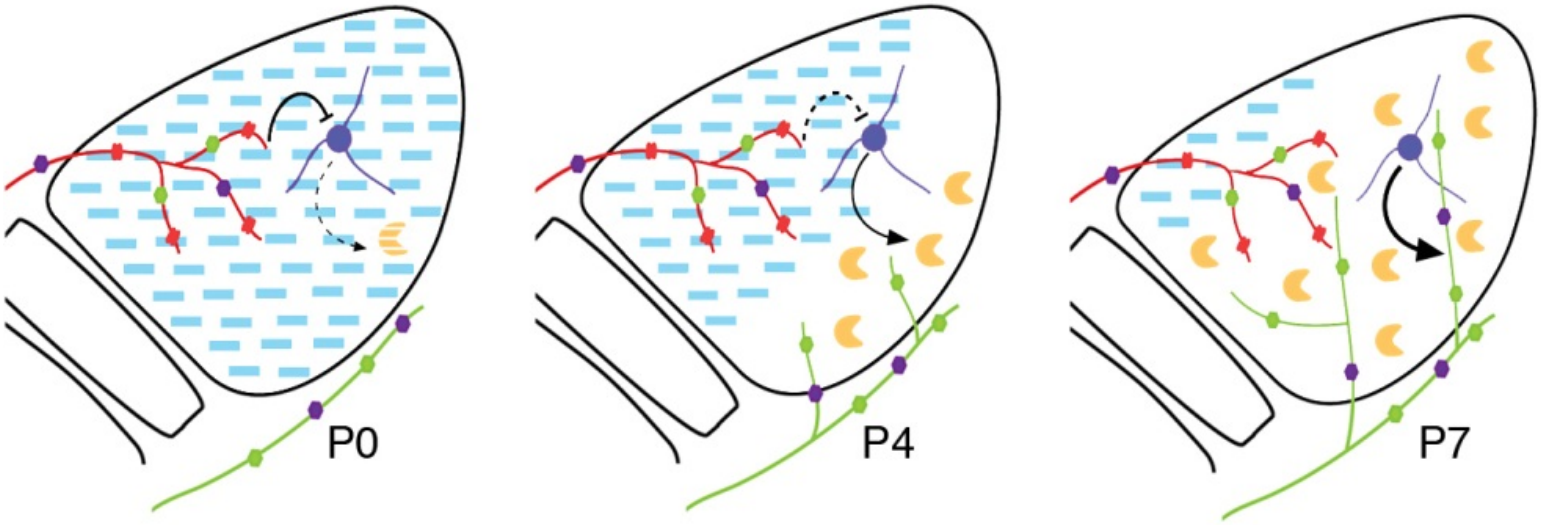

relay neuron

retinal axon

cortical axon

aggrecanase

aggrecan

α3β1 integrin

PTPRs

NgRs

Chapter VI

Discussion

Understanding the mechanisms that drive both the timing and distribution of retinal and non-retinal inputs onto relay neurons in dLGN is important as I sought to elucidate mechanisms that coordinate the formation of multiple inputs in one target region. During this project, I have identified a novel role for aggrecan, an inhibitory CSPG enriched in neonatal mouse dLGN, in preventing the premature invasion of cortical axons into dLGN, and I believe that discovering mechanisms that regulate the timing of innervation in the CNS will likely contribute to the development of targeted therapies for pathological conditions that effect axon guidance and synaptic targeting.

Relay neurons in the dLGN project thalamocortical axons to layer IV of visual cortex. Different sets of cortical neurons in layer VI of visual cortex send descending corticothalamic (CT) axons to form reciprocal, feedback connections onto relay neurons in dLGN (Sherman and Guillery, 2002). Waiting periods for growing axons have been reported in the chick hindlimb and the spinal cord, and the purpose of the waiting period is hypothesized to allow for maturation of axonal targets (Sharma et al., 1994; Wang and Scott, 2000; Deck et al., 2013). My results indicate that RGCs are beginning to form functional synapses and differentiation just prior to the degradation of the aggrecan stop signal and layer VI fiber entry into dLGN. These results suggest that the function of the aggrecan mediated delay of CG innervation is congruent with previous reports of waiting periods in the CNS.

Distinct cellular populations react differently to aggrecan

Aggrecan is one of the most well characterized CSPGs in the CNS. Reports have illustrated that the growth of many types of axons can be inhibited by aggrecan (Snow and Letourneau, 1992). In response to SCI, aggrecan secretion by reactive astrocytes limits the amount of axon regeneration at the glial scar, and aggrecan is the focus for therapies to facilitate functional regeneration in the injured spinal cord (McKeon et al., 1991; Silver and Miller, 2004; Busch et al., 2009). Recent evidence has been provided showing that serotonergic neurons in the spinal cord exhibit an unusual viability and axon sprouting in the aggrecan rich glial scar; therefore, aggrecan does not have the same effect on all cell types (Hawthorne et al., 2011). My results showed that layer VI cortical neurites were repelled by aggrecan *in vitro.* Combined with *in vivo* analyses and manipulations, I concluded that aggrecan was not only sufficient to repel layer VI axon outgrowth but also was necessary to delay CG fiber invasion in dLGN.

These results also presented a fascinating paradox. Previous studies have shown that aggrecan inhibits retinal axon outgrowth in vitro; however, aggrecan in dLGN prevented CG innervation from P0-P3 while permitting RG innervation and synapse development (Snow and Letourneau, 1992). My observations could be attributed to differing cells abilities to overcome aggrecan inhibition through interactions with particular growth-promoting substances, such as laminin or neurotrophin-3 (Snow et al., 1990; Fawcett, 2006). There is also evidence that embryonic neurons can overcome the inhibition presented by high concentrations of aggrecan by altering the expression levels of integrin receptors in their cell surface (Condic et al., 1999; Tan et al., 2011). Lack of aggrecan inhibition may also be explained, in part, by complexity of

in vivo systems in which aggrecan can mediate inhibition through at least 4 different receptors including the leukocyte antigen-related protein tyrosine phosphatase receptor (LAR), protein tyrosine phosphatase sigma (PTPσ), nogo receptor 1 (NgR1) and nogo receptor 3 [NgR3 (Fisher et al., 2011; Dickendesher et al., 2012; Sharma et al., 2012)]. Interactions become even more complex as the CS-GAG domain of aggrecan is composed of at least five different CS sulfation patterns, and evidence has shown that these CS-GAGs have differing levels of inhibitory function (Gilbert et al., 2005). In the dynamic CNS environment, growth cones from distinct cell types could react differently to aggrecan due to the presence of growth factors or activity based receptor expression.

Activity dependent alteration of aggrecan in CNS

. Aggrecan expression can be altered in response to epileptic seizures, and CSPGs have been shown to be dysregulated in schizophrenic patients (McRae et al., 2010; Berretta, 2013). In the visual cortex, aggrecan expression is regulated by experience-dependent retinal activity. Numerous reports have indicated decreased aggrecan expression at the perineuronal net (PNN), a structure shown to limit plasticity after the closure of the critical period, in response to visual deprivation or dark-rearing during early visual development (Sur et al, 1988; Lander et al., 1997). The effect of the lost aggrecan enhances plasticity of neurons ensheathed in PNNs and prolongs the critical period (Kind et al., 2013).

Since altered retinal activity can change the expression of aggrecan, I performed experiments to gauge the effect of loss of retinal activity on aggrecan expression. The *math5*$^{-/-}$ mutants contain a targeted deletion of the Math5 transcription factor, which is

crucial for differentiation of retinal progenitor cells to RGCs. In the absence of Math5, 95% of RGCs are never formed (Wang et al., 2001). Through *math5*$^{-/-}$ cross-breeding with the *golli-tau-gfp* mice, I was able to analyze the effects of silencing retinal input in dLGN on CG innervation, and I was also able to determine how molecular expression of aggrecan was altered in the absence of retinal instruction. The *math5*$^{-/-}$ mouse model was particularly useful because I did not have to stress the mice with surgery, such as encucleation, which could have triggered immune responses known to alter cellular activities in the brain. Aggrecan degradation in both systems occurred in a mediolateral pattern, thus establishing a gradient into which layer VI axons projected once aggrecan-IR was low. As reported in the *math5*$^{-/-}$ mice, I observed accelerated CG fiber innervation by 1-2 d compared to WT *golli-tau-gfp* mice, and I discovered that aggrecan signal was degraded 1-2 earlier in the *math5*$^{-/-}$ mice.

These results prompted me to use qPCR to probe *acan* gene expression in dLGN to see if the loss of retinal activity included a direct effect on the level of mRNA transcription; unfortunately, the aggrecan transcription mirrored normal WT aggrecan expression throughout development, and no significant difference in *acan* mRNA was observed in age matched *golli-tau-gfp* and *math5*$^{-/-}$ dLGN samples. Microarray analyses revealed that there was a family of *adamts* genes that were upregulated in dLGN compared to vLGN at P3, and they continued to increase expression during the development period. Nearly half of the ADAMTS family members, including ADAMTS1, 4, 5, 8, 9, 12, 15, 16, 18, and 19, have been characterized as functional aggrecanases (Llamazares et al., 2007; Tortorella and Malfait, 2008).

My transcriptional profile analyses provided more questions than answers, as is often the case, and I had to take much care in designing a meaningful study due to redundant functions of ADAMTS members. The ADAMTS family of enzymes has selective activity on a plethora of extracellular proteoglycans including other members of the lectican family (Stanton et al., 2011). Although there was no direct effect on aggrecan expression, this information prompted a reformulation of my original hypothesis to include the possibility that aggrecanases might be regulated by retinal inputs instead of aggrecan. Although I originally thought aggrecan was directly affected by retinal input, these results provide new and exciting avenues of research for regulation of aggrecan in other areas of the brain.

Outside of the CNS, reports of aberrant aggrecan levels often include analysis of ADAMTS/aggrecanases, but ADAMTS family member interactions with aggrecan in the CNS remains unknown. Many of the previous reports on altered aggrecan expression in the visual system do not mention aggrecanases as potential regulators of aggrecan. During the course of my experimentation, I generated riboprobes for *adamts4* which show global CNS expression in the developing mouse brain, and probes directed towards *adamts15* indicate mRNA expression in medial thalamus, dLGN, and particular subsets of cells in hippocampus (Data not shown). Therefore, I assert that ADAMTS/aggrecanase expression and activity analyses could potentially be more important for the regulation of critical periods and plasticity in CNS than previously reports have suggested, and analyses of ADAMTS enzymes should be performed along with aggrecan expression analyses.

Regulation and function of ADAMTS in CNS

Most of the ADAMTS metalloproteinases were established as aggrecanases in osteoarthritis studies outside of the CNS (Fosgang and Rogerson, 2010). Closely related molecules from the ADAM (a disintegrin and metalloproteinase) family have been identified as mediators of amyloid precursor proteins in Alzheimer's disease, but functional studies of ADAMTS family members in the CNS are in their infancy (Allinson et al., 2003; Bernstein et al., 2003; Krstic et al., 2012). This lack of characterization made it difficult to choose a particular ADAMTS/aggrecanase for my digestion experiments. ADAMTS12 has not yet been well characterized in terms of CNS function, like many of the ADAMTS members, but it has been shown to possess enzymatic activities directed towards aggrecan (Llamazares et al., 2007). Recent publications had shown some promising effects of ADAMTS4 in CNS, one of which reported ADAMTS4 mediated fuctional recovery in response to spinal cord injury (Tauchi et al., 2012). Ultimately, I decided that this study must include ADAMTS4 because of its upregulation in dLGN at the early postnatal ages, high aggrecanase activity, and availability.

Although my experiments focused on ADAMTS4 degradation of aggrecan, I cannot discount the diversity of upregulated *adamts* mRNAs because they may not have only redundant functions, but they could offer more insight into how ADAMTS proteins work together during development to modify the ECM, in order to guide axons or promote synaptogenesis. Previous reports, outside of the CNS, illustrated coordination of ADAMTS5, ADAMTS9, and ADAMTS20 for the resorption of interdigital webs. ADAMTS2, ADAMTS3, and ADAMTS14 have been shown to synergistically degrade procollagens I and III (McCulloch et al., 2009; Le Goff et al., 2006).

Cooperative functions of ADAMTS were also suggested though evolutionary analysis that hypothesized that each ADAMTS might display some subfunctionalization and specialization in certain tissues (Huxley-Jones et al., 2005). Reports on the assimilation of multiple ADAMTS proteinases to degrade one class of molecule provide interesting prospects for future research, especially since I observed modest changes in the regulation of many of the *adamts* mRNAs in the microarray comparison of the early postnatal dLGN expression in *golli-tau-gfp* and *math5*$^{-/-}$. Although I did not find as many ADAMTS metalloproteinases to be altered significantly in the *math5*$^{-/-}$, I did discover a modest increase in many of the adamts family members that contain aggrecanase activity, including *adamts*4*, adamts*8*, adamts*9*, adamts*15*,* and *adamts*16. *Adamts12* mRNA levels were significantly upregulated, and there was also a significant 27% increase amongst the entire family of *adamts* aggrecanases. Since the ADAMTS enzymes have redundant functions, I believe that these increases provide ample explanation for early aggrecan degradation in the *math5*$^{-/-}$ mice.

I extensively reported expression data in my analyses regarding ADAMTS, but I must also recognize the possible effects of molecules that contribute to the activity profiles of ADAMTS enzymes. Multiple regulators of ADAMTS metalloproteinase activity have been documented. Tissue inhibitors of metalloproteinases (TIMPs) contain 4 members, but currently only TIMP1 and TIMP3 have identified roles in the inhibition of ADAMTS metallproteinases (Murphy, 2011). Although neither was identified as significantly altered in expression analyses, maintenance of TIMP levels combined with modest increases in multiple ADAMTS proteins may contribute to greatly increased

aggrecan degradation and accelerated timing of layer VI innervation in dLGN in the *math5*$^{-/-}$ set of experiments.

Another possible level of regulation for ADAMTS could be achieved by a completely different set of molecules from the TIMPS. ADAMTS are not immediately active upon translation, and they must have metalloproteinase propeptides cleaved, post-translationally, before they become enzymatically functional (Apte, 2009). In addition to enzymatic digestion of the prodomain, ADAMTS4 activation occurs through C-terminal truncation by MMP-17 [(matrix metalloproteinase-17) Gao et al., 2002; Gao et al., 2004]. Aggrecanase activating and inhibiting factors can potentially be generated by RGCs and dLGN neurons ; therefore, retinal input may alter activities of the ADAMTS either directly through secretion of these factors or through induction of relay neurons to produce and secrete them (Kay et al., 2011).

ADAMTS versus MMP degradation of aggrecan

Earlier in this manuscript, I briefly made the case for using rhADAMTS4 in my experimental paradigms. In this section I will revisit this argument and compare ADAMTS4 with other MMPs, instead of just focusing on other ADAMTS aggrecanases, to solidify my justification for ADAMTS4 digestion of aggrecan *in vivo*.

MMP-3, -7, and -8 are all able to reverse the inhibition of neurite outgrowth due to the presence of CSPGs, so they appear to have as much potential as ADAMTS4 to degrade aggrecan if used *in vivo.* However, ADAMTS4 can cleave multiple fragments of aggrecan, and it has been hypothesized that partial ADAMTS4 digestion of aggrecan results in bioactive fragments that could produce neurite outgrowth, much like what has

been shown to occur when ADAMTS molecules cleave versican and brevican *in vivo* (Sandy et al., 1991; McCulloch et al., 2009; Viapiano et al., 2008).

Another advantage of ADAMTS4 over MMP digestion *in vivo* is the inability of ADAMTS4 to process laminin, which has been to shown to aid in the suppression of CSPG inihibitory signaling (Cua et al., 2013; Snow et al., 1996). Furthermore, although both ADAMTS4 and many MMPs cleave a multitude of differing target molecules within the CNS,exogenous delivery of MMPs has been shown to cause neurotoxicity *in vivo* due to a lack of localized, targeted protease activity (Xue et al., 2009; Gu et al., 2005; Cua et al., 2013).

ADAMTS4 has a proteolysis-independent mechanism for inducing neurite outgrowth, and it has been shown to be effective in allowing axon regeneration in response to spinal cord injury (Hamel et al, 2008; Tauchi et al., 2012). Finally, ADAMTS4 has been reported to be more effective than chABC in decreasing CSPG inhibition, and chABC has been well characterized for its effectiveness in restoring axon outgrowth in the spinal cord (Cua et al., 2013). Together these reports led me to believe that ADAMTS4 could potentially be the most effective route for aggrecan degradation *in vivo.*

Possible role for aggrecan in establishment of RF circuitry in dLGN

Much of this dissertation focused on the mechanisms that keep layer VI fibers out of dLGN until RG axons begin to mature, but little has been discussed regarding how aggrecan might affect RG synapse formation with relay neurons. Retinal activity coordinates the establishment of proper eye-specific domains in the mouse dLGN, and

the combination of repellent ephrin-A molecular guidance molecules and retinal activity work together in the development of topographic maps in retino-recipient nuclei (Feldheim et al., 1998; Torborg and Feller, 2005; Pfeiffenberger et al., 2006; Feller, 2009.) Furthermore, topographic mapping in SC and V1 are aligned through the generation of normal spontaneous retinal waves (Triplett et al., 2009). These reports support the notion that RF connections with relay neurons are very important in the establishment of visual circuitry.

RGCs innervate the dLGN and form immature synapses at perinatal ages in the mouse (Godement et al., 1984; Hong and Chen, 2011). During the first postnatal week, when aggrecan is abundant in dLGN, 10-20 weak synapses from different RGCs converge onto single relay neurons (Chen and Regehr. 2000). During this competition phase, only the most suitable synapses will become functional, and the rest will be retracted. Aggrecan could have multiple functions during this period. First, CS-GAGs have been shown to sequester growth factors, masking them from binding receptors, until a sheddase, like any of the ADAMTS aggrecanase enzymes, degrades the CS domains and allows the growth cone to interact with the growth factors (Muir et al., 1989; Sanes, 2003). As the axons compete for space, correctly formed RGC inputs could prompt aggrecanse distribution to a specific location leading to the unmasking of growth factors that promote synaptic differentiation and maturation.

RGCs express different guidance receptors which allow them to traverse to different sides of the brain. Expression patterns of molecules, or combinations of expression patterns, also lead to the divergent pathways when selective targeting occurs in the CNS (Petros and Mason, 2008). As aggrecan is degraded from the

medial edge to lateral border, RGC axons containing multiple CSPG receptors or extremely sensitive receptors could defasciculate and move to areas where aggrecan has been degraded. RGC axons that have no CSPG receptors or express high levels of CAMs will form synaptic contacts in the areas where aggrecan levels are still robust. This axon sorting model fits well with the competition phase because growth factors would become more abundant to particular growth cones as sensitive fibers move to more hospitable areas.

The assembly of neural circuits requires both specific temporal and spatial organization. Mechanisms that drive the spatial control of axon guidance have been well described, but the function and regulation of temporal controls of axon pathfinding remain largely unknown. This manuscript details both a molecular mechanism for temporal control of axons and its activity based regulation. My results suggest that the timing of dLGN innervation by layer VI CG axons is regulated by aggrecan, and I provide evidence for a signaling cascade by which transcriptional control of ADAMTS/aggrecanases is mediated by RGC activity. Furthermore, these results support the recent claim that retinal inputs instruct the timing of layer CG innervation in dLGN (Seabrook et al., 2013). This study provides insight into the role of waiting periods in the establishment of functional connectivity in CNS and reveals a novel function for aggrecan in the developing nervous system.

List of References

Alilain, W. J., Horn, K. P., Hu, H., Dick, T. E., & Silver, J. (2011). Functional regeneration of respiratory pathways after spinal cord injury. *Nature, 475*(7355), 196-200.

Allinson, T. M., Parkin, E. T., Turner, A. J., & Hooper, N. M. (2003). ADAMs family members as amyloid precursor protein alpha-secretases. *Journal of Neuroscience Research, 74*(3), 342-352.

Ango, F., di Cristo, G., Higashiyama, H., Bennett, V., Wu, P., & Huang, Z. J. (2004). Ankyrin-based subcellular gradient of neurofascin, an immunoglobulin family protein, directs GABAergic innervation at purkinje axon initial segment. *Cell, 119*(2), 257-272.

Apte, S. S. (2009). A disintegrin-like and metalloprotease (reprolysin-type) with thrombospondin type 1 motif (ADAMTS) superfamily: Functions and mechanisms. *The Journal of Biological Chemistry, 284*(46), 31493-31497.

Aspberg, A. (2012). The different roles of aggrecan interaction domains. *The Journal of Histochemistry and Cytochemistry : Official Journal of the Histochemistry Society, 60*(12), 987-996.

Badea, T. C., Cahill, H., Ecker, J., Hattar, S., & Nathans, J. (2009). Distinct roles of transcription factors brn3a and brn3b in controlling the development, morphology, and function of retinal ganglion cells. *Neuron, 61*(6), 852-864.

Barnard, A. R., Hattar, S., Hankins, M. W., & Lucas, R. J. (2006). Melanopsin regulates visual processing in the mouse retina. *Current Biology : CB, 16*(4), 389-395.

Berretta, S. (2012). Extracellular matrix abnormalities in schizophrenia. *Neuropharmacology, 62*(3), 1584-1597.

Bickford, M. E., Slusarczyk, A., Dilger, E. K., Krahe, T. E., Kucuk, C., & Guido, W. (2010). Synaptic development of the mouse dorsal lateral geniculate nucleus. *The Journal of Comparative Neurology, 518*(5), 622-635.

Brittis, P. A., Canning, D. R., & Silver, J. (1992). Chondroitin sulfate as a regulator of neuronal patterning in the retina. *Science (New York, N.Y.), 255*(5045),733-736.

Brittis, P. A., Lemmon, V., Rutishauser, U., & Silver, J. (1995). Unique changes of ganglion cell growth cone behavior following cell adhesion molecule perturbations: A time-lapse study of the living retina. *Molecular and Cellular Neurosciences, 6*(5), 433-449.

Brittis, P. A., & Silver, J. (1995). Multiple factors govern intraretinal axon guidance: A time-lapse study. *Molecular and Cellular Neurosciences, 6*(5), 413-432.

Busch, S. A., Horn, K. P., Silver, D. J., & Silver, J. (2009). Overcoming macrophage-mediated axonal dieback following CNS injury. *The Journal of Neuroscience : The Official Journal of the Society for Neuroscience, 29*(32), 9967-9976.

Butts, D. A., Kanold, P. O., & Shatz, C. J. (2007). A burst-based "hebbian" learning rule at retinogeniculate synapses links retinal waves to activity-dependent refinement. *PLoS Biology, 5*(3), e61.

Chalupa, L. M., & Gunhan, E. (2004). Development of on and off retinal pathways and retinogeniculate projections. *Progress in Retinal and Eye Research, 23*(1), 31-51.

Chen, C., & Regehr, W. G. (2000). Developmental remodeling of the retinogeniculate synapse. *Neuron, 28*(3), 955-966.

Chen, S. K., Chew, K. S., McNeill, D. S., Keeley, P. W., Ecker, J. L., Mao, B. Q., . . . Hattar, S. (2013). Apoptosis regulates ipRGC spacing necessary for rods and cones to drive circadian photoentrainment. *Neuron, 77*(3), 503-515.

Chen, S. Y., & Cheng, H. J. (2009). Functions of axon guidance molecules in synapse formation. *Current Opinion in Neurobiology, 19*(5), 471-478.

Chen, Z., Gore, B. B., Long, H., Ma, L., & Tessier-Lavigne, M. (2008). Alternative splicing of the Robo3 axon guidance receptor governs the midline switch from attraction to repulsion. *Neuron, 58*(3), 325-332.

Condic, M. L., Snow, D. M., & Letourneau, P. C. (1999). Embryonic neurons adapt to the inhibitory proteoglycan aggrecan by increasing integrin expression. *The Journal of Neuroscience : The Official Journal of the Society for Neuroscience, 19*(22), 10036-10043.

Cosenza, R. M., & Moore, R. Y. (1984). Afferent connections of the ventral lateral geniculate nucleus in the rat: An HRP study. *Brain Research, 310*(2), 367-370.

Crawford, D. C., Jiang, X., Taylor, A., & Mennerick, S. (2012). Astrocyte-derived thrombospondins mediate the development of hippocampal presynaptic plasticity in vitro. *The Journal of Neuroscience : The Official Journal of the Society for Neuroscience, 32*(38), 13100-13110.

Cua, R. C., Lau, L. W., Keough, M. B., Midha, R., Apte, S. S., & Yong, V. W. (2013). Overcoming neurite-inhibitory chondroitin sulfate proteoglycans in the astrocyte matrix. *Glia, 61*(6), 972-984.

Cudeiro, J., & Sillito, A. M. (2006). Looking back: Corticothalamic feedback and early visual processing. *Trends in Neurosciences, 29*(6), 298-306.

Dakubo, G. D., Wang, Y. P., Mazerolle, C., Campsall, K., McMahon, A. P., & Wallace, V. A. (2003). Retinal ganglion cell-derived sonic hedgehog signaling is required for optic disc and stalk neuroepithelial cell development. *Development (Cambridge, England), 130*(13), 2967-2980.

Deck, M., Lokmane, L., Chauvet, S., Mailhes, C., Keita, M., Niquille, M., . . . Garel, S. (2013). Pathfinding of corticothalamic axons relies on a rendezvous with thalamic projections. *Neuron, 77*(3), 472-484.

Demb, J. B. (2007). Cellular mechanisms for direction selectivity in the retina. *Neuron, 55*(2), 179-186.

Dickendesher, T. L., Baldwin, K. T., Mironova, Y. A., Koriyama, Y., Raiker, S. J., Askew, K. L., Giger, R. J. (2012). NgR1 and NgR3 are receptors for chondroitin sulfate proteoglycans. *Nature Neuroscience, 15*(5), 703-712.

Dino, M. R., Harroch, S., Hockfield, S., & Matthews, R. T. (2006). Monoclonal antibody cat-315 detects a glycoform of receptor protein tyrosine phosphatase beta/phosphacan early in CNS development that localizes to extrasynaptic sites prior to synapse formation. *Neuroscience, 142*(4), 1055-1069.

Dityatev, A., Schachner, M., & Sonderegger, P. (2010). The dual role of the extracellular matrix in synaptic plasticity and homeostasis. *Nature Reviews.Neuroscience, 11*(11), 735-746.

Domowicz, M., Krueger, R. C., Li, H., Mangoura, D., Vertel, B. M., & Schwartz, N. B. (1996). The nanomelic mutation in the aggrecan gene is expressed in chick chondrocytes and neurons. *International Journal of Developmental Neuroscience : The Official Journal of the International Society for Developmental Neuroscience, 14*(3), 191-201.

Drager, U. C. (1985). Birth dates of retinal ganglion cells giving rise to the crossed and uncrossed optic projections in the mouse. *Proceedings of the Royal Society of London.Series B, Containing Papers of a Biological Character.Royal Society (Great Britain), 224*(1234), 57-77.

Dudanova, I., & Klein, R. (2013). Integration of guidance cues: Parallel signaling and crosstalk. *Trends in Neurosciences, 36*(5), 295-304.

Erisir, A., Van Horn, S. C., & Sherman, S. M. (1997). Relative numbers of cortical and brainstem inputs to the lateral geniculate nucleus. *Proceedings of the National Academy of Sciences of the United States of America, 94*(4), 1517-1520.

Fawcett, J. W. (2006). Overcoming inhibition in the damaged spinal cord. *Journal of Neurotrauma, 23*(3-4), 371-383.

Feldheim, D. A., & O'Leary, D. D. (2010). Visual map development: Bidirectional signaling, bifunctional guidance molecules, and competition. *Cold Spring Harbor Perspectives in Biology, 2*(11),

Feldheim, D. A., Vanderhaeghen, P., Hansen, M. J., Frisen, J., Lu, Q., Barbacid, M., & Flanagan, J. G. (1998). Topographic guidance labels in a sensory projection to the forebrain. *Neuron, 21*(6), 1303-1313.

Feller, M. B. (2009). Retinal waves are likely to instruct the formation of eye-specific retinogeniculate projections. *Neural Development, 4*, 24-8104-4-24.

Feller, M. B., Wellis, D. P., Stellwagen, D., Werblin, F. S., & Shatz, C. J. (1996). Requirement for cholinergic synaptic transmission in the propagation of spontaneous retinal waves. *Science (New York, N.Y.), 272*(5265), 1182-1187.

Fenrich, K. K., Skelton, N., MacDermid, V. E., Meehan, C. F., Armstrong, S., Neuber-Hess, M. S., & Rose, P. K. (2007). Axonal regeneration and development of de novo axons from distal dendrites of adult feline commissural interneurons after a proximal axotomy. *The Journal of Comparative Neurology, 502*(6), 1079-1097.

Fisher, D., Xing, B., Dill, J., Li, H., Hoang, H. H., Zhao, Z., Li, S. (2011). Leukocyte common antigen-related phosphatase is a functional receptor for chondroitin sulfate proteoglycan axon growth inhibitors. *The Journal of Neuroscience : The Official Journal of the Society for Neuroscience, 31*(40), 14051 14066.

Forster, E., Zhao, S., & Frotscher, M. (2001). Hyaluronan-associated adhesive cues control fiber segregation in the hippocampus. *Development (Cambridge,England), 128*(15), 3029-3039.

Fosang, A. J., & Rogerson, F. M. (2010). Identifying the human aggrecanase. *Osteoarthritis and Cartilage / OARS, Osteoarthritis Research Society, 18*(9), 1109-1116.

Fox, M. A., & Guido, W. (2011). Shedding light on class-specific wiring: Development of intrinsically photosensitive retinal ganglion cell circuitry. *Molecular Neurobiology, 44*(3), 321-329.

Fox, M. A., & Sanes, J. R. (2007). Synaptotagmin I and II are present in distinct subsets of central synapses. *The Journal of Comparative Neurology, 503*(2), 280-296.

Fox, M. A., & Umemori, H. (2006). Seeking long-term relationship: Axon and target communicate to organize synaptic differentiation. *Journal of*

Neurochemistry, 97(5), 1215-1231.

Frischknecht, R., & Gundelfinger, E. D. (2012). The brain's extracellular matrix and its role in synaptic plasticity. *Advances in Experimental Medicine and Biology, 970*, 153-171.

Gao, G., Plaas, A., Thompson, V. P., Jin, S., Zuo, F., & Sandy, J. D. (2004). ADAMTS4 (aggrecanase-1) activation on the cell surface involves C-terminal cleavage by glycosylphosphatidyl inositol-anchored membrane type 4-matrix metalloproteinase and binding of the activated proteinase to chondroitin sulfate and heparan sulfate on syndecan-1. *The Journal of Biological Chemistry, 279*(11), 10042-10051.

Gao, G., Westling, J., Thompson, V. P., Howell, T. D., Gottschall, P. E., & Sandy, J. D. (2002). Activation of the proteolytic activity of ADAMTS4 (aggrecanase-1) by C-terminal truncation. *The Journal of Biological Chemistry, 277*(13), 11034-11041.

Giamanco, K. A., Morawski, M., & Matthews, R. T. (2010). Perineuronal net formation and structure in aggrecan knockout mice. *Neuroscience, 170*(4), 1314-1327.

Gilbert, R. J., McKeon, R. J., Darr, A., Calabro, A., Hascall, V. C., & Bellamkonda, R. V. (2005). CS-4,6 is differentially upregulated in glial scar and is a potent inhibitor of neurite extension. *Molecular and Cellular Neurosciences, 29*(4), 545-558.

Goldberg, J. L., & Barres, B. A. (2000). The relationship between neuronal survival and regeneration. *Annual Review of Neuroscience, 23*, 579-612.

Goldberg, J. L., Espinosa, J. S., Xu, Y., Davidson, N., Kovacs, G. T., & Barres, B. A. (2002). Retinal ganglion cells do not extend axons by default: Promotion by neurotrophic signaling and electrical activity. *Neuron, 33*(5), 689-702.

Golgi, C. (1875) Sull fina stuttura dei bulbi olfattori. *Riv. Sper. Freniat. Reggio-Emilia* 1:405-425

Goodman, C. S., & Shatz, C. J. (1993). Developmental mechanisms that generate precise patterns of neuronal connectivity. *Cell, 72 Suppl*, 77-98.

Grant, E., Hoerder-Suabedissen, A., & Molnar, Z. (2012). Development of the corticothalamic projections. *Frontiers in Neuroscience, 6*, 53.

Gu, Z., Cui, J., Brown, S., Fridman, R., Mobashery, S., Strongin, A. Y., & Lipton, S. A. (2005). A highly specific inhibitor of matrix metalloproteinase-9 rescues laminin from proteolysis and neurons from apoptosis in transient focal cerebral ischemia. *The Journal of Neuroscience : The Official Journal of the Society for Neuroscience, 25*(27), 6401-6408.

Guido, W. (2008). Refinement of the retinogeniculate pathway. *The Journal of*

Physiology, 586(Pt 18), 4357-4362

Guillery, R. W., & Sherman, S. M. (2002). Thalamic relay functions and their role in corticocortical communication: Generalizations from the visual system. *Neuron, 33*(2), 163-175.

Hamel, M. G., Ajmo, J. M., Leonardo, C. C., Zuo, F., Sandy, J. D., & Gottschall, P. E. (2008). Multimodal signaling by the ADAMTSs (a disintegrin and metalloproteinase with thrombospondin motifs) promotes neurite extension. *Experimental Neurology, 210*(2), 428-440.

Harrison, R.G. (1907). Observations on the living developing nerve fiber. *Anat. Rec.* 1:116-118

Harrison, R.G. (1910). The outgrowth of the nerve fiber as a mode of protoplasmic movement. J. Exp. Zool. 9:787-846

Hattar, S., Kumar, M., Park, A., Tong, P., Tung, J., Yau, K. W., & Berson, D. M. (2006). Central projections of melanopsin-expressing retinal ganglion cells in the mouse. *The Journal of Comparative Neurology, 497*(3), 326-349.

Hattar, S., Liao, H. W., Takao, M., Berson, D. M., & Yau, K. W. (2002). Melanopsin-containing retinal ganglion cells: Architecture, projections, and intrinsic photosensitivity. *Science (New York, N.Y.), 295*(5557), 1065-1070.

Hawthorne, A. L., Hu, H., Kundu, B., Steinmetz, M. P., Wylie, C. J., Deneris, E. S., & Silver, J. (2011). The unusual response of serotonergic neurons after CNS injury: Lack of axonal dieback and enhanced sprouting within the inhibitory environment of the glial scar. *The Journal of Neuroscience : The Official Journal of the Society for Neuroscience, 31*(15), 5605-5616.

Herrera, E., Brown, L., Aruga, J., Rachel, R. A., Dolen, G., Mikoshiba, K., . . . Mason, C. A. (2003). Zic2 patterns binocular vision by specifying the uncrossed retinal projection. *Cell, 114*(5), 545-557.

Hindges, R., McLaughlin, T., Genoud, N., Henkemeyer, M., & O'Leary, D. (2002). EphB forward signaling controls directional branch extension and arborization required for dorsal-ventral retinotopic mapping. *Neuron, 35*(3), 475-487.

Hong, Y. K., & Chen, C. (2011). Wiring and rewiring of the retinogeniculate synapse. *Current Opinion in Neurobiology, 21*(2), 228-237.

Huberman, A. D., Feller, M. B., & Chapman, B. (2008). Mechanisms underlying development of visual maps and receptive fields. *Annual Review of Neuroscience, 31*, 479-509.

Huberman, A. D., & Niell, C. M. (2011). What can mice tell us about how vision works? *Trends in Neurosciences, 34*(9), 464-473.

Huxley-Jones, J., Apte, S. S., Robertson, D. L., & Boot-Handford, R. P. (2005). The characterisation of six ADAMTS proteases in the basal chordate ciona intestinalis provides new insights into the vertebrate ADAMTS family. *The International Journal of Biochemistry & Cell Biology, 37*(9), 1838-1845.

Jacobs, E. C., Campagnoni, C., Kampf, K., Reyes, S. D., Kalra, V., Handley, V., . . . Campagnoni, A. T. (2007). Visualization of corticofugal projections during early cortical development in a tau-GFP-transgenic mouse. *The European Journal of Neuroscience, 25*(1), 17-30.

Jaubert-Miazza, L., Green, E., Lo, F. S., Bui, K., Mills, J., & Guido, W. (2005). Structural and functional composition of the developing retinogeniculate pathway in the mouse. *Visual Neuroscience, 22*(5), 661-676.

Jones, E. G. (2002). Thalamic circuitry and thalamocortical synchrony. *Philosophical Transactions of the Royal Society of London.Series B, Biological Sciences, 357*(1428), 1659-1673.

Kandel, E. R., Schwartz, J. H., & Thomas, M. J. (Eds.). (2000). *Principles of neural science* (4th ed.). New York, NY: McGraw-Hill.

Kay, J. N., De la Huerta, I., Kim, I. J., Zhang, Y., Yamagata, M., Chu, M. W., Sanes, J. R. (2011). Retinal ganglion cells with distinct directional preferences differ in molecular identity, structure, and central projections. *The Journal of Neuroscience : The Official Journal of the Society for Neuroscience, 31*(21), 7753-7762.

Kind, P. C., Sengpiel, F., Beaver, C. J., Crocker-Buque, A., Kelly, G. M., Matthews, R. T., & Mitchell, D. E. (2013). The development and activity-dependent expression of aggrecan in the cat visual cortex. *Cerebral Cortex (New York, N.Y.: 1991), 23*(2), 349-360.

Kirkby, L. A., & Feller, M. B. (2013). Intrinsically photosensitive ganglion cells contribute to plasticity in retinal wave circuits. *Proceedings of the National Academy of Sciences of the United States of America, 110*(29), 12090-12095.

Kolodkin, A. L., & Tessier-Lavigne, M. (2011). Mechanisms and molecules of neuronal wiring: A primer. *Cold Spring Harbor Perspectives in Biology, 3*(6),

Krstic, D., Rodriguez, M., & Knuesel, I. (2012). Regulated proteolytic processing of reelin through interplay of tissue plasminogen activator (tPA), ADAMTS-4, ADAMTS-5, and their modulators. *PloS One, 7*(10).

Kwok, J. C., Afshari, F., Garcia-Alias, G., & Fawcett, J. W. (2008). Proteoglycans in the central nervous system: Plasticity, regeneration and their stimulation with chondroitinase ABC. *Restorative Neurology and Neuroscience, 26*(2-3), 131-145.

Lander, C., Kind, P., Maleski, M., & Hockfield, S. (1997). A family of activity-dependent neuronal cell-surface chondroitin sulfate proteoglycans in cat visual cortex. *The Journal of Neuroscience : The Official Journal of the Society for Neuroscience, 17*(6), 1928-1939.

Landry, C. F., Pribyl, T. M., Ellison, J. A., Givogri, M. I., Kampf, K., Campagnoni, C. W., & Campagnoni, A. T. (1998). Embryonic expression of the myelin basic protein gene: Identification of a promoter region that targets transgene expression to pioneer neurons. *The Journal of Neuroscience : The Official Journal of the Society for Neuroscience, 18*(18), 7315-7327.

Langley, J.N. (1895). Note on regeneration of pre-ganglionic fibers of the sympathetic. *J. Physiol. (London)* 18:280-284

Langley, J.N. (1906). On nerve-endings and on special excitable substances in cells. *Croonian Lecture*. 78 170-194.

Le Goff, C., Somerville, R. P., Kesteloot, F., Powell, K., Birk, D. E., Colige, A. C., & Apte, S. S. (2006). Regulation of procollagen amino-propeptide processing during mouse embryogenesis by specialization of homologous ADAMTS proteases: Insights on collagen biosynthesis and dermatosparaxis. *Development (Cambridge, England), 133*(8), 1587-1596.

Lentz, S. I., Knudson, C. M., Korsmeyer, S. J., & Snider, W. D. (1999). Neurotrophins support the development of diverse sensory axon morphologies. *The Journal of Neuroscience : The Official Journal of the Society for Neuroscience, 19*(3), 1038-1048.

Lindsay, R. M. (1988). Nerve growth factors (NGF, BDNF) enhance axonal regeneration but are not required for survival of adult sensory neurons. *The Journal of Neuroscience : The Official Journal of the Society for Neuroscience, 8*(7), 2394-2405.

Livak, K. J., & Schmittgen, T. D. (2001). Analysis of relative gene expression data using real-time quantitative PCR and the 2(-delta delta C(T)) method. *Methods (San Diego, Calif.), 25*(4), 402-408.

Llamazares, M., Obaya, A. J., Moncada-Pazos, A., Heljasvaara, R., Espada, J., Lopez-Otin, C., & Cal, S. (2007). The ADAMTS12 metalloproteinase exhibits anti-tumorigenic properties through modulation of the ras-dependent ERK signalling pathway. *Journal of Cell Science, 120*(Pt 20), 3544-3552.

Luo, L., & Flanagan, J. G. (2007). Development of continuous and discrete neural maps. *Neuron, 56*(2), 284-300.

Marcus, R. C., Blazeski, R., Godement, P., & Mason, C. A. (1995). Retinal axon divergence in the optic chiasm: Uncrossed axons diverge from crossed axons within a midline glial specialization. *The Journal of Neuroscience : The Official Journal of the Society for Neuroscience, 15*(5 Pt 2), 3716-3729.

Massey, J. M., Hubscher, C. H., Wagoner, M. R., Decker, J. A., Amps, J., Silver, J., & Onifer, S. M. (2006). Chondroitinase ABC digestion of the perineuronal net promotes functional collateral sprouting in the cuneate nucleus after cervical spinal cord injury. *The Journal of Neuroscience : The Official Journal of the Society for Neuroscience, 26*(16), 4406-4414.

McCulloch, D. R., Nelson, C. M., Dixon, L. J., Silver, D. L., Wylie, J. D., Lindner, V., . . . Apte, S. S. (2009). ADAMTS metalloproteases generate active versican fragments that regulate interdigital web regression. *Developmental Cell, 17*(5), 687-698.

McKeon, R. J., Hoke, A., & Silver, J. (1995). Injury-induced proteoglycans inhibit the potential for laminin-mediated axon growth on astrocytic scars. *Experimental Neurology, 136*(1), 32-43.

McKeon, R. J., Schreiber, R. C., Rudge, J. S., & Silver, J. (1991). Reduction of neurite outgrowth in a model of glial scarring following CNS injury is correlated with the expression of inhibitory molecules on reactive astrocytes. *The Journal of Neuroscience : The Official Journal of the Society for Neuroscience, 11*(11), 3398-3411.

McRae, P. A., Rocco, M. M., Kelly, G., Brumberg, J. C., & Matthews, R. T. (2007). Sensory deprivation alters aggrecan and perineuronal net expression in the mouse barrel cortex. *The Journal of Neuroscience : The Official Journal of the Society for Neuroscience, 27*(20), 5405-5413.

Morawski, M., Bruckner, G., Arendt, T., & Matthews, R. T. (2012). Aggrecan: Beyond cartilage and into the brain. *The International Journal of Biochemistry & Cell Biology, 44*(5), 690-693.

Muir, D., Sonnenfeld, K., & Berl, S. (1989). Growth cone advance mediated by fibronectin-associated filopodia is inhibited by a phorbol ester tumor promoter. *Experimental Cell Research, 180*(1), 134-149.

Muir-Robinson, G., Hwang, B. J., & Feller, M. B. (2002). Retinogeniculate axons undergo eye-specific segregation in the absence of eye-specific layers. *The Journal of Neuroscience : The Official Journal of the Society for Neuroscience, 22*(13), 5259-5264.

Murphy, G. (2011). Tissue inhibitors of metalloproteinases. *Genome Biology, 12*(11), 233-2011-12-11-233.

Pak, W., Hindges, R., Lim, Y. S., Pfaff, S. L., & O'Leary, D. D. (2004). Magnitude of binocular vision controlled by islet-2 repression of a genetic program that specifies laterality of retinal axon pathfinding. *Cell, 119*(4), 567-578.

Palade, G.E. and Palay, S.L. (1954) Electron microscope observations of interneuronal and neuromuscular synapses. *Anat. Rec*. 118:335-336

Petros, T. J., Rebsam, A., & Mason, C. A. (2008). Retinal axon growth at the optic chiasm: To cross or not to cross. *Annual Review of Neuroscience, 31*, 295-315.

Pfeiffenberger, C., Cutforth, T., Woods, G., Yamada, J., Renteria, R. C., Copenhagen, D. R., . Feldheim, D. A. (2005). Ephrin-as and neural activity are required for eye-specific patterning during retinogeniculate mapping. *Nature Neuroscience, 8*(8), 1022-1027.

Pfeiffenberger, C., Yamada, J., & Feldheim, D. A. (2006). Ephrin-as and patterned retinal activity act together in the development of topographic maps in the primary visual system. *The Journal of Neuroscience : The Official Journal of the Society for Neuroscience, 26*(50), 12873-12884.

Porter, S., Clark, I. M., Kevorkian, L., & Edwards, D. R. (2005). The ADAMTS metalloproteinases. *The Biochemical Journal, 386*(Pt 1), 15-27.

Powell, A. W., Sassa, T., Wu, Y., Tessier-Lavigne, M., & Polleux, F. (2008). Topography of thalamic projections requires attractive and repulsive functions of netrin-1 in the ventral telencephalon. *PLoS Biology, 6*(5), e116.

Provencio, I., Rodriguez, I. R., Jiang, G., Hayes, W. P., Moreira, E. F., & Rollag, M. D. (2000). A novel human opsin in the inner retina. *The Journal of Neuroscience : The Official Journal of the Society for Neuroscience, 20*(2), 600-605.

Quina, L. A., Pak, W., Lanier, J., Banwait, P., Gratwick, K., Liu, Y., Turner, E. E. (2005). Brn3a-expressing retinal ganglion cells project specifically to thalamocortical and collicular visual pathways. *The Journal of Neuroscience : The Official Journal of the Society for Neuroscience, 25*(50), 11595-11604.

Ramon y Cajal, S. (1892). Nuevo concepto de la histologia de los centros nerviosos. *Rev. Cien med. Barcelona* 18.

Ramon y Cajal, S. (1909). Histologie du Systeme Nerveux de l'Homme et des Vertebres.

Ramon y Cajal, S. (1913). Sobre un Nuevo proceder de impregnacion de la neuroglia y sus resultadosen los centros nerviosos del hombre y animals. *Trab. Lab. Invest. Biol. Univ. Madrid.* 11:219-237

Raper, J., & Mason, C. (2010). Cellular strategies of axonal pathfinding. *Cold Spring Harbor Perspectives in Biology, 2*(9), a001933.

Rebsam, A., & Mason, C. A. (2011). Cadherins as matchmakers. *Neuron, 71*(4), 566-568.

Rebsam, A., Petros, T. J., & Mason, C. A. (2009). Switching retinogeniculate axon laterality leads to normal targeting but abnormal eye-specific segregation that is activity dependent. *The Journal of Neuroscience : The Official Journal of the Society for Neuroscience, 29*(47), 14855-14863.

Renna, J. M., Weng, S., & Berson, D. M. (2011). Light acts through melanopsin to alter retinal waves and segregation of retinogeniculate afferents. *Nature Neuroscience, 14*(7), 827-829.

Rio-Hortega, P.d. (1919). El tercer element de los centros nerviosos. I. La microglia normal. II. Intervencion de la microglia en los procesos patologicos. (Celulas En bastoncito y cuerpos granulo-adiposos). III. Naturaleza probable de la microglia. *Bol. Soc. Esp. Biol.* 9:69-129

Rittenhouse, E., Dunn, L. C., Cookingham, J., Calo, C., Spiegelman, M., Dooher, G. B., & Bennett, D. (1978). Cartilage matrix deficiency (cmd): A new autosomal recessive lethal mutation in the mouse. *Journal of Embryology and Experimental Morphology, 43*, 71-84.

Sabatier, C., Plump, A. S., Le, M., Brose, K., Tamada, A., Murakami, F., . . . Tessier-Lavigne, M. (2004). The divergent robo family protein rig-1/Robo3 is a negative regulator of slit responsiveness required for midline crossing by commissural axons. *Cell, 117*(2), 157-169.

Sandy, J. D., Neame, P. J., Boynton, R. E., & Flannery, C. R. (1991). Catabolism of aggrecan in cartilage explants. identification of a major cleavage site within the interglobular domain. *The Journal of Biological Chemistry, 266*(14), 8683-8685

Sanes, J. R. (2003). The basement membrane/basal lamina of skeletal muscle. *The Journal of Biological Chemistry, 278*(15), 12601-12604.

Sanes, J. R., & Yamagata, M. (2009). Many paths to synaptic specificity. *Annual Review of Cell and Developmental Biology, 25*, 161-195.

Sanes, J. R., & Zipursky, S. L. (2010). Design principles of insect and vertebrate visual systems. *Neuron, 66*(1), 15-36.

Schmidt, T. M., Do, M. T., Dacey, D., Lucas, R., Hattar, S., & Matynia, A. (2011). Melanopsin-positive intrinsically photosensitive retinal ganglion cells: From form to function. *The Journal of Neuroscience : The Official Journal of the Society for*

Neuroscience, 31(45), 16094-16101.

Seabrook, T. A., El-Danaf, R. N., Krahe, T. E., Fox, M. A., & Guido, W. (2013). Retinal input regulates the timing of corticogeniculate innervation. *The Journal of Neuroscience: The Official Journal of the Society for Neuroscience, 33*(24), 10085-10097.

Sharma, K., Korade, Z., & Frank, E. (1994). Development of specific muscle and cutaneous sensory projections in cultured segments of spinal cord. *Development (Cambridge, England), 120*(5), 1315-1323.

Sharma, K., Selzer, M. E., & Li, S. (2012). Scar-mediated inhibition and CSPG receptors in the CNS. *Experimental Neurology, 237*(2), 370-378.

Sheldon, M., Rice, D. S., D'Arcangelo, G., Yoneshima, H., Nakajima, K., Mikoshiba, K., Curran, T. (1997). Scrambler and yotari disrupt the disabled gene and produce a reeler-like phenotype in mice. *Nature, 389*(6652), 730-733.

Shen, Y., Tenney, A. P., Busch, S. A., Horn, K. P., Cuascut, F. X., Liu, K., Flanagan, J. G. (2009). PTPsigma is a receptor for chondroitin sulfate proteoglycan, an inhibitor of neural regeneration. *Science (New York, N.Y.), 326*(5952), 592-596.

Shepherd, G.M. (1991). Foundations of the Neuron Doctrine. New York: Oxford University Press.

Sherman, S. M. (2012). Thalamocortical interactions. *Current Opinion in Neurobiology, 22*(4), 575-579.

Sherrington, C.S. (1897). The central nervous system. Macmillan, London.

Sherrington, C.S. (1900). The spinal cord. Pentland, Edinburgh

Sillito, A. M., Cudeiro, J., & Jones, H. E. (2006). Always returning: Feedback and sensory processing in visual cortex and thalamus. *Trends in Neurosciences, 29*(6), 307-316.

Silver, J., & Miller, J. H. (2004). Regeneration beyond the glial scar. *Nature Reviews.Neuroscience, 5*(2), 146-156.

Snow, D. M., Brown, E. M., & Letourneau, P. C. (1996). Growth cone behavior in the presence of soluble chondroitin sulfate proteoglycan (CSPG), compared to behavior on CSPG bound to laminin or fibronectin. *International Journal of Developmental Neuroscience : The Official Journal of the International Society for Developmental Neuroscience, 14*(3), 331-349.

Snow, D. M., Lemmon, V., Carrino, D. A., Caplan, A. I., & Silver, J. (1990). Sulfated proteoglycans in astroglial barriers inhibit neurite outgrowth in vitro. *Experimental*

Neurology, 109(1), 111-130.

Snow, D. M., & Letourneau, P. C. (1992). Neurite outgrowth on a step gradient of chondroitin sulfate proteoglycan (CS-PG). *Journal of Neurobiology, 23*(3), 322-336.

Snow, D. M., Smith, J. D., Cunningham, A. T., McFarlin, J., & Goshorn, E. C. (2003). Neurite elongation on chondroitin sulfate proteoglycans is characterized by axonal fasciculation. *Experimental Neurology, 182*(2), 310-321.

SPERRY, R. W. (1963). Chemoaffinity in the orderly growth of nerve fiber patterns and connections. *Proceedings of the National Academy of Sciences of the United States of America, 50*, 703-710.

Stafford, B. K., Sher, A., Litke, A. M., & Feldheim, D. A. (2009). Spatial-temporal patterns of retinal waves underlying activity-dependent refinement of retinofugal projections. *Neuron, 64*(2), 200-212.

Stanton, H., Melrose, J., Little, C. B., & Fosang, A. J. (2011). Proteoglycan degradation by the ADAMTS family of proteinases. *Biochimica Et Biophysica Acta, 1812*(12), 1616-1629.

Steinmetz, M. P., Horn, K. P., Tom, V. J., Miller, J. H., Busch, S. A., Nair, D., Silver, J. (2005). Chronic enhancement of the intrinsic growth capacity of sensory neurons combined with the degradation of inhibitory proteoglycans allows functional regeneration of sensory axons through the dorsal root entry zone in the mammalian spinal cord. *The Journal of Neuroscience : The Official Journal of the Society for Neuroscience, 25*(35), 8066-8076.

Su, J., Gorse, K., Ramirez, F., & Fox, M. A. (2010). Collagen XIX is expressed by interneurons and contributes to the formation of hippocampal synapses. *The Journal of Comparative Neurology, 518*(2), 229-253.

Su, J., Haner, C. V., Imbery, T. E., Brooks, J. M., Morhardt, D. R., Gorse, K., Fox, M. A. (2011). Reelin is required for class-specific retinogeniculate targeting. *The Journal of Neuroscience : The Official Journal of the Society for Neuroscience, 31*(2), 575-586.

Sur, M., Frost, D. O., & Hockfield, S. (1988). Expression of a surface-associated antigen on Y-cells in the cat lateral geniculate nucleus is regulated by visual experience. *The Journal of Neuroscience : The Official Journal of the Society for Neuroscience, 8*(3), 874-882.

Tan, C. L., Kwok, J. C., Patani, R., Ffrench-Constant, C., Chandran, S., & Fawcett, J. W. (2011). Integrin activation promotes axon growth on inhibitory chondroitin sulfate proteoglycans by enhancing integrin signaling. *The Journal of Neuroscience : The Official Journal of the Society for Neuroscience, 31*(17), 6289-6295.

Tauchi, R., Imagama, S., Natori, T., Ohgomori, T., Muramoto, A., Shinjo, R.,Kadomatsu, K. (2012). The endogenous proteoglycan-degrading enzyme ADAMTS-4 promotes functional recovery after spinal cord injury. *Journal of Neuroinflammation, 9*, 53-2094-9-53.

Tessier-Lavigne, M., & Goodman, C. S. (1996). The molecular biology of axon guidance. *Science (New York, N.Y.), 274*(5290), 1123-1133.

Torborg, C. L., & Feller, M. B. (2005). Spontaneous patterned retinal activity and the refinement of retinal projections. *Progress in Neurobiology, 76*(4), 213-235.

Tortorella, M. D., & Malfait, A. M. (2008). Will the real aggrecanase(s) step up: Evaluating the criteria that define aggrecanase activity in osteoarthritis. *Current Pharmaceutical Biotechnology, 9*(1), 16-23.

Triplett, J. W., & Feldheim, D. A. (2012). Eph and ephrin signaling in the formation of topographic maps. *Seminars in Cell & Developmental Biology, 23*(1), 7-15.

Triplett, J. W., Owens, M. T., Yamada, J., Lemke, G., Cang, J., Stryker, M. P., & Feldheim, D. A. (2009). Retinal input instructs alignment of visual topographic maps. *Cell, 139*(1), 175-185.

Truett, G. E., Heeger, P., Mynatt, R. L., Truett, A. A., Walker, J. A., & Warman, M. L. (2000). Preparation of PCR-quality mouse genomic DNA with hot sodium hydroxide and tris (HotSHOT). *Biotechniques, 29*(1), 52, 54.

Van Hooser, S. D., Heimel, J. A., & Nelson, S. B. (2005). Functional cell classes and functional architecture in the early visual system of a highly visual rodent. *Progress in Brain Research, 149*, 127-145.

Van Horn, S. C., Erisir, A., & Sherman, S. M. (2000). Relative distribution of synapses in the A-laminae of the lateral geniculate nucleus of the cat. *The Journal of Comparative Neurology, 416*(4), 509-520.

Viapiano, M. S., Hockfield, S., & Matthews, R. T. (2008). BEHAB/brevican requires ADAMTS-mediated proteolytic cleavage to promote glioma invasion. *Journal of Neuro-Oncology, 88*(3), 261-272.

Wang, G., & Scott, S. A. (2000). The "waiting period" of sensory and motor axons in early chick hindlimb: Its role in axon pathfinding and neuronal maturation. *The Journal of Neuroscience : The Official Journal of the Society for Neuroscience, 20*(14), 5358-5366.

Wang, G., & Scott, S. A. (2008). Retinoid signaling is involved in governing the waiting period for axons in chick hindlimb. *Developmental Biology, 321*(1), 216-226.

Wang, S. W., Kim, B. S., Ding, K., Wang, H., Sun, D., Johnson, R. L., Gan, L. (2001). Requirement for math5 in the development of retinal ganglion cells. *Genes & Development, 15*(1), 24-29.

Watanabe, H., Kimata, K., Line, S., Strong, D., Gao, L. Y., Kozak, C. A., & Yamada, Y. (1994). Mouse cartilage matrix deficiency (cmd) caused by a 7 bp deletion in the aggrecan gene. *Nature Genetics, 7*(2), 154-157.

Watanabe, H., Nakata, K., Kimata, K., Nakanishi, I., & Yamada, Y. (1997). Dwarfism and age-associated spinal degeneration of heterozygote cmd mice defective in aggrecan. *Proceedings of the National Academy of Sciences of the United States of America, 94*(13), 6943-6947.

Williams, S. E., Grumet, M., Colman, D. R., Henkemeyer, M., Mason, C. A., & Sakurai, T. (2006). A role for nr-CAM in the patterning of binocular visual pathways. *Neuron, 50*(4), 535-547.

Williams, S. E., Mann, F., Erskine, L., Sakurai, T., Wei, S., Rossi, D. J., Henkemeyer, M. (2003). Ephrin-B2 and EphB1 mediate retinal axon divergence at the optic chiasm. *Neuron, 39*(6), 919-935.

Xie, Y., Skinner, E., Landry, C., Handley, V., Schonmann, V., Jacobs, E., Campagnoni, A. (2002). Influence of the embryonic preplate on the organization of the cerebral cortex: A targeted ablation model. *The Journal of Neuroscience : The Official Journal of the Society for Neuroscience, 22*(20), 8981-8991.

Xue, M., Fan, Y., Liu, S., Zygun, D. A., Demchuk, A., & Yong, V. W. (2009). Contributions of multiple proteases to neurotoxicity in a mouse model of intracerebral haemorrhage. *Brain : A Journal of Neurology, 132*(Pt 1), 26-36.

Yamada, E. S., Silveira, L. C., Gomes, F. L., & Lee, B. B. (1996). The retinal ganglion cell classes of new world primates. *Revista Brasileira De Biologia, 56 Su 1 Pt 2*, 381-396.

Yamagata, M., Weiner, J. A., & Sanes, J. R. (2002). Sidekicks: Synaptic adhesion molecules that promote lamina-specific connectivity in the retina. *Cell,110*(5), 649-660.

Yang, Z., Ding, K., Pan, L., Deng, M., & Gan, L. (2003). Math5 determines the competence state of retinal ganglion cell progenitors. *Developmental Biology, 264*(1), 240-254.

Yin, Y., Henzl, M. T., Lorber, B., Nakazawa, T., Thomas, T. T., Jiang, F., Benowitz, L. I. (2006). Oncomodulin is a macrophage-derived signal for axon regeneration in retinal ganglion cells. *Nature Neuroscience, 9*(6), 843-852.

Zhou, Z., Meng, Y., Asrar, S., Todorovski, Z., & Jia, Z. (2009). A critical role of rho-

kinase ROCK2 in the regulation of spine and synaptic function. *Neuropharmacology, 56*(1), 81-89.

Zimmermann, D. R., & Dours-Zimmermann, M. T. (2008). Extracellular matrix of the central nervous system: From neglect to challenge. *Histochemistry and Cell Biology, 130*(4), 635-653.

Zipursky, S. L., & Sanes, J. R. (2010). Chemoaffinity revisited: Dscams, protocadherins, and neural circuit assembly. *Cell, 143*(3), 343-353.

Appendix A

Probing for the Presence of GFAP-positive Astrocytes and Iba-1-positive Microglia in Experimental Models

Figure A1: Disassociated cortical cultures from embryonic tissue contain few GFAP-positive astrocytes. (Left Frame) Low-magnification fluorescent image of GFAP labeled astrocytes in P0 cortical culture. Note the network of astrocytes that fills most of the field. (Middle and Right Frames)Higher-magnification fluorescent images of GFAP labeled astrocytes from cortical culture obtained from E16 mice. Scale bars are 200 µm.

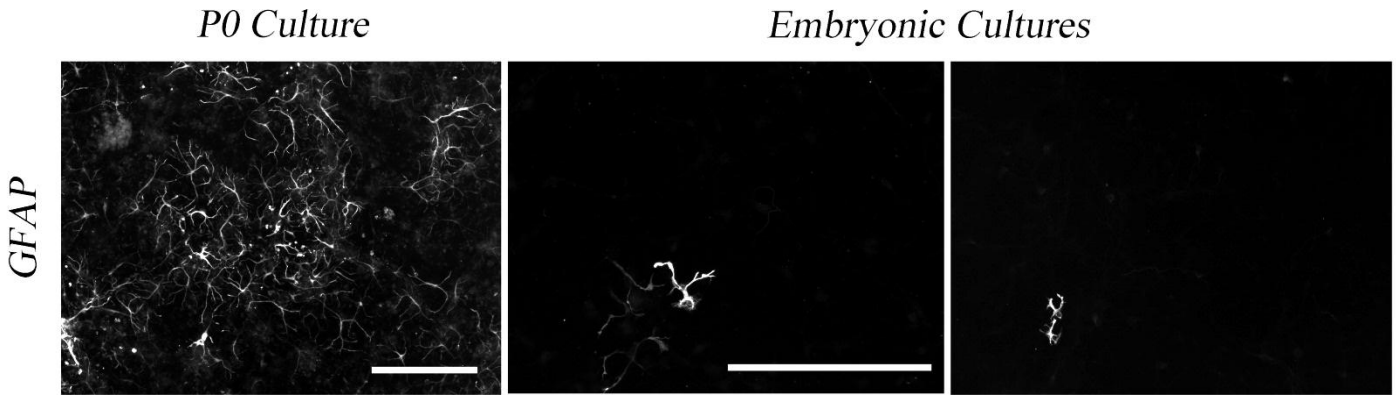
P0 Culture
Embryonic Cultures
GFAP

Figure A2: GFAP positive astrocytes and Iba-1 positive microglia in bilateral injected tissues. (Top Row) Fluorescent images indicating GFAP positive astrocytes, within dLGN, one day post-neonatal injection of PNase (Left), chABC (Middle), or ADAMTS4 (Right). (Bottom Row) Fluorescent images showing Iba-1 positive microglial proliferation in dLGN from mice treated with the same conditions as above. chABC-injected (Middle) tissues show the most Iba1 positive cells, while fewer microglia are stained in PNase (Left) and ADAMTS4 (Right) treated animals. dLGN are encircled with dots. Scale bar is 200µm.

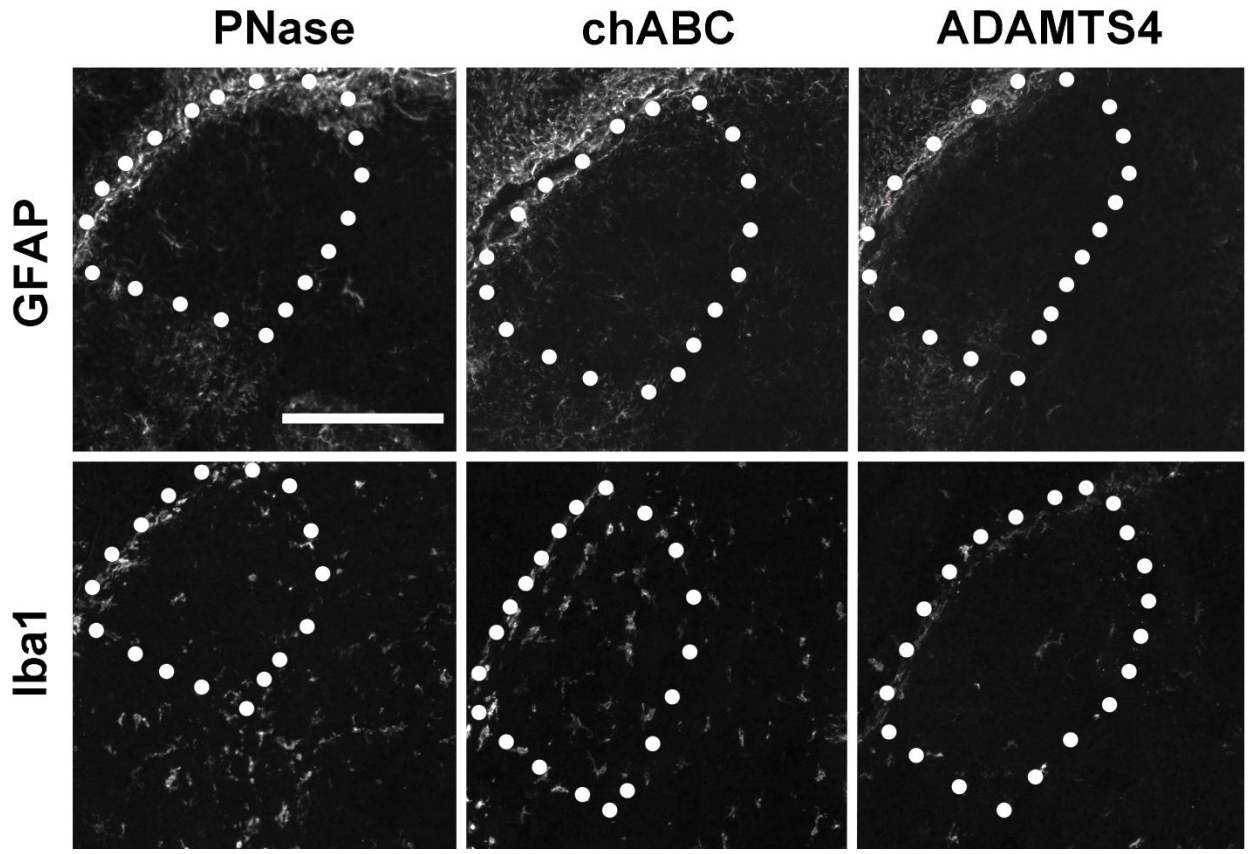
PNase
chABC
ADAMTS4
GFAP
Iba1

Figure A3: Comparison of GFAP positive astrocytes and Iba-1 positive microglia in *golli-tau-gfp* and *math5*$^{-/-}$ mice. (Left Panel) GFAP immunostained sections in *golli-tau-gfp* and *math5*$^{-/-}$ mice show very few astrocytes at P0 and at the time when CG axons begin to invade dLGN. (Right Panel) Iba-1 positive microglia are sparsely expressed in dLGN in both *golli-tau-gfp* and *math5*$^{-/-}$ mice at P0 and as CG fibers innervate dLGN. dLGN are encircled with dots. Scale bar is 200µm.

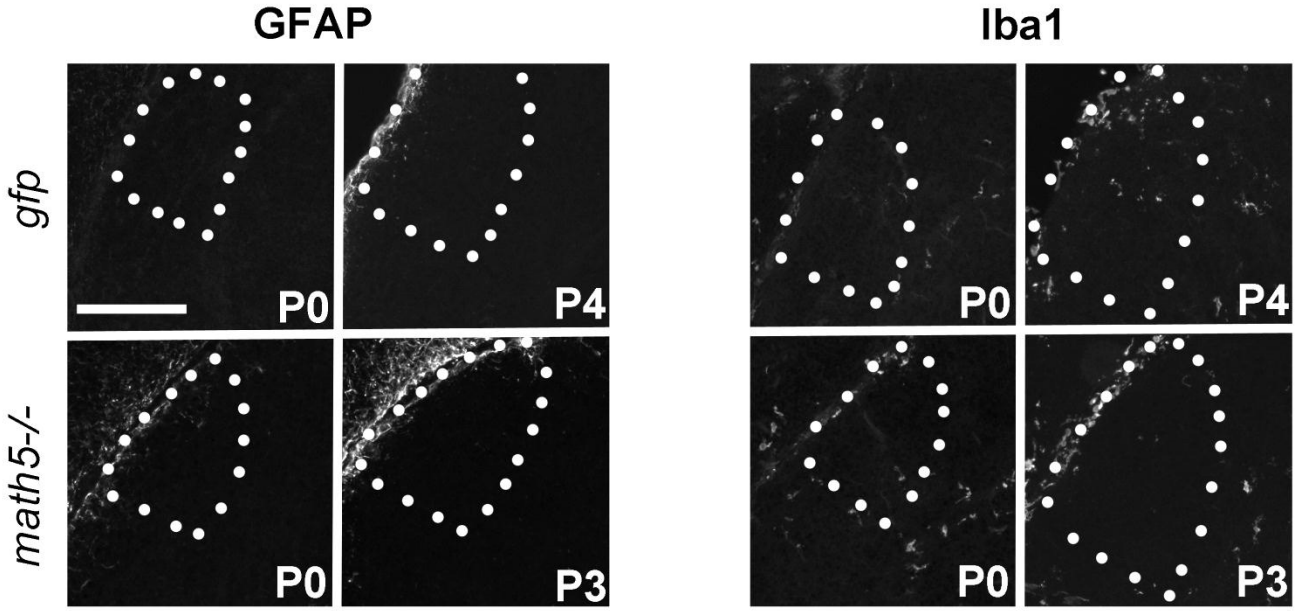
GFAP
Iba1
gfp
math5-/-
P0
P4
P0
P3
P0
P4
P0
P3

Appendix B

Retinal Innervation in *acan*^{cmd} Mice

Figure B1: Retinal projections innervate dLGN in the absence of aggrecan. (Top panel) Cat315 immunostained thalamus at E16 in WT and *acan*^{cmd} mice. Labeling of thalamus does not occur using cat315 in the absence of functional aggrecan, thus showing cat315 specificity. (Bottom Panel) Retinal labeling with DiI just after birth in WT and *acan*^{cmd} mice show that retinal projections find their targets in the presence or absence of aggrecan, but there appears to be some disorganization in axon fasciculation of *acan*^{cmd} mice. dLGN are encircled with dots. Scale bars are 200µm.

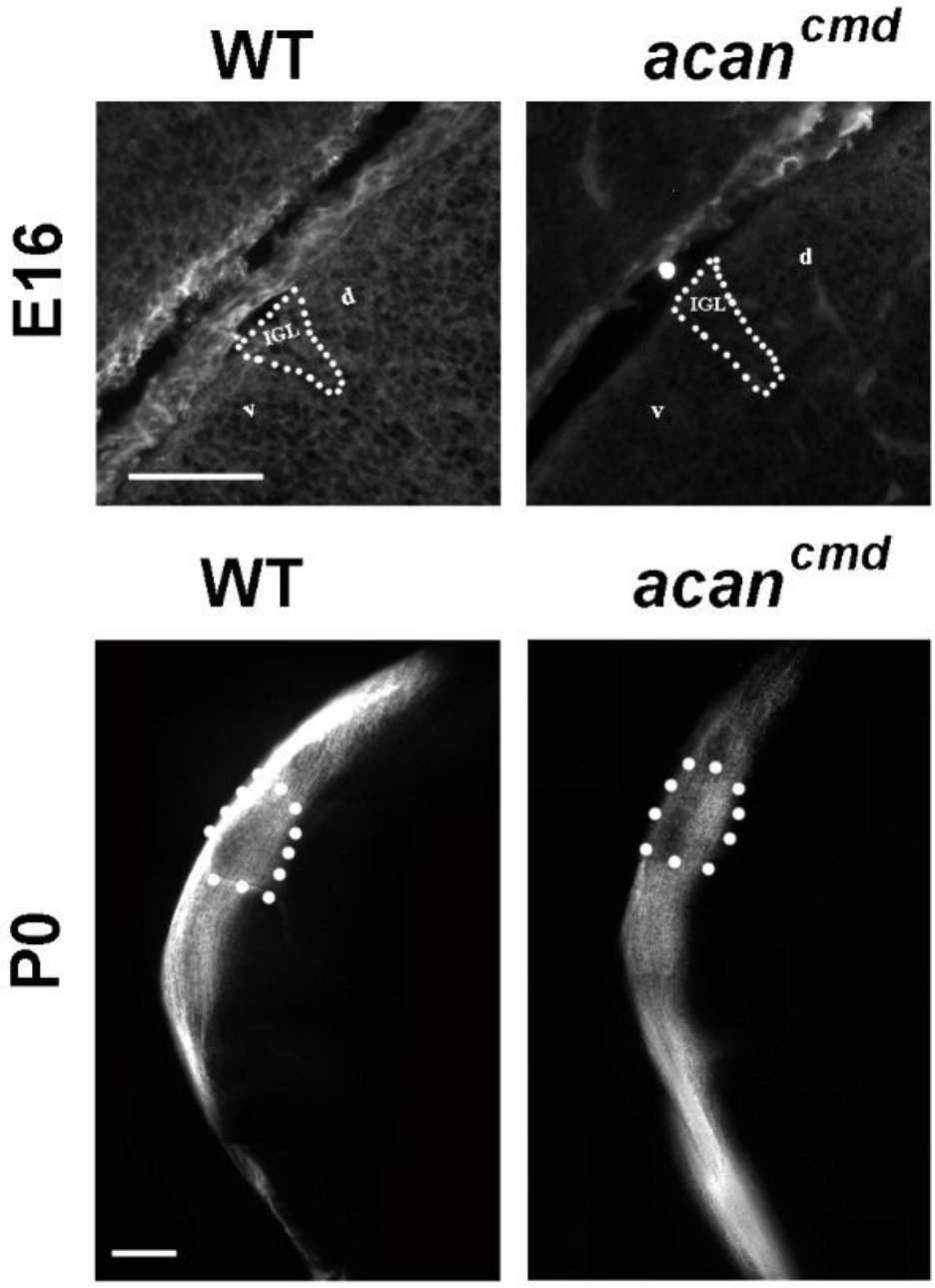
WT
acan cmd
E16
d
IGL
v
d
IGL
v
WT
acan cmd
P0

Vita

Justin Brooks was born in Richmond, Virginia on June 13, 1982. He graduated from St. Christopher's High School in 2000 and attended Virginia Tech. He received the undergraduate research award and a Bachelor's degree in Biochemistry in 2004. Subsequently, he attended VCU in the PhD program for Biochemistry for one year before exploring his options in industry. After years of boredom, he realized that continuing his education was his only option. Justin joined the laboratory of Dr. Michael Fox in January, 2010. He has presented numerous posters detailing his work over the past 4 years and has won multiple awards at Central Virginia Chapter of the Society for Neuroscience. He is a member of the Society for Neuroscience, American Association for the Advancement of Science and American Society for Neurochemistry.

Manuscripts resulting from Justin's work at Virginia Commonwealth University.

Su, J., Haner, C. V., Imbery, T. E., Brooks, J. M., Morhardt, D. R., Gorse, K., & Fox, M.A(2011). Reelin is required for class-specific retinogeniculate targeting. *The Journal of Neuroscience : The Official Journal of the Society for Neuroscience, 31*(2), 575-586.

Singh, R., Su, J., Brooks, J., Terauchi, A., Umemori, H., & Fox, M. A. (2012). Fibroblast growth factor 22 contributes to the development of retinal nerve terminals in the dorsal lateral geniculate nucleus. *Frontiers in Molecular Neuroscience, 4*, 61.

Brooks, J.M., Su, J., Levy, C., Wang, J.S., Seabrook, T.A., Guido, W., Fox, M.A**.** "A molecular mechanism regulating the timing of corticogeniculate innervation." Cell Reports. 2013*.*